博士論文

Inverse Problems for Acoustic Measurement with Nonlinear Saturation Effects: Theory and Applications

（非線形飽和現象を伴う音響計測のための逆問題における理論と応用）

植野 夏樹

Abstract

The objectives of this thesis are twofold: first, to establish a unifying framework of inverse problems for acoustic measurement, especially considering nonlinear saturation effects; and second, to propose practical methods for two specific topics of acoustic measurement, the restoration of saturated sound signals and the estimation of sound fields, where existing and proposed theories on inverse problems are fully utilized. Most current methods related to acoustic measurement problems are classified as linear inverse problems, where a linear relationship between the target acoustic quantity and the observed signal is assumed. In practice, however, observation is often affected by nonlinear saturation effects in various situations of acoustic measurement, which cannot be dealt with in these methods. The former part of this thesis presents a new formulation for inverse problems with nonlinear saturation effects and also provides efficient algorithms to solve the proposed formulation. In the latter part, several practical methods for restoring saturated sound signals and estimating sound fields are proposed on the basis of the methodological framework presented in the former part. Also, experimental evaluations are provided in comparison with other current practical methods proposed in the corresponding fields, and the validity of the proposed methods is demonstrated.

Contents

Chapter 1

Introduction

1.1 Background

This thesis deals with the problem of estimating various acoustic quantities from indirect observation, as illustrated in Figure 1.1, which is referred to as the *acoustic measurement problem*. Here, the term "acoustic quantity" will be used in a broad sense to include (temporal) sound signals, (spatio-temporal) sound fields, and various other acoustic-related parameters. Acoustic measurement techniques, as well as other measurement techniques, not only are an end in themselves but also form the foundation of a wide variety of applications. In automatic speech recognition [1,2] and computational auditory event analysis [3,4], for example, speech signals or environmental sound signals have to be captured with a certain degree of accuracy. As another example, sound field measurement techniques have various applications in spatial audio technologies, including binaural reproduction [5,6], sound field reproduction [7,8], and spatial active noise control [9]. Particularly in recent decades, so much progress has been made in these applications that it is now possible, or almost possible, to put these techniques into practice in the real world. Also, an accurate measurement (calibration) of the directivity and frequency response of sensors such as microphones and loudspeakers can be regarded as one type of acoustic

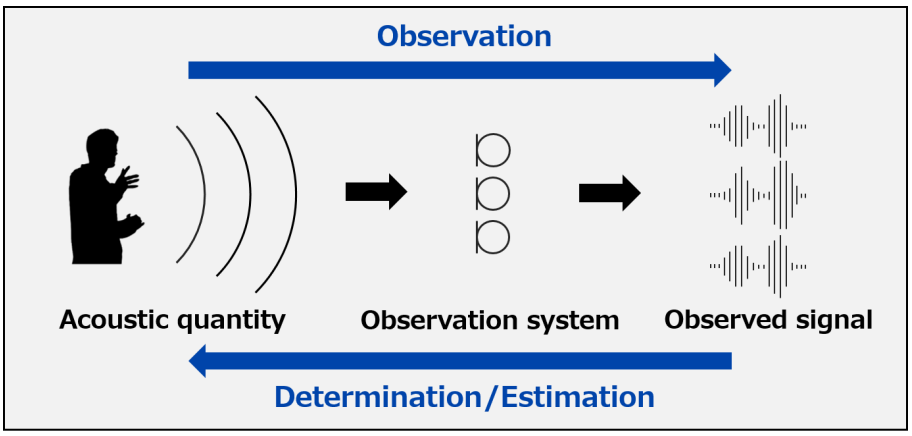

Fig. 1.1: Acoustic measurement problem.

measurement problem, which will improve the performance of these applied techniques and broaden their scope.

As well as the variety of target acoustic quantities, there are diverse types of sensing devices and systems used in acoustic measurement. These can be classified on the basis of their principles (e.g., transduction mechanisms) and also their functions (e.g., directivity and frequency response). Therefore, various combinations of situations are possible in acoustic measurement problems. Although each of them seems a different problem at first glance, we can often find common characteristics in their underlying mathematical models. This abstract viewpoint, based not on the physical mechanism or application but on the mathematical model, is often taken in the research field called *inverse problems* [10–13], and it is effective because various seemingly independent problems can be treated in a unified manner.

1.2 Classification of Acoustic Measurement Problems

From the viewpoint of inverse problems, acoustic measurement problems are typically classified depending on whether or not the *superposition principle*, i.e., linearity between the acoustic quantity of interest and the observed signal, holds in the observation. A typical example of linear observation is the sampling of sound signals [14–16]. Also, in the measurement of sound fields using multiple microphones [8, 17–25], the superposition property holds well regardless of the microphones' directivity and frequency response as long as the observed signal is within their dynamic range. These problems can be dealt with as *linear inverse problems*, and many useful theories and efficient algorithms have been proposed and investigated for linear inverse problems, although they have not been fully applied in the context of acoustic measurement. On the other hand, for example, in sound source localization problems [26–28] and sensor localization problems [29, 30], the target quantity, i.e., the positions of the sound sources or sensors, and the observed signals have a complex nonlinear relationship even if an ideal observation within the dynamic range is achieved. These problems are usually studied with further mathematical classification and are beyond the scope of this thesis.

In addition to the above classification, the intrinsic nonlinearity of sensing devices and systems is also important, even though little attention has been paid to it in the literature related to acoustic measurement problems. For example, capacitive microphones have complex nonlinear behaviors caused by elastic and electrostatic forces [31], and (pre)amplifiers have nonlinear saturation effects owing to the transfer characteristics of transistors [32]. The degree of nonlinearity depends on the design of the sensors and the input intensity; inexpensive systems often suffer from a non-negligible degree of nonlinearity. Therefore, even in acoustic measurement problems that are typically categorized as linear ones, the above nonlinearities have to be considered under such non-ideal conditions.

1.3 Scope and Objectives

The theoretical scope of this thesis includes linear inverse problems as a special case and also covers saturation effects arising in observation systems, which are one of the most common nonlinear phenomena but have not been considered in most existing studies on acoustic measurement problems. Although not all nonlinear effects such as hysteresis can be described as saturation, the overall behaviors of observation systems can often be well approximated by it [33]. At least, nonlinearities caused by (pre)amplifiers are modeled well as saturation effects, i.e., a monotonic relationship between input and output signals [32]. Therefore, a unifying framework for inverse problems considering nonlinear saturation effects is helpful in improving estimation accuracy in various situations. Conversely, the establishment of such a framework will also lead to the practical realization of novel measurement systems suffering severe saturation effects but having advantages in other aspects, such as sampling rate, signal-to-noise ratio, manufacturing cost, and nondestructivity.

While dealing with abstract theories on inverse problems, this thesis also focuses on two specific topics of acoustic measurement problems: the restoration of saturated sound signals and the estimation of sound fields. This is not intended only to provide applications of the theories presented in this thesis; it is also motivated by the fact that even existing theories on linear inverse problems have not been fully applied in current methods of acoustic measurement. From both academic and practical viewpoints, it is desirable to reduce the gap between abstract theories in inverse problems and practical methods in the fields of application. In particular, even in cases of linear observation, estimation accuracy of current practical methods can be improved by exploiting several theories on Hilbert spaces [34, 35], and these theories are proven to be effective also in formulations considering nonlinear saturation effects. Other possible applications, such as the estimation of room transfer functions and head-related transfer functions, are not described in detail in this thesis; however, it is expected that efficient estimation methods for various other acoustic quantities can also be established in a similar manner on the basis of the presented methodology.

On the basis of the above discussion, the objectives of this thesis are

- to establish a unifying framework of inverse problems considering nonlinear saturation effects;
- to propose efficient estimation methods for sound signals and sound fields, where existing and proposed theories on inverse problems are fully applied.

Here, the objectives are given rather abstractly; they are reiterated in more detail after summarizing related studies in Chapter 2.

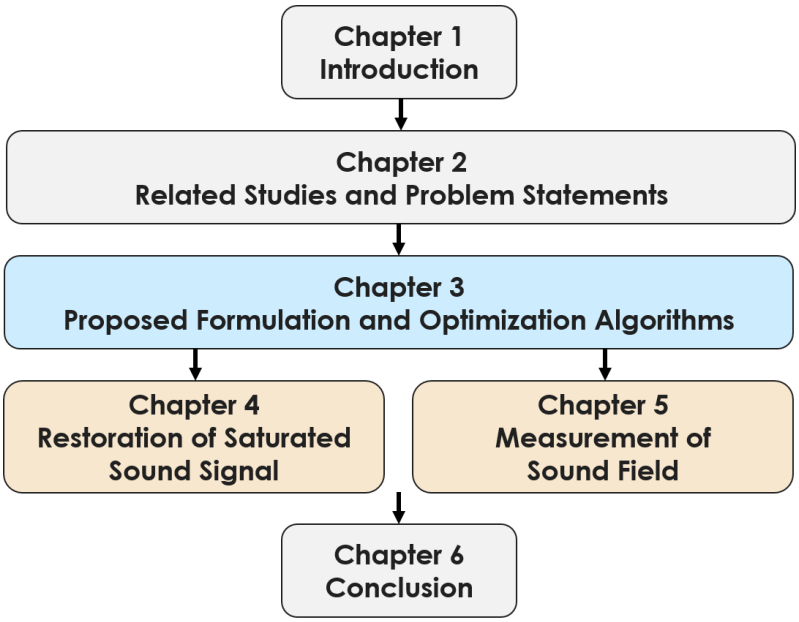

Fig. 1.2: Outline of thesis.

1.4 Outline

The organization of this thesis is given in Figure 1.2. Chapter 2 introduces the mathematical framework of an inverse problem for acoustic measurement, which is formulated as an optimization problem of a certain class, summarizes its related studies, and clarifies current problems to be addressed in this thesis. In Chapter 3, a new formulation for the inverse problems defined in Chapter 2 is proposed, and its theoretical comparison with other current formulations is discussed. Efficient optimization algorithms for the proposed formulation are also provided. Chapters 4 and 5 deal with two different specific topics of acoustic measurement problems, which are structured independently from each other but both are based on the theoretical framework provided in Chapters 2 and 3. These two chapters are not just application examples; each of them includes several contributions in the corresponding research field. Chapter 4 focuses on restoration problems of saturated sound signals, whereas Chapter 5 focuses on sound field estimation problems. Finally, Chapter 6 concludes this thesis.

1.5 Mathematical Notations

Since many mathematical symbols will be used throughout this thesis, they will be defined independently in each chapter unless explicitly referred to. However, the following basic notations are used throughout this thesis.

- $\mathbb{N}$: set of all natural numbers including zero

- $\mathbb{Z}$: set of all integers
  - $[\![m, n]\!]$: set of all integers between m and n inclusive ($m, n \in \mathbb{Z}$, $m \leq n$)
- $\mathbb{R}$: set of all natural numbers
- $\mathbb{C}$: set of all complex numbers
  - i: imaginary unit in $\mathbb{C}$
  - z^*: complex conjugate of z ($z \in \mathbb{C}$)
- $\mathbb{S}_n$: unit circle or sphere in $\mathbb{R}^{n+1}$ ($n \in \{1, 2\}$)
- $\int_{x \in X} f(x) \, \mathrm{d}\mu$: integral of f over X with respect to the Lebesgue measure (f is a measurable function on a measurable set $X \subseteq \mathbb{R}$)
- $\int_{\boldsymbol{x} \in \mathbb{S}_n} f(\boldsymbol{x}) \, \mathrm{d}\chi$: circular or spherical integral of f (f is a measurable function on $\mathbb{S}_n$, $n \in \{1, 2\}$)

Chapter 2

Related Studies and Problem Statements

The goals of this chapter are to provide a mathematical formulation of an acoustic measurement problem, which will be described as an optimization problem called an inverse problem, and to clarify current difficulties in dealing with this problem. For these goals, a general framework of inverse problems is introduced first in Section 2.1. In Section 2.2, by focusing on several characteristics in acoustic measurement, the mathematical class of inverse problems of interest is clarified, which also defines a practical class of acoustic measurement problems within the scope of the theories provided in this thesis. Section 2.3 provides an overview of related studies, and the problems to be addressed in this thesis are stated in Section 2.4.

2.1 General Framework of Inverse Problem

An inverse problem is a process of determining or estimating a quantity of interest from its indirect observation, whose theory has been under intensive investigation in engineering, applied mathematics, and many other fields. A mathematical description of an inverse problem is given as follows. Let $\mathcal{U}$ and $\mathcal{S}$ denote sets consisting of all possible candidates for quantities of interest and observed signals, respectively. Then, the relationship between the quantity of interest and the observed signal, called a *forward problem*, is given by a *forward operator*, which is a mapping from $\mathcal{U}$ to $\mathcal{S}$, i.e.,

$$A : \mathcal{U} \to \mathcal{S}. \tag{2.1}$$

In other words, from the quantity of interest $u \in \mathcal{U}$, the observed signal $s \in \mathcal{S}$ (in a noise-free case) is given by

$$s = A(u). \tag{2.2}$$

In the context of an inverse problem, the forward operator A is assumed to be given. The goal of the inverse problem is to estimate the unknown quantity $u \in \mathcal{U}$ from the given observed signal $s \in \mathcal{S}$.

If A is bijective and there is no observation noise, the estimation problem is simple, at least in the mathematical sense, because for any given $s \in \mathcal{S}$, there exists a unique $u \in \mathcal{U}$ satisfying (2.2). Unfortunately, these conditions are not satisfied in many practical situations. In acoustic measurement problems, in particular, we often face the following situations:

- The quantity of interest is an infinite-dimensional vector, whereas the observed signal is a finite-dimensional vector.
- The observation is affected by noninjective saturation effects.
- The observation is affected by noises.

In such cases, one cannot determine the unknown quantity uniquely from the observed signal only by (2.2). Therefore, one has to exploit some physical, statistical, or empirical assumption on the target quantity (and sometimes also on the observational noise) and to determine the most "reasonable" one on the basis of some criterion. This strategy can be formulated as the following optimization problem:

$$\underset{u \in \mathcal{U}}{\text{minimize}} \; Q(u) \coloneqq L_s(u) + R(u). \tag{2.3}$$

Here, $Q : \mathcal{U} \to \mathbb{R} \cup \{\infty\}$ is an *objective function* evaluating the overall reasonability of the quantity of interest, $L_s : \mathcal{U} \to \mathbb{R} \cup \{\infty\}$ is a *loss function* evaluating the consistency between the quantity of interest and the observed signal, and $R : \mathcal{U} \to \mathbb{R} \cup \{\infty\}$ is a *regularization function* evaluating the reasonability of the quantity of interest based on some prior knowledge or assumption independently of the observation. Hereafter, the term "inverse problem" is defined to mean the estimation problem of the quantity of interest based on (2.3), which is also often called an ill-posed inverse problem[*1] in the literature.

Once the problem of (2.3) has been defined, its optimal solution is determined in the mathematical sense. In practice, however, it is not always a trivial task to obtain the optimal solution of (2.3); rather, only a few specific cases admit (computable) closed-form solutions. Instead, *iterative algorithms* are typically used in a large class of optimization problems, where approximate solutions are generated sequentially. Here, it should be noted that the available algorithms and their characteristics, such as the convergence property and computational cost, depend on the class of the objective function. Owing to these algorithmic factors, even if the validity of the formulation is supported from stochastic or other perspectives, it does not necessarily yield accurate and efficient estimation

[*1] This does not correspond to the well-known definition given by Hadamard [36]. In Hadamard's definition, the inverse problem is said to be well-posed if the following three conditions are satisfied:
- existence of the solution, i.e., surjectivity of A,
- uniqueness of the solution, i.e., injectivity of A,
- stability of the solution, i.e., continuity of the inverse of A (under certain a topology on $\mathcal{U}$ and $\mathcal{S}$),

and otherwise said to be ill-posed. However, the definition given in the manuscript is also often used depending on the context.

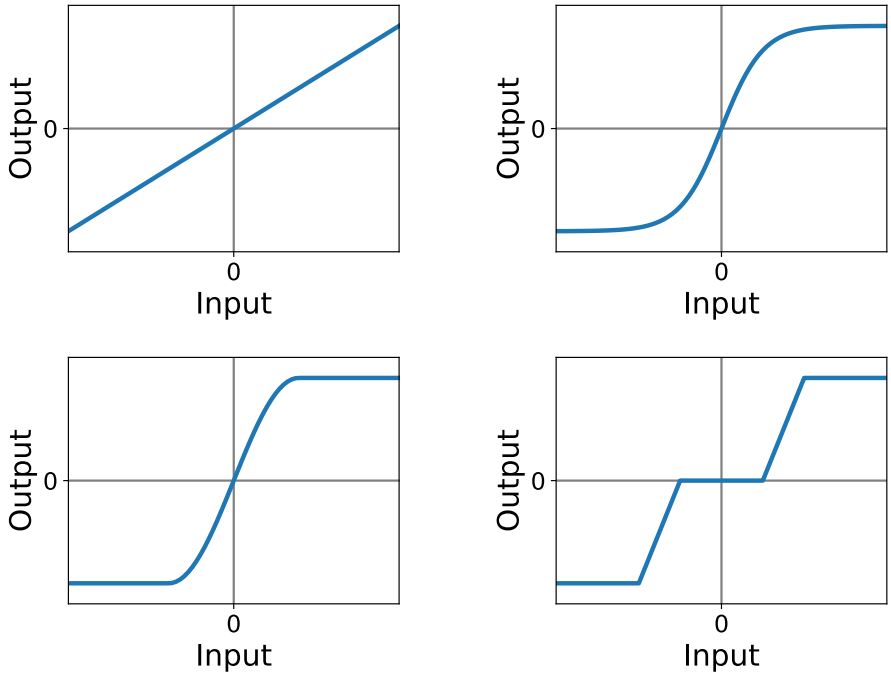

Fig. 2.1: Examples of monotone and Lipschitz continuous functions.

in practice. Hence, to establish a "good" estimation method, one has to simultaneously consider formulation and optimization algorithms, which is one of the distinctive features in considering inverse problems.

2.2 Acoustic Measurement as Inverse Problems

As described in Section 1.3, the acoustic measurement of interest in this thesis is modeled as a combination of linear observation and nonlinear saturation effects. These observational settings can be described mathematically as a forward problem in Section 2.1 with the following conditions:

- $\mathcal{U}$ is a Hilbert space over $\mathbb{K} \in \{\mathbb{R}, \mathbb{C}\}$ with an inner product $\langle \cdot, \cdot \rangle_{\mathcal{U}} : \mathcal{U} \times \mathcal{U} \to \mathbb{K}$.
- $\mathcal{S}$ is a finite-dimensional Hilbert space over $\mathbb{K}$ with an inner product $\langle \cdot, \cdot \rangle_{\mathcal{S}} : \mathcal{S} \times \mathcal{S} \to \mathbb{K}$.
- A can be decomposed as $A = f \circ D$, where $D : \mathcal{U} \to \mathcal{S}$ is a bounded linear mapping and $f : \mathcal{S} \to \mathcal{S}$ is a (possibly nonlinear) cyclically monotone and Lipschitz continuous mapping.

The definitions of a Hilbert space and a bounded linear mapping are given in Appendix A.1. One of the main contributions of this thesis is to take the nonlinear function f into consideration; if f is the identity mapping, the above conditions correspond to those of linear inverse problems. Here, a mapping $f : \mathcal{S} \to \mathcal{S}$ is said to be cyclically

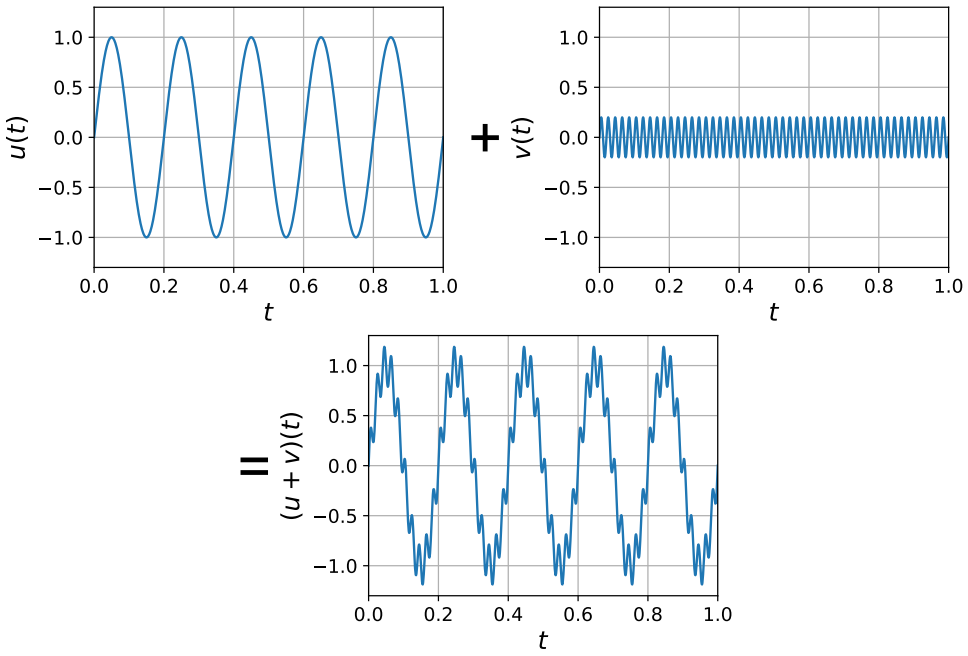

Fig. 2.2: Superposition of sound signals.

monotone if there exists some positive-definite linear mapping $\Lambda : \mathcal{S} \to \mathcal{S}$ satisfying

$$\sum_{n=1}^{N} \left\langle z^{(n+1)}, f(z^{(n+1)}) - f(z^{(n)}) \right\rangle_{\Lambda} \geq 0 \tag{2.4}$$

for all $N \in \mathbb{N}$ and $z^{(1)}, \ldots, z^{(N+1)} \in \mathcal{S}$ such that $z^{(N+1)} = z^{(1)}$. Here, $\langle \cdot, \cdot \rangle_{\Lambda} : \mathcal{S} \times \mathcal{S} \to \mathbb{K}$ is an inner product induced by Λ, defined as $\langle z, w \rangle_{\Lambda} \coloneqq \langle z, \Lambda w \rangle_{\mathcal{S}}$ for $z, w \in \mathcal{S}$. For such Λ, f is also said to be cyclically monotone with respect to Λ, more specifically. A simple case is when $\mathcal{S} = \mathbb{R}^N$ with $N \in \mathbb{N}$ and f is an elementwise monotonically nondecreasing and Lipschitz continuous function (see Figure 2.1, for example), where Λ can be taken as any diagonal matrix with positive diagonal elements. Note that cyclically monotone functions are not necessarily invertible as shown by this figure.

Here, acoustic measurement problems have been defined in an abstract form. To make it easier to understand specific situations, several practical examples are provided briefly with an intuitive explanation (with as little mathematical formulation as possible) in the following subsections, which will be described again in more detail with a mathematical formulation in later chapters on specific applications.

2.2.1 Measurement of Sound Signal

A sound signal is described as a relation from time to amplitude, which means that it can be regarded as a function, for example, from $\mathbb{R}$ to $\mathbb{R}$ for a continuous-time signal and from $\mathbb{Z}$ to $\mathbb{R}$ for a discrete-time signal. Therefore, in the measurement of a sound

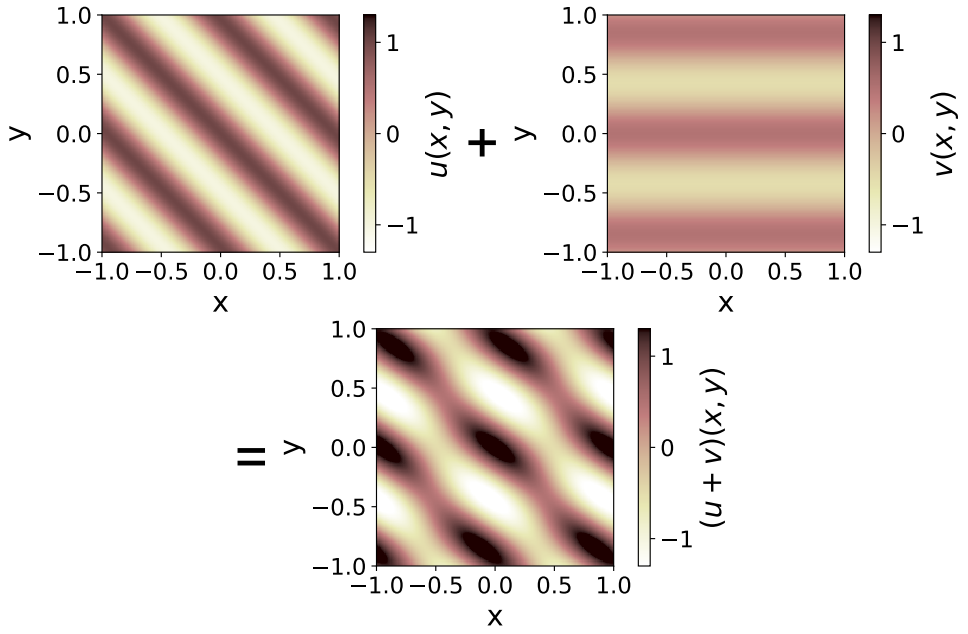

Fig. 2.3: Superposition of sound fields.

signal, $\mathcal{U}$ can be defined as a function space, and the summation in this space can be regarded intuitively as a superposition of sounds (see Figure 2.2). Furthermore, a linear constraint, such as square integrability or bandlimitation, can also be exploited on $\mathcal{U}$. For example, the scalar multiplication and superposition of bandlimited signals are also bandlimited; therefore, all bandlimited signals also constitute a linear space. Such spaces can be regarded as Hilbert spaces with an appropriate definition of an inner product.

The measurement of a sound signal is basically realized by sampling the output signal resulting from the target sound via a linear time-invariant system. A linear time-invariant system is described by its impulse response; the output signal is given by the convolution of the input signal and the impulse response. Since the convolution is a linear operation with respect to input signals for a fixed impulse response, and the sampling is also a linear processing, the relationship between the input and sampled signals can be described using a linear mapping. If the saturation effect can be regarded as an elementwise processing (without any hysteresis characteristics), it can be modeled by a cyclically monotone mapping.

2.2.2 Measurement of Sound Field

Let Ω be a two-dimensional or three-dimensional (nonempty open) region of interest. A sound field in Ω is described by a function $u : \Omega \times \mathbb{R} \to \mathbb{R}$, where $u(\boldsymbol{r}, t)$ denotes the (infinitesimal) variation of acoustic pressure from its equilibrium value at position $\boldsymbol{r} \in \Omega$ and time $t \in \mathbb{R}$. When Ω does not include any sound sources, u can be well modeled as a

solution of the following wave equation [37]:

$$\left(\Delta - \frac{1}{c^2}\frac{\partial^2}{\partial t^2}\right) u = 0, \tag{2.5}$$

where Δ is the Laplace operator and $c \in \mathbb{R}$ denotes the speed of sound, which is assumed to be constant in Ω. This is obviously a linear equation; scalar multiples and sums of solutions of (2.5) also satisfy (2.5). If we consider a time-harmonic sound field given by

$$u(\boldsymbol{r}, t) = \tilde{u}(\boldsymbol{r}) \exp(-i\omega t) \quad (\boldsymbol{r} \in \Omega,\ t \in \mathbb{R}) \tag{2.6}$$

with $\tilde{u} : \Omega \to \mathbb{C}$ and an angular frequency $\omega \in \mathbb{R}$ (the harmonic time dependence $\exp(-i\omega t)$ will be used in this thesis according to conventions in the field of spatial acoustics [37]), $\tilde{u}$ satisfies the following Helmholtz equation [37]:

$$(\Delta + k^2)\tilde{u} = 0, \tag{2.7}$$

which is also a linear equation. As described above, all solutions of the wave equation or Helmholtz equation constitute a linear space, where the summation in this space can be regarded intuitively as a superposition of sound fields (see Figure 2.3). Also, a more specific class of sound fields, such as superpositions of plane-wave functions, can be considered as a linear space $\mathcal{U}$, which is often useful in theoretical treatment. Such spaces have infinite dimensions; however, they can be regarded as Hilbert spaces with appropriate definitions of inner products.

Consider the measurement of a sound field using multiple microphones with (given) arbitrary directivities, frequency responses, and sampling times. Since directivities and frequency responses are linear characteristics, the relationship between a target sound field and sampled signals can be described using a linear mapping. If the saturation effect can be regarded as an elementwise processing, it can be modeled as a cyclically monotone mapping even if the saturation characteristics are different for each microphone.

2.2.3 Other Applications

Although the above examples are the main applicational interest in this thesis, the presented theories are also applicable in the measurement of various other acoustic quantities. For example, various linear characteristics of microphones, such as directivity and frequency response, can be regarded in an abstract manner as a linear mapping describing the relationship between input sound signals or sound fields and output signals. The set of all linear mappings between two given linear spaces can also be regarded as a linear space in a natural manner, and obtaining an output signal from a given input signal can be regarded as a linear processing with respect to the unknown linear characteristics. Therefore, the proposed model can also be used in such situations. As another example, a room impulse response, which describes an impulse response between two arbitrary source and

receiver positions in a given reverberant environment, can also be regarded in an abstract manner as a linear mapping describing the relationship between a direct sound field and a reverberant sound field. In principle, any acoustic quantity allowing such representation is also within the scope of the theories presented in this thesis.

2.3 Related Studies

This section introduces several previous studies related to inverse problems of interest in this thesis to clarify current difficulties to be addressed.

2.3.1 Overview of Iterative Methods for Continuous Optimization

As described in Section 2.2, optimization problems of interest in this thesis are defined on Hilbert spaces, which means that they are classified as continuous optimization problems. As a preliminary for discussing inverse problems from algorithmic perspectives, this section gives an overview of iterative algorithms for continuous optimization problems. The notions of convexity, (Fréchet) derivative, and proximal operator will be used hereafter, whose definitions are given in Appendix A.2.

Although there have been numerous iterative algorithms for continuous optimization proposed in the literature [38–44], their underlying approaches are classified mainly into three types: the *smooth optimization approach*, *majorization-minimization approach*, and *proximal approach*. First, many well-established algorithms, such as gradient descent methods, nonlinear conjugate gradient descent methods, Newton's method, and quasi-Newton methods, are based on the use of the first-order or second-order derivatives of the objective function [38, 40, 41, 45, 46]; such an approach is here referred to as the smooth optimization approach. These are classical but still standard methods, and a wide variety of modification and acceleration methods have also been proposed in the literature. The convergence property has been well investigated under some additional conditions, such as the Lipschitz continuity of the derivative of an objective function. This approach is widely applicable to differentiable objective functions; however, the class of differentiable functions has no longer been sufficiently comprehensive in the field of inverse problems ever since the concept of sparsity emerged in this field [47, 48]. In recent decades, a wide variety of nonsmooth regularization functions promoting the sparsity of a target quantity (in a certain representation) have been demonstrated to be effective in various inverse problems including acoustic measurement [22, 24, 25]. Therefore, an alternative scheme is required to solve such nonsmooth optimization problems.

Various iterative algorithms based on a majorization-minimization approach [44, 49] have been proposed to solve smooth and nonsmooth optimization problems. A key idea of the majorization-minimization approach is the design of a *surrogate function* described

as follows. Let $Q : \mathcal{U} \to \mathbb{R} \cup \{\infty\}$ be an original objective function and $\breve{Q} : \mathcal{U} \times \mathcal{U} \to \mathbb{R} \cup \{\infty\}$ be a function satisfying the following conditions:

- $Q(u) \leq \breve{Q}(u, v)$ for all $u, v \in \mathcal{U}$.
- $Q(u) = \breve{Q}(u, u)$ for all $u \in \mathcal{U}$.

Such a function $\breve{Q}$ is called a surrogate function of Q. If one can design a surrogate function $\breve{Q}$ that can be easily minimized with respect to the first variable for any fixed second variable, a sequence of approximate solutions $u^{(0)}, u^{(1)}, \ldots \in \mathcal{U}$ can be obtained by

$$u^{(k+1)} = \operatorname*{arg\,min}_{u \in \mathcal{U}} \breve{Q}(u, u^{(k)}) \tag{2.8}$$

with an arbitrary initial value $u^{(0)} \in \mathcal{U}$. Note that there exist various surrogate functions for one objective function. Although the practical efficiency of the algorithm highly depends on the design of the surrogate function, the obtained sequence is always guaranteed to decrease or keep the value of the objective function, which is proved from the inequality

$$Q(u^{(k+1)}) \leq \breve{Q}(u^{(k+1)}, u^{(k)}) \leq \breve{Q}(u^{(k)}, u^{(k)}) = Q(u^{(k)}). \tag{2.9}$$

However, it is generally difficult to confirm the convergence of a generated sequence to a global or local optimal solution. Another drawback of this approach is the lack of a comprehensive way to design "good" surrogate functions for a wide class of objective functions. For example, consider an optimization problem of the following form:

$$\operatorname*{minimize}_{u \in \mathcal{U}} \; Q(u) \coloneqq Q_1(u) + \cdots + Q_N(u) \tag{2.10}$$

with $N \in \mathbb{N}$ and $Q_1, \ldots, Q_N : \mathcal{U} \to \mathbb{R} \cup \{\infty\}$. Obviously, the summation of surrogate functions for $Q_1, \ldots, Q_N$ is a surrogate function of Q. However, even if one can design good surrogate functions for each of $Q_1, \ldots, Q_N$, their summation is not necessarily easy to minimize for the first variable. Therefore, one has to consider the compatibility of multiple surrogate functions.

Nonsmooth optimization problems have also been tackled from another viewpoint, called a proximal approach [43]. A major characteristic in this approach is the use of a proximal operator, which is also defined via an optimization problem but computable in closed form for various practically used nonsmooth functions. Although the details will be provided in Chapter 3, in combination with the concept of the alternating direction method of multipliers [50], several sophisticated optimization algorithms based on the proximal approach are applicable to functions belonging to the following classes:

1. a differentiable function whose gradient is Lipschitz continuous and available as a computable operator,
2. a function whose proximal operator is available as a computable operator,

3. a composite function of a bounded linear operator and a function satisfying condition 1 or 2, and
4. a finite summation of functions, each of which satisfies condition 3.

Here, consider again the optimization problem of (2.10). In contrast to the majorization-minimization approach, the proximal approach is generally applicable as long as each of $Q_1, \ldots, Q_N$ belongs to the above class; therefore, one does not need to consider the compatibility between them. Moreover, in a manner similar to that in the smooth optimization approach, the convergence of a generated sequence to a global or local optimal solution is guaranteed under quite general conditions, and there are also various acceleration methods in the proximal approach.

In any of the approaches described above, the convexity of an objective function takes an important role. In most iterative algorithms, convergence to a global optimal solution is guaranteed for convex objective functions. For nonconvex objective functions, on the other hand, only convergence to some local optimal solution is guaranteed in most algorithms; therefore, the goodness of the obtained solution often depends on the initial solution and parameters used in the algorithm. In the context of inverse problems, various convex and nonconvex formulations, especially for regularization functions, have been proposed; an appropriate choice depends on the situation. However, a convex formulation is useful at least in the following two respects. First, when a convex formulation gives a better performance than nonconvex ones or a practically sufficient performance, even if not better performance, the convex formulation is preferable owing to its reliable convergence independent of the initial solution. Second, a solution obtained by some convex formulation can also be used as an initial solution in another nonconvex formulation. Since a good initial solution is obtained by the convex formulation, the use of this initial solution is expected to give a better performance than that of baseless or random initial solutions even in the nonconvex formulation. For the convex formulation of (2.3), of course, the loss function should be convex.

2.3.2 Linear and Nonlinear Inverse Problems

Consider again the inverse problem of (2.3) with the assumptions given in Section 2.2. When f is the identity mapping (i.e., when saturation effects can be ignored), this inverse problem is called a *linear inverse problem*, and there have been numerous works on regularization methods and optimization algorithms for linear inverse problems [47, 51, 52] including those related to acoustic measurement [22, 24, 25, 53]. In linear inverse problems, the quadratic loss function, denoted hereafter by $L_s^{(\mathrm{quad})} : \mathcal{U} \to \mathbb{R} \cup \{\infty\}$, is used in most cases. The quadratic loss function is defined as

$$L_s^{(\mathrm{quad})}(u) \coloneqq \frac{1}{2}\|f(Lu) - s\|_\Lambda^2 \quad (u \in \mathcal{U}) \tag{2.11}$$

with a positive-definite bounded linear mapping $\Lambda : \mathcal{S} \to \mathcal{S}$, where $\|\cdot\|_\Lambda : \mathcal{S} \to [0, \infty)$ is the norm induced by the inner product $\langle \cdot, \cdot \rangle_\Lambda$. In this case, the optimization problem takes the following form:

$$\underset{u \in \mathcal{U}}{\text{minimize}} \; Q(u) \coloneqq \frac{1}{2}\|f(Lu) - s\|_\Lambda^2 + R(u), \tag{2.12}$$

which is also called *regularized least squares*. In linear inverse problems, the quadratic loss function has several mathematically tractable properties, such as convexity and differentiability. Hence, the main topic in the research of linear inverse problems is the formulation of a regularization function exploiting various prior knowledge on the target quantity and the optimization theory for problems having the form of (2.12).

On the other hand, when f is nonlinear, as in the problem of interest in this thesis, the inverse problem is called a *nonlinear inverse problem*. In contrast to linear inverse problems, there are relatively few works on nonlinear inverse problems related to acoustic measurement, especially with optimization algorithms. It is difficult, or almost impossible, to obtain useful results for a general nonlinear inverse problem owing to its excessive generality. For example, consider the commonly used regularized least squares given by (2.12) in cases of nonlinear f. The regularization methods proposed in linear inverse problems are expected to be effective also in this case, at least in a theoretical sense, because the role of regularization is independent of the observation. From the optimization viewpoint, however, the situation changes significantly. Owing to the nonlinearity (and possible nondifferentiability) of f, the quadratic loss function is not necessarily convex or even differentiable in general; therefore, well-established optimization algorithms proposed in linear inverse problems do not necessarily work well, or might not even be applicable, in nonlinear inverse problems. As seen in this example, the mathematical tractability of the loss function is also important in considering nonlinear inverse problems.

2.3.3 Previous Works with Respect to Loss Function

There are several previous works on nonlinear inverse problems related to those of interest in this thesis [54–57]. Although these works focus on a specific application, called a signal declipping problem, the underlying theories and formulations can be generalized to the problem defined in Section 2.2. In these works, tractable formulations of loss functions are provided, which can be classified into two types: the *hard constraint function* [55] and the *soft consistency function* [54, 56, 57].

The hard constraint function, hereafter denoted by $L_s^{(\mathrm{hard})} : \mathcal{U} \to \mathbb{R} \cup \{\infty\}$, is defined as

$$L_s^{(\mathrm{hard})}(u) \coloneqq \begin{cases} 0 & (Du \in f^{-1}(s)) \\ \infty & (Du \in \mathcal{S} \setminus f^{-1}(s)) \end{cases}, \tag{2.13}$$

where $f^{-1}(s) \subseteq \mathcal{S}$ is defined as $f^{-1}(s) \coloneqq \{z \in \mathcal{S} \mid f(z) = s\}$. For $s \in \mathrm{image}(f)$, this

function is proper, lower-semicontinuous, lower-bounded, and convex because $f^{-1}(s)$ is a nonempty, closed, and convex set (see Section 3.2 for a proof). Furthermore, this function can be decomposed as

$$L_s^{(\mathrm{hard})} = H_s^{(\mathrm{hard})} \circ D \tag{2.14}$$

with a function $H_s^{(\mathrm{hard})} : \mathcal{S} \to \mathbb{R} \cup \{\infty\}$ defined as

$$H_s^{(\mathrm{hard})}(z) \coloneqq \begin{cases} 0 & (z \in f^{-1}(s)) \\ \infty & (z \in \mathcal{S} \setminus f^{-1}(s)) \end{cases}. \tag{2.15}$$

Here, the proximal operator of $H_s^{(\mathrm{hard})}$ is given by

$$\mathrm{prox}^{\gamma}_{H_s^{(\mathrm{hard})}}(z) \coloneqq \mathrm{proj}_{f^{-1}(s)}(z) \quad (z \in \mathcal{S}) \tag{2.16}$$

for any $\gamma \in (0, \infty)$, where $\mathrm{proj}_{f^{-1}(s)}(\cdot) : \mathcal{S} \to \mathcal{S}$ denotes the orthogonal projection into $f^{-1}(s)$. In many practical cases, this proximal operator can be calculated easily. For example, if $\mathcal{S} = \mathbb{R}^N$ with $N \in \mathbb{N}$ and f is given by an elementwise operation as

$$f(\mathbf{z}) = \begin{bmatrix} f_1(z_1) \\ \cdots \\ f_N(z_N) \end{bmatrix} \quad (\mathbf{z} \coloneqq [z_1, \ldots, z_N]^{\mathsf{T}} \in \mathbb{R}^N) \tag{2.17}$$

with monotonically nondecreasing functions $f_1, \ldots, f_N : \mathbb{R} \to \mathbb{R}$, we have

$$\mathrm{proj}_{f^{-1}(\mathbf{s})}(\mathbf{z}) = \begin{bmatrix} \mathrm{proj}_{f^{-1}(s_1)}(z_1) \\ \cdots \\ \mathrm{proj}_{f^{-1}(s_N)}(z_N) \end{bmatrix} \quad (\mathbf{z} \coloneqq [z_1, \ldots, z_N]^{\mathsf{T}}) \tag{2.18}$$

for any $\mathbf{s} \coloneqq [z_1, \ldots, z_N]^{\mathsf{T}} \in \mathrm{image}(f)$. Therefore, the proximal operator can be reduced to simple univariable operations. Using this proximal operator, several iterative algorithms based on the proximal approach can be applied with an arbitrary regularization function whose proximal operator or derivative is available. The hard constraint loss function was proposed for noise-free situations (e.g., the signal restoration problem from a hard clipping effect caused by an analog-to-digital converter is focused on in [55]). Conversely, this loss function is not suitable in noisy observation because it leaves no margin for inconsistency.

On the other hand, the soft consistency function, hereafter denoted by $L_s^{(\mathrm{soft})} : \mathcal{U} \to \mathbb{R} \cup \{\infty\}$, is defined as

$$L_s^{(\mathrm{soft})}(u) \coloneqq \min_{z \in f^{-1}(s)} \left\{ \frac{1}{2} \|Du - z\|_{\mathcal{S}}^2 \right\} \quad (u \in \mathcal{U}). \tag{2.19}$$

For $s \in \mathrm{image}(f)$, this function is also proper, lower-semicontinuous, lower-bounded, and convex because $f^{-1}(s)$ is a nonempty, closed, and convex set. Furthermore, this function can be decomposed as

$$L_s^{(\mathrm{soft})} = H_s^{(\mathrm{soft})} \circ D \tag{2.20}$$

with a function $H_s^{(\mathrm{soft})} : \mathcal{S} \to \mathbb{R} \cup \{\infty\}$ defined as

$$H_s^{(\mathrm{soft})}(z) \coloneqq \min_{w \in f^{-1}(s)} \left\{ \frac{1}{2} \|z - w\|_{\mathcal{S}}^2 \right\} \quad (z \in \mathcal{S}). \tag{2.21}$$

Here, $H_s^{(\mathrm{hard})}$ is differentiable, whose derivative is given by

$$\nabla H_s^{(\mathrm{hard})}(z) = z - \mathrm{proj}_{f^{-1}(s)}(z). \tag{2.22}$$

Since this derivative is 1-Lipschitz continuous, several algorithms based on the proximal approach can be applied with various regularization functions. In contrast to the hard clipping function, the soft clipping function seems to be suitable for noisy observations at first glance since inconsistency between u and s is allowed to some extent. Indeed, Rencker et al. [57] discussed the influence of observational noises before saturation effects. However, this loss function is also discontinuous with respect to s in general; therefore, even a small observational noise after saturation may markedly affect the estimation results. In addition, these two loss functions are defined only for $s \in \mathrm{image}(f)$; if s takes a value outside $\mathrm{image}(f)$ owing to the observation noise, one cannot even use these formulations since $f^{-1}(s)$ becomes an empty set. Hence, a robust loss function with a continuous sensitivity to s is desired for acoustic measurement problems considering observation noises after saturation effects.

2.4 Problem Statements

By summarizing Section 2.3, one can see the following facts with respect to the acoustic measurement problems of interest in this thesis:

- An effective formulation of a loss function that is mathematically tractable and robust against observation noises after saturation effects is still to be established.
- Various regularization functions have been proposed in the literature, and the appropriate choice depends on the target quantity and situation.

On the basis of the above discussion, the main objectives in this thesis are as follows:

- to design a formulation allowing both high estimation accuracy (especially robustness against observational noises after saturation) and computational efficiency;
- to provide an optimization algorithm for the above formulation that can be used comprehensively with various classes of regularization functions;
- to apply the proposed framework to several practical problems with appropriate regularization methods and demonstrate the validity of the proposed estimation methods by experiments in comparison with other current methods.

The first two objectives are related to the abstract (case-independent) methodology, which

will be described in Chapter 3, and the last one is related to the concrete (case-dependent) applications, which will be described in Chapters 4 and 5.

Chapter 3

Proposed Formulation and Optimization Algorithms

This chapter presents a new formulation of a loss function that is robust to observation noises and also mathematically tractable from the optimization viewpoint. Section 3.1 provides the definition and several properties of the proposed loss function, whose proofs are given in Section 3.2. Section 3.3 gives a comparison between the proposed and previous formulations. In Sections 3.4 and 3.5, optimization theories and algorithms are provided for Hilbertian and non-Hilbertian regularization functions, respectively.

3.1 Proposed Loss Function

Let $\Lambda : \mathcal{S} \to \mathcal{S}$ be a positive-definite bounded linear mapping such that f is monotone with respect to Λ. Moreover, let $F : \mathcal{S} \to \mathbb{R}$ be a potential function of f (in the sense of the Fréchet derivative with respect to the inner product $\langle \cdot, \cdot \rangle_\Lambda$), i.e.,

$$\nabla_\Lambda F = f, \tag{3.1}$$

where $\nabla_\Lambda F : \mathcal{S} \to \mathcal{S}$ denotes the derivative of F with respect to the inner product $\langle \cdot, \cdot \rangle_\Lambda$. Such a function is given by

$$F(z) = F(w) + \int_0^1 \langle f(w + t(z - w)), z - w \rangle_\Lambda \, \mathrm{d}t \quad (z \in \mathcal{S}) \tag{3.2}$$

with arbitrary $w \in \mathcal{S}$; however, the concrete form of F is not significant because it does not appear in the proposed estimation algorithm. Note that the existence of the potential function is guaranteed by the cyclical monotonicity of f [58]. Then, the proposed loss function $L_s : \mathcal{U} \to \mathbb{R} \cup \{\infty\}$ is defined for $s \in \mathrm{image}(f)$ as

$$L_s(u) \coloneqq F(Du) - F(z) - \langle s, Du - z \rangle_\Lambda \quad (u \in \mathcal{U}) \tag{3.3}$$

with arbitrary $z \in f^{-1}(s)$. Note that (3.3) is well defined regardless of the choice of z in (3.3) and w in (3.2) (see Section 3.2 for a proof).

Here, the proposed loss function satisfies the following divergence-like properties:

1. $L_s(u) \geq 0$ for all $u \in \mathcal{U}$ and $s \in \mathrm{image}(f)$.
2. $L_s(u) = 0$ if and only if $s = f(Du)$ for all $u \in \mathcal{U}$ and $s \in \mathrm{image}(f)$.

Moreover, it also satisfies the following two properties:

3. $L_s(u)$ is differentiable and convex with respect to $u \in \mathcal{U}$ for any fixed $s \in \mathrm{image}(f)$.
4. $L_s(u)$ is continuous and convex with respect to $s \in \mathrm{image}(f)$ for any fixed $u \in \mathcal{U}$.

Proofs of the above four properties are provided in Section 3.2. In particular, the derivative of L_s (with respect to the inner product $\langle \cdot, \cdot \rangle_{\mathcal{S}}$), denoted by $\nabla L_s : \mathcal{U} \to \mathcal{U}$, is given by

$$\nabla L_s(u) = D^* \Lambda(f(Du) - s) \quad (u \in \mathcal{U}). \tag{3.4}$$

Moreover, since f is Lipschitz continuous by the assumption in Section 2.2, $\nabla L_s : \mathcal{U} \to \mathcal{U}$ is also Lipschitz continuous with a Lipschitz constant $\mathrm{Lip}(f) \times \|DD^*\Lambda\|_{\mathrm{op}}$, where $\mathrm{Lip}(f)$ denotes the minimum Lipschitz constant of f and $\| \cdot \|_{\mathrm{op}}$ denotes the operator norm.

This loss function is defined only for $s \in \mathrm{image}(f)$ in the strict sense. However, by omitting the terms irrelevant to $u \in \mathcal{U}$ from (3.3), an essentially equivalent loss function $\tilde{L}_s : \mathcal{U} \to \mathbb{R} \cup \{\infty\}$ can be defined as

$$\tilde{L}_s(u) \coloneqq F(Du) - \langle s, Du \rangle_{\Lambda} \quad (u \in \mathcal{U}) \tag{3.5}$$

for any $s \in \mathcal{S}$ regardless of whether s is in $\mathrm{image}(f)$ or not. This extension is practically significant since s may take a value outside $\mathrm{image}(f)$ owing to observation noises. Note that such an extension is impossible in the previous hard constraint loss function and soft consistency loss function.

3.2 Proofs for Properties of Proposed Loss Function

As a preliminary, several basic properties with respect to f are briefly summarized. Let $F^* : \mathcal{S} \to \mathbb{R} \cup \{\infty\}$ be the convex conjugate [40] of F, defined as

$$F^*(w) \coloneqq \sup_{z \in \mathcal{S}} \{\langle w, z \rangle_{\Lambda} - F(z)\} \quad (z \in \mathcal{S}). \tag{3.6}$$

Then, from the differentiability of F, we have

$$f(z) = s \Leftrightarrow F^*(s) = \langle s, z \rangle_{\Lambda} - F(z) \tag{3.7}$$

and therefore

$$\partial_{\Lambda} F^*(s) = f^{-1}(s) \tag{3.8}$$

for $z, s \in \mathcal{S}$, where $\partial_{\Lambda} F^*(s) \subseteq \mathcal{S}$ denotes the subderivative of F^* at $s \in \mathcal{S}$ with respect to the inner product $\langle \cdot, \cdot \rangle_{\Lambda}$. Moreover, since the subderivative of the convex function is a closed convex set from its definition, we have the closedness and convexity of $f^{-1}(s)$ for any s.

Using these properties, the propositions described in Section 3.1 will be proved. First, the independence with respect to $w \in \mathcal{S}$ in (3.2) and $z \in f^{-1}(s)$ in (3.3) is proved as follows. From (3.1), we have

$$L_s(u) = \int_0^1 \langle f(z + t(Du - z)) - s, Du - z \rangle_\Lambda \, \mathrm{d}t \quad (u \in \mathcal{U}) \tag{3.9}$$

for any $w \in \mathcal{S}$ in (3.2), which means L_s is well defined independently of w. Also, again from (3.1), we have

$$(F(z') - \langle s, z' \rangle_\Lambda) - (F(z) - \langle s, z \rangle_\Lambda) = \int_0^1 \langle f(z + t(z' - z)) - s, z' - z \rangle_\Lambda \, \mathrm{d}t \tag{3.10}$$

for any $z, z' \in f^{-1}(s)$. Here, from the convexity of $f^{-1}(s)$, we have $f(z + t(z' - z)) = s$ for all $t \in [0, 1]$. Therefore, we obtain

$$(F(z') - \langle s, z' \rangle_\Lambda) - (F(z) - \langle s, z \rangle_\Lambda) = 0 \quad \forall z, z' \in f^{-1}(s), \tag{3.11}$$

which means L_s is well defined independently of $z \in f^{-1}(s)$ in (3.3).

Next, the four properties of the proposed loss function given in Section 3.1 will be proved. In (3.9), we have

$$\langle f(z + t(Du - z)) - s, Du - z \rangle_\Lambda \geq 0 \quad \forall t \in [0, 1] \tag{3.12}$$

from the cyclical monotonicity of f. Therefore, we have the first property, i.e., $L_s(u) \geq 0$.

The second property can be obtained from the following proposition:

$$w \in f^{-1}(s) \Leftrightarrow F(w) - F(z) = \langle s, w - z \rangle_\Lambda , \tag{3.13}$$

where z is an arbitrary element of $f^{-1}(s)$. First, we have

$$\begin{aligned} w \in f^{-1}(s) &\Leftrightarrow w \in \partial_\Lambda F^*(s) \\ &\Leftrightarrow F^*(y) \geq F^*(s) + \langle y - s, w \rangle_\Lambda \quad \forall y \in \mathcal{S} \\ &\Rightarrow F^*(f(w)) \geq F^*(s) + \langle f(w) - s, w \rangle_\Lambda . \end{aligned} \tag{3.14}$$

On the other hand, from the definition of F^*, the following relation holds for any $z, w \in \mathcal{S}$:

$$\begin{aligned} &F(w) - F(z) - \langle f(z), w - z \rangle_\Lambda \\ &= F^*(f(z)) - F^*(f(w)) - \langle f(z) - f(w), w \rangle_\Lambda \\ &\geq 0. \end{aligned} \tag{3.15}$$

Therefore, we obtain

$$w \in f^{-1}(s) \Rightarrow F(w) - F(z) - \langle s, w - z \rangle_\Lambda = 0. \tag{3.16}$$

Conversely, from the relation

$$F(w) - F(z) - \langle s, w - z \rangle_\Lambda = 0 \Leftrightarrow F^*(f(w)) - F^*(s) = \langle f(w) - s, w \rangle_\Lambda \tag{3.17}$$

and the inequality

$$F^*(y) - F^*(f(w)) \geq \langle y - f(w), w \rangle_\Lambda \quad \forall y, w \in \mathcal{S}, \tag{3.18}$$

we have

$$\begin{aligned} F(w) - F(z) - \langle s, w - z \rangle_\Lambda = 0 &\Leftrightarrow F^*(y) - F^*(s) \geq \langle y - s, w \rangle_\Lambda \\ &\Leftrightarrow w \in \partial_\Lambda F^*(s) \\ &\Leftrightarrow w \in f^{-1}(s). \end{aligned} \tag{3.19}$$

Therefore, we obtain the second property.

The third property can be obtained immediately from (3.3) and (3.1). For the fourth property, first we obtain

$$L_s(u) = F^*(s) - F^*(Du) - \langle s - f(Du), Du \rangle_\Lambda \quad (u \in \mathcal{U}) \tag{3.20}$$

from (3.15). Here, let $\Gamma_u : \mathcal{S} \to \mathbb{R} \cup \{\infty\}$ be defined for fixed $u \in \mathcal{U}$ as

$$\Gamma_u(s) \coloneqq L_s(u) \quad (s \in \mathcal{S}). \tag{3.21}$$

Since F^* is convex, Γ_u is continuous in image(f) and convex, whose subderivative is given by

$$\partial_\Lambda \Gamma_u(s) = \left\{ z - Du \;\middle|\; z \in f^{-1}(s) \right\}. \tag{3.22}$$

3.3 Comparison with Previous Formulations

This section provides a theoretical comparison between the proposed loss function and the three loss functions described in Section 2.3, i.e., the quadratic loss function, hard constraint loss function, and soft consistency loss function. First, the proposed loss function and quadratic loss function have continuous sensitivity with respect to the observed signal, whereas the other two functions do not. This continuity is desired in cases where observation noises are added after saturation effects. From an optimization viewpoint, on the other hand, the proposed loss function, as well as the hard constraint loss function and soft consistency loss function, is preferable to the quadratic loss function owing to its convexity and differentiability. From the above discussion, one can see that the proposed loss function has both robustness against observation noises and mathematical tractability. These properties are also summarized in Table 3.1. Moreover, for an intuitive explanation, examples in the one-dimensional case, i.e., $\mathcal{S} = \mathbb{R}$, are shown in Figures 3.1, 3.2, and 3.3. One can see discontinuity in the vertical direction where f is partially constant in Figure 3.3, whereas Figure 3.1 shows continuity over the entire domain in both the vertical and horizontal directions. Also, nonconvexity in the horizontal direction can be seen in Figure 3.2, whereas Figure 3.1 shows convexity in both the vertical and horizontal directions.

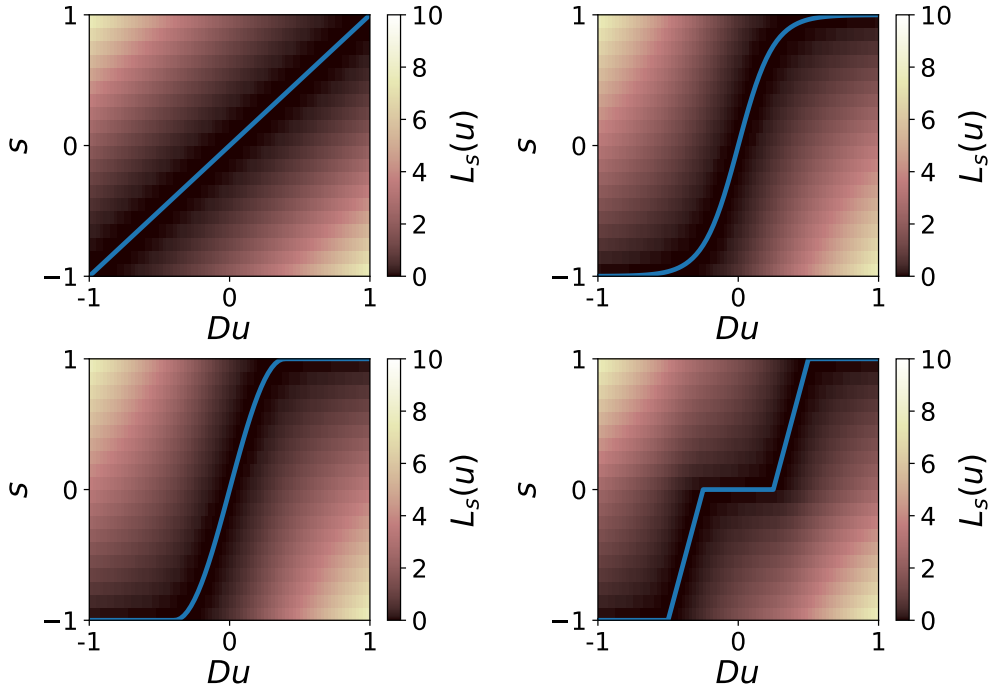

Fig. 3.1: Examples of proposed loss function.

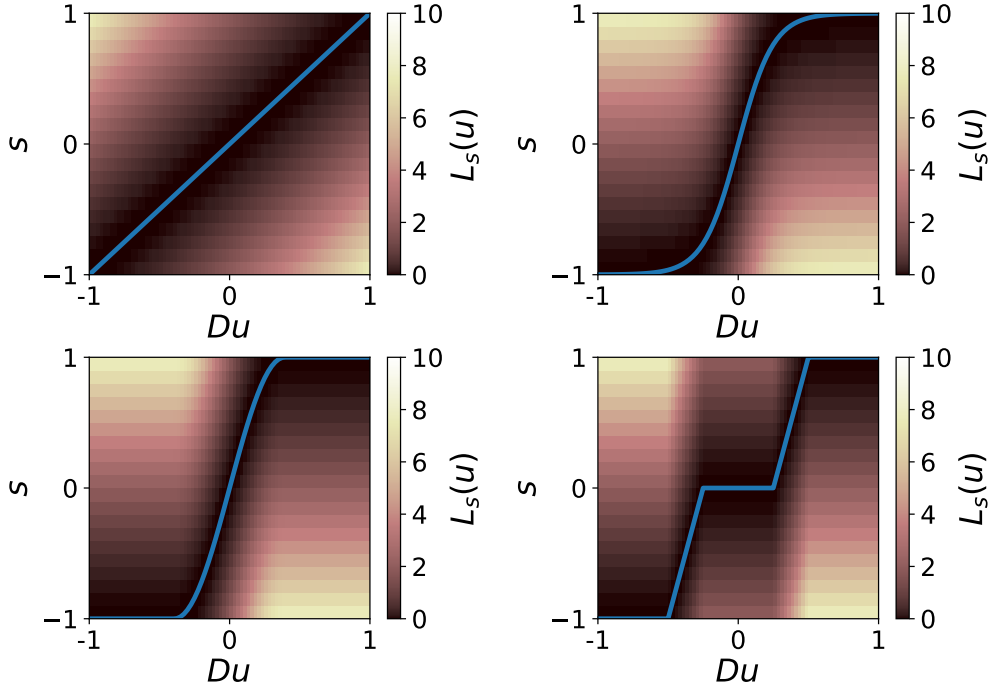

Fig. 3.2: Examples of quadratic loss function.

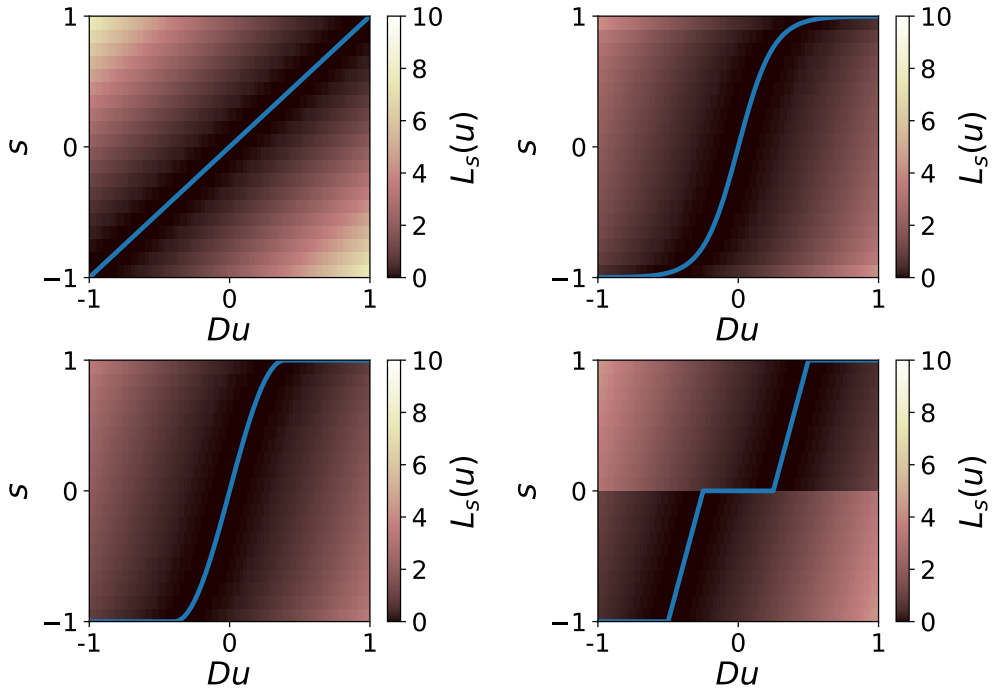

Fig. 3.3: Examples of soft consistency loss function.

Table 3.1: Properties of loss functions.

	Convexity	Continuity with respect to observed signal
Proposed loss function	Yes	Yes
Quadratic loss function	No	Yes
Hard constraint loss function	Yes	No
Soft consistency loss function	Yes	No

3.4 Optimization Theories and Algorithms for Hilbertian Regularization

First, consider the specific case of the Hilbertian regularization, i.e.,

$$R(u) = \frac{\lambda}{2}\|u\|_{\mathcal{U}}^2 \quad (u \in \mathcal{U}), \tag{3.23}$$

where $\lambda \in (0, \infty)$ is a constant parameter called a regularization parameter. This formulation is also called the *Tikhonov–Phillips regularization*. Compared with the general (non-Hilbertian) case, the Hilbertian regularization yields the following three tractable properties:

- existence of the closed-form solution in cases of linear observation;
- availability of the representer theorem;
- differentiability.

These properties are discussed in detail in the following subsections.

3.4.1 Closed-Form Solution for Linear Observation

When f is the identity mapping, i.e.,

$$f(z) = z \quad (z \in \mathcal{S}), \tag{3.24}$$

the loss function is represented as

$$L_s(u) = \frac{1}{2}\|Du - s\|_\Lambda^2 \quad (u \in \mathcal{U}), \tag{3.25}$$

i.e., the proposed loss function corresponds to the quadratic loss function. In this case, the problem of (2.3) has the same form as the ordinary linear regression with Tikhonov–Phillips regularization, and its solution can be obtained in a closed form as follows. First, the objective function is given by

$$Q(u) = \frac{1}{2}\|Du - s\|_\Lambda^2 + \frac{\lambda}{2}\|u\|_\mathcal{U}^2 \quad (u \in \mathcal{U}), \tag{3.26}$$

which can be rewritten as

$$Q(u) = u^*(D^*\Lambda D + \lambda I_\mathcal{U})u - u^*D^*\Lambda s - s^*\Lambda D u + \|s\|_\mathcal{S}^2 \quad (u \in \mathcal{U}), \tag{3.27}$$

where $I_\mathcal{U}$ is the identity mapping on $\mathcal{U}$. Here, u^* and D^* are the adjoints of u and D, respectively, whose definition is given in Appendix A.1. Since $D^*\Lambda D + \lambda I_\mathcal{U}$ is positive-definite and therefore invertible, it can be further rewritten as

$$\begin{aligned} Q(u) = {} & \left[u - (D^*\Lambda D + \lambda I_\mathcal{U})^{-1}D^*\Lambda s\right]^*(D^*\Lambda D + \lambda I_\mathcal{U})\left[u - (D^*\Lambda D + \lambda I_\mathcal{U})^{-1}D^*\Lambda s\right] \\ & + s^*\left[\Lambda D(D^*\Lambda D + \lambda I_\mathcal{U})^{-1}D^*\Lambda + I_\mathcal{S}\right]s \quad (u \in \mathcal{U}). \end{aligned} \tag{3.28}$$

Again from the positive definiteness of $D^*\Lambda D + \lambda I_\mathcal{U}$, i.e., $u^*(D^*\Lambda D + \lambda I_\mathcal{U})u > 0$ for all $u \in \mathcal{U} \setminus \{0\}$, we can see that Q is minimized at $u^{(\mathrm{opt})} \in \mathcal{U}$ given by

$$u^{(\mathrm{opt})} = (D^*\Lambda D + \lambda I_\mathcal{U})^{-1}D^*\Lambda s. \tag{3.29}$$

At first glance, the calculation of $(D^*\Lambda D + \lambda I_\mathcal{U})^{-1}$ seems difficult for infinite-dimensional $\mathcal{U}$. Actually, this infinite-dimensional calculation can be avoided by using the identity $(D^*\Lambda D + \lambda I_\mathcal{U})^{-1}D^*\Lambda = D^*\Sigma(K + \lambda\Sigma)^{-1}$ with $\Sigma \coloneqq \Lambda^{-1}$ and $K \coloneqq DD^*$, from which we obtain

$$u^{(\mathrm{opt})} = D^*\Sigma(K + \lambda\Sigma)^{-1}s. \tag{3.30}$$

In this form, $(K + \lambda\Sigma)^{-1}$ can be calculated since $DD^* + \lambda\Sigma$ is a linear mapping on a finite-dimensional linear space $\mathcal{S}$, i.e., it admits a matrix representation. This formula is computationally useful also when $\mathcal{U}$ has a finite but much larger dimension than $\mathcal{S}$ since it allows dimensional reduction in the calculation of the matrix inversion.

Here, it should be noted that $u^{(\mathrm{opt})}$ can be represented in the form of

$$u^{(\mathrm{opt})} = D^*\alpha \tag{3.31}$$

with certain $\alpha \in \mathcal{S}$. Actually, this property holds for more general cases, which is described in the following section.

3.4.2 Representer Theorem

When f is nonlinear, the optimization problem takes the following form:

$$\underset{u\in\mathcal{U}}{\text{minimize}}\ Q(u) \coloneqq H_s(Du) + \frac{\lambda}{2}\|u\|_{\mathcal{U}}^2, \tag{3.32}$$

where $H_s : \mathcal{S} \to \mathbb{R} \cup \{\infty\}$ is defined as

$$H_s(z) \coloneqq F(z) - \langle s, z\rangle_\Lambda \quad (z \in \mathcal{S}). \tag{3.33}$$

In this case, it is generally difficult to obtain the closed-form solution of (3.32); however, there are several general properties given as follows. First, the objective function is convex and coercive even when $s \in \mathcal{S} \setminus \mathrm{image}(f)$; therefore, there always exists a unique optimal solution. Here, the coerciveness can be proved as follows. For arbitrary $u_0 \in \mathcal{U} \setminus \{0\}$, let $q : \mathbb{R} \to \mathbb{R} \cup \{\infty\}$ be defined as

$$q(t) \coloneqq Q(tu_0) \quad (t \in \mathbb{R}), \tag{3.34}$$

which can be rewritten as

$$q(t) = F(tz_0) - t\langle s, z_0\rangle_\Lambda + \frac{\lambda}{2}t^2\|u_0\|_{\mathcal{U}}^2 \quad (t \in \mathbb{R}). \tag{3.35}$$

From the differentiability of F, q is also differentiable, whose derivative is given by

$$\begin{aligned}\frac{\partial q(t)}{\partial t} &= \langle f(tz_0) - s, z_0\rangle_\Lambda + \lambda\|u_0\|_{\mathcal{U}}^2 t \\ &= \langle f(tz_0) - f(t0), z_0 - 0\rangle_\Lambda + \lambda\|u_0\|_{\mathcal{U}}^2 t + \langle f(0) - s, z_0\rangle_\Lambda .\end{aligned} \tag{3.36}$$

Here, from the monotonicity of f, the term $\langle f(tz_0) - f(t0), z_0 - 0\rangle_\Lambda$ is nonnegative for all $t \in \mathbb{R}$. Therefore, we have

$$\lim_{t\to\infty} \frac{\partial q(t)}{\partial t} = \infty, \tag{3.37}$$

which yields the coerciveness of Q.

Moreover, from the representer theorem [34,59–63], one can see that the optimal solution of (3.32) lies within a finite-dimensional linear subspace given as coimage(D), called the

coimage of D. The coimage can be regarded as a generalization of the row space in matrix algebra to general Hilbert spaces, and coimage(D) is characterized by

$$\mathrm{coimage}(D) = \mathrm{image}(D^*). \tag{3.38}$$

In particular, the representer theorem states that any optimal solution $u^{(\mathrm{opt})} \in \mathcal{U}$ of

$$\underset{u\in\mathcal{U}}{\text{minimize}}\ Q(u) \coloneqq H(Du) + g(\|u\|_{\mathcal{U}}) \tag{3.39}$$

with an arbitrary function $H : \mathcal{U} \to \mathbb{R} \cup \{\infty\}$ and an arbitrary strictly monotonically increasing function $g : [0, \infty) \to \mathbb{R}$ admits a representation in the form of

$$u^{(\mathrm{opt})} = D^*\alpha \tag{3.40}$$

with certain $\alpha \in \mathcal{S}$ [34,60–63]. We can easily see that (3.32) satisfies the above conditions of the representer theorem and that the optimal α in (3.40) is given as a solution of

$$\underset{\alpha\in\mathcal{S}}{\text{minimize}}\ Q^{(*)}(\alpha) \coloneqq H_s(K\alpha) + \frac{\lambda}{2}\|\alpha\|_K^2. \tag{3.41}$$

Here, $K : \mathcal{S} \to \mathcal{S}$ is a bounded linear mapping called the Gram operator generated by D^*, which is defined as $K \coloneqq DD^*$, and $\|\cdot\|_K$ is a seminorm on $\mathcal{S}$ induced by the inner product $\langle\cdot,\cdot\rangle_K : \mathcal{S} \times \mathcal{S} \to \mathbb{K}$, defined as $\langle\alpha, \alpha'\rangle_K \coloneqq \langle\alpha, K\alpha'\rangle_{\mathcal{S}}$ for $\alpha, \alpha' \in \mathcal{S}$. Therefore, we only need to seek the optimal solution within the finite-dimensional Hilbert space $\mathcal{S}$ instead of the original Hilbert space $\mathcal{U}$. This technique of dimensional reduction is often used in the field of machine learning, especially in function interpolation methods called *kernel methods* [64], because of its affinity with theories on reproducing kernel Hilbert spaces [65]. As shown above, however, it can also be used in more general situations including acoustic measurement problems, which is described in later chapters in more detail.

3.4.3 Optimization Algorithms

Since the optimization problem of (3.41) is convex and differentiable, many well-established iterative algorithms are available. Here, two iterative algorithms are provided as Algorithms 1 and 2.

Algorithm 1 is based on the gradient descent method with a constant step size parameter. Several acceleration methods, such as Nesterov's one [46], can also be applied. Note that the derivative of $Q^{(*)}$ with respect to the inner product $\langle\cdot,\cdot\rangle_K$ is used here, which is denoted by $\nabla_K Q^{(*)} : \mathcal{S} \to \mathcal{S}$ and given by

$$\nabla_K Q^{(*)}(\alpha) = \Lambda(f(K\alpha) - s) + \lambda\alpha \quad (\alpha \in \mathcal{S}), \tag{3.42}$$

instead of the derivative with respect to the inner product $\langle\cdot,\cdot\rangle_{\mathcal{S}}$, given by

$$\nabla Q^{(*)}(\alpha) = K\Lambda(f(K\alpha) - s) + \lambda K\alpha \quad (\alpha \in \mathcal{S}). \tag{3.43}$$

Algorithm 1 Gradient descent algorithm for Hilbertian regularization

Require: $\alpha \in \mathcal{S}$, $\gamma \in (0, 2/(\mathrm{Lip}(f) \times \|K\Lambda\|_{\mathrm{op}} + \lambda))$

  repeat

    $\alpha \leftarrow \alpha - \gamma[\Lambda(f(K\alpha) - s) + \lambda\alpha]$

  end

  return $\hat{u} = D^*\alpha$

This is to keep the correspondence of the metric between the two spaces, i.e., the equality

$$\langle u, u' \rangle_{\mathcal{U}} = \langle \alpha, \alpha' \rangle_K , \tag{3.44}$$

holding for any $u, u' \in \mathcal{U}$ and $\alpha, \alpha' \in \mathcal{S}$ satisfying $u = D^*\alpha$ and $u' = D^*\alpha'$. In other words, Algorithm 1 can also be interpreted as the gradient descent method of Q in the original space $\mathcal{U}$ with the inner product $\langle \cdot, \cdot \rangle_{\mathcal{U}}$. However, the convergence itself can be guaranteed even when the derivative given in (3.43) is used with $\gamma \in (0, 2/(\mathrm{Lip}(f) \times \|K^2\Lambda\|_{\mathrm{op}} + \lambda\|K\|_{\mathrm{op}}))$.

On the other hand, Algorithm 2 is based on the majorization-minimization approach, which is derived as follows. First, from the Lipschitz continuity of f, we have [66]

$$F(z) \leq F(w) + \langle f(w), z - w \rangle_\Lambda + \frac{\beta}{2}\|z - w\|_\Lambda^2 \quad \forall z, w \in \mathcal{S} \tag{3.45}$$

for $\beta \in (0, \mathrm{Lip}(f)]$, where the equality holds for $z = w$. Therefore, we can define a surrogate function $\breve{Q}^{(*)}(\alpha, \alpha') : \mathcal{S} \times \mathcal{S} \to \mathbb{R} \cup \{\infty\}$ as

$$\begin{aligned} \breve{Q}^{(*)}(\alpha, \alpha') = \frac{\beta}{2}\|K(\alpha - \alpha)\|_\Lambda^2 + \langle f(K\alpha'), K(\alpha - \alpha') \rangle_\Lambda + H_s(K\alpha') \\ - \langle s, K\alpha \rangle_\Lambda + \frac{\lambda}{2}\|\alpha\|_K^2 \quad (\alpha, \alpha' \in \mathcal{S}). \end{aligned} \tag{3.46}$$

This surrogate function is a quadratic function with respect to the first variable; therefore, it can be minimized in a closed form, and we can obtain Algorithm 2. Since this algorithm can be regarded as an iterative operation of the regularized least squares, it is referred here to as the *iterative least squares algorithm*. Although the calculation of $(K + \gamma\lambda\Sigma)^{-1}$ is required in this algorithm, it can be calculated before we obtain the observed signal s. Note that this algorithm gives the closed-form solution when f is the identity mapping and $\gamma = 1$, which can be confirmed by comparison with (3.30).

3.5 Optimization Theories and Algorithms for Non-Hilbertian Regularization

Next, we consider more general cases of non-Hilbertian regularization. In practical situations, such regularization functions are often used in the context of sparsity-based inverse

Algorithm 2 Iterative least squares algorithm for Hilbertian regularization

Require: $\alpha \in \mathcal{S}$, $\gamma \in (0, 1/\mathrm{Lip}(f)]$

  repeat

    $\alpha \leftarrow (K + \gamma\lambda\Sigma)^{-1}[K\alpha - \gamma(f(K\alpha) - s)]$

  end

  return $\hat{u} = D^*\alpha$

problems.

3.5.1 Classification of Non-Hilbertian Regularization

Although the term "non-Hilbertian" can be used in a wide sense, most practically used non-Hilbertian regularization functions are designed for promoting sparsity. A typical example of a sparsity-promoting function is the l_p norm or pseudonorm function [47] on $\mathbb{R}^N$ with $N \in \mathbb{N}$ and $0 < p < 2$, i.e.,

$$R(\mathbf{u}) = \sum_{n=1}^{N} |u_1|_p^p \quad (\mathbf{u} \coloneqq [u_1, \ldots, u_N]^\mathsf{T} \in \mathbb{R}^N). \tag{3.47}$$

As in this example, many sparsity-promoting regularization functions have nondifferentiable points. However, practically used nonsmooth regularization functions can be classified into the following two types. One is a function $R : \mathcal{U} \to \mathbb{R} \cup \{\infty\}$ that is "majorizable" by a quadratic function, whose surrogate function, denoted by $\breve{R} : \mathcal{U} \times \mathcal{U}$, is given by

$$\breve{R}(u, u') = \langle u, u \rangle_{W(u')} + C(u') \tag{3.48}$$

with some constant $C(u') \in \mathbb{R}$ and (easily computable) positive-definite bounded linear mapping $W(u') : \mathcal{U} \to \mathcal{U}$, where $\langle \cdot, \cdot \rangle_{W(u')} : \mathcal{U} \times \mathcal{U} \to \mathbb{K}$ is the inner product induced by $W(u')$. The l_p norm or pseudonorm functions defined above are typical examples of such functions [47]. For these functions, we can apply the majorization-minimization approach. The other is a function $R : \mathcal{U} \to \mathbb{R} \cup \{\infty\}$ whose proximable operator is available. The l_1 norm function is a typical example of such functions [43]. For these functions, we can apply the proximal approach. Note that, in either approach, the convexity of R is not required. Although it is difficult to guarantee the convergence to the global solution for nonconvex R, a wide variety of regularization functions, which exhibit high performance in practice, can be used with these approaches.

3.5.2 Optimization Algorithm

Here, two iterative algorithms are provided as Algorithms 3 and 4. Algorithm 3 is based on the proximal approach, which is called the *proximal-linearized alternating direction method*

Algorithm 3 PL-ADMM algorithm for non-Hilbertian regularization

Require: $u \in \mathcal{U}$, $v \in \mathcal{S}$, $z \in \mathcal{S}$, $\rho \in (0, \infty)$, $\gamma \in (0, 1/(\rho\|K\|_{\mathrm{op}})]$, $\mu \in (0, 1/(\rho + \|\Lambda\|_{\mathrm{op}} \times \mathrm{Lip}(f))]$

repeat

$u \leftarrow \mathrm{prox}_R^{\gamma}(u - \gamma D^*[v + \rho(Du - z)])$

$z \leftarrow z - \mu\left(\Lambda(f(z) - s) - [v + \rho(Du - z)]\right)$

$v \leftarrow v + \rho(Du - z)$

end

return $\hat{u} = u$

Algorithm 4 Iterative reweighted least squares algorithm for non-Hilbertian regularization

Require: $u \in \mathcal{U}$, $\gamma \in (0, 1/\mathrm{Lip}(f)]$

repeat

$u \leftarrow (D^*\Lambda D + \gamma W(u))^{-1} D^*\Lambda[Du - \gamma(f(Du) - s)]$

end

return $\hat{u} = u$

of multipliers (PL-ADMM) [50,66]. This algorithm can be applied when the proximal operator of R is available. Algorithm 4 is based on the majorization-minimization approach, which is called the *iterative reweighted least squares algorithm* [47]. This algorithm can be applied when the surrogate function of R is given by (3.48).

Chapter 4

Restoration of Saturated Sound Signal

This chapter focuses on specific applicational problems of the restoration of saturated sound signals. Although the basic framework follows the theories provided in Chapters 2 and 3, experimental comparisons with other signal restoration methods are also presented. In Section 4.1, the research background and related studies on restoration problems of saturated sound signals are summarized. Signal restoration methods based on two different strategies are proposed in Sections 4.2 and 4.3.

4.1 Research Background

Saturation is an essentially inevitable nonlinear phenomenon in the measurement of any types of signals including sound signals. Highly distorted signals due to this phenomenon not only degrade their perceptual quality [67, 68] but also have negative effects in various applications at later stages [69]. Restoring such signals is of great interest as a common problem to be solved.

There have been many attempts to solve this problem or related ones in the literature [54–56, 69–76]. In [70], the signal is restored using oversampling (i.e., sampling with a frequency higher than the Nyquist rate, which is determined by the Nyquist–Shannon sampling theorem [16]). Since no other assumptions are imposed on target signals, this method is expected to be applicable to a wide variety of signals, although observation richer than usual is required. However, only a specific saturation effect, a hard clipping effect, is considered in this method, and its theory cannot be applied directly to various saturation effects caused by sensors and amplifiers.

Sparsity-based signal restoration methods have also attracted considerable attention for their restoration accuracy in various practical situations [54–56, 71, 73–76]. In these methods, some sparse structure on the target signal is assumed, and an optimization problem is formulated to induce the sparsity of the estimated signal, which is evaluated by a sparsity-promoting regularization function, while keeping the consistency between the

estimated signal and the observed signal, which is evaluated by a loss function. Obviously, such a sparsity assumption is not necessarily satisfied for all possible signals; however, it is reported to work well practically for various signals observed in the real world. In these methods, the hard constraint loss function and soft consistency loss function described in Section 2.3 are used. Therefore, the formulated optimization problems can be solved using various iterative algorithms based on the proximal approach [54–56, 76]. These methods exhibit high restoration accuracy for real data as well as for artificially created data in noise-free cases, or at least in noisy cases only before saturation effects. These assumptions are justified, for example, when considering a hard clipping effect caused by an analog-to-digital converter. When considering saturation caused by sensors and amplifiers, on the other hand, we often need to consider observation noises after saturation effects; however, there has been little theoretical or experimental investigation for such cases.

The following sections present new comprehensive signal restoration algorithms applicable to noisy observation on the basis of the loss function proposed in Chapter 3, which exhibits a continuous sensitivity against the observed signal, as opposed to the loss functions proposed in other previous works. Section 4.2 presents a restoration method where only the bandlimitation of target signals is assumed as in [70]. This method is applicable to various saturation functions and sampling schemes, including oversampling and more general nonuniform sampling. Section 4.3 presents a sparsity-based restoration method. In this method, the basic framework follows that proposed in [55]; however, the use of the proposed loss function leads to a significant improvement in restoration accuracy in noisy cases. In each section, experimental results are also provided to demonstrate the validity of the proposed method.

4.2 Signal Restoration from Nonuniform Samples

4.2.1 Formulation

A bandlimited signal can be modeled as a function $u : \mathbb{R} \to \mathbb{R}$ that admits the form of

$$u(t) = \frac{1}{\sqrt{2\pi}} \int_{\omega \in \Omega} \hat{u}(\omega) \exp(i\omega t) \, \mathrm{d}\mu \quad (t \in \mathbb{R}) \tag{4.1}$$

with some $\hat{u} \in \mathcal{L}_2(\Omega, \mathbb{C})$, where $\Omega \coloneqq [-\omega_{\max}, \omega_{\max}]$ denotes the bandlimitation of the signal with $\omega_{\max} \in (0, \infty)$. Let $\mathscr{F}$ denote the function transformation from $\hat{u}$ to u in (4.1), i.e., the inverse Fourier transform, and $\tilde{\mathcal{L}}_2(\Omega, \mathbb{C})$ be the set defined as

$$\tilde{\mathcal{L}}_2(\Omega, \mathbb{C}) \coloneqq \{\hat{u} \in \mathcal{L}_2(\Omega, \mathbb{C}) \mid \hat{u}(-\omega) = \hat{u}(\omega)^* \ \forall \omega \in \Omega\} . \tag{4.2}$$

Then, the set of all bandlimited signals can be given by

$$\mathcal{U} \coloneqq \left\{ \mathscr{F}\hat{u} \;\middle|\; \hat{u} \in \tilde{\mathcal{L}}_2(\Omega, \mathbb{C}) \right\} . \tag{4.3}$$

Moreover, let $\langle \cdot, \cdot \rangle_{\mathcal{U}} : \mathcal{U} \times \mathcal{U} \to \mathbb{R}$ be an inner product defined as

$$\langle u, v \rangle_{\mathcal{U}} \coloneqq \int_{t \in \mathbb{R}} u(t) v(t) \, \mathrm{d}\mu. \tag{4.4}$$

Then, $\mathcal{U}$ is a real Hilbert space with an inner product $\langle u, v \rangle_{\mathcal{U}}$ and, as noted in [14, 15], a reproducing kernel Hilbert space with a reproducing kernel $\kappa : \mathbb{R} \times \mathbb{R} \to \mathbb{R}$ given by

$$\kappa(t, t') \coloneqq \frac{\omega_{\max}}{\pi} \mathrm{sinc}(\omega_{\max}(t - t')) \quad (t, t' \in \mathbb{R}), \tag{4.5}$$

i.e., the following equality holds:

$$\langle \kappa(\cdot, t), u \rangle_{\mathcal{U}} = u(t) \quad (u \in \mathcal{U},\ t \in \mathbb{R}). \tag{4.6}$$

Here, $\mathrm{sinc}(\cdot) : \mathbb{R} \to \mathbb{R}$ is the unnormalized sinc function defined as

$$\mathrm{sinc}(z) \coloneqq \begin{cases} \sin(z)/z & z \in \mathbb{R} \setminus \{0\} \\ 1 & z = 0 \end{cases}. \tag{4.7}$$

Consider a signal sampled at $N \in \mathbb{N}$ points $t_1, \ldots, t_N \in \mathbb{R}$ with a nonlinear saturation effect. The relationship between the unknown bandlimited signal $u \in \mathcal{U}$ and the observed signals $s_1, \ldots, s_N \in \mathbb{R}$ is given by

$$s_n = f_0(u(t_n)) + \epsilon_n \quad (n \in [\![1, N]\!]), \tag{4.8}$$

where $f_0 : \mathbb{R} \to \mathbb{R}$ is a monotonically nondecreasing and Lipschitz continuous function representing the saturation effect and $\epsilon_1, \ldots, \epsilon_N \in \mathbb{R}$ denote the observation noises. From (4.6), the above relationship can be rewritten as

$$\mathbf{s} = f(Du) + \boldsymbol{\epsilon}, \tag{4.9}$$

where $\mathbf{s} \in \mathbb{R}^N$ and $\boldsymbol{\epsilon} \in \mathbb{R}^N$ are defined as

$$\mathbf{s} \coloneqq \begin{bmatrix} s_1 \\ \vdots \\ s_N \end{bmatrix}, \ \boldsymbol{\epsilon} \coloneqq \begin{bmatrix} \epsilon_1 \\ \vdots \\ \epsilon_N \end{bmatrix}, \tag{4.10}$$

$D : \mathcal{U} \to \mathbb{R}^N$ is a bounded linear operator defined as

$$Du \coloneqq \begin{bmatrix} \langle \kappa_1, u \rangle_{\mathcal{U}} \\ \vdots \\ \langle \kappa_N, u \rangle_{\mathcal{U}} \end{bmatrix} \quad (u \in \mathcal{U}), \tag{4.11}$$

and $f : \mathbb{R}^N \to \mathbb{R}^N$ is a monotone mapping defined as

$$f(\mathbf{z}) \coloneqq \begin{bmatrix} f_0(z_1) \\ \vdots \\ f_0(z_N) \end{bmatrix} \quad (\mathbf{z} \coloneqq [z_1, \ldots, z_N]^{\mathsf{T}} \in \mathbb{R}^N). \tag{4.12}$$

Here, $\kappa_1, \ldots, \kappa_N \in \mathcal{U}$ are defined as

$$\kappa_n(t) = \kappa(t_n, t) \quad (t \in \mathbb{R},\ n \in [\![1, N]\!]). \tag{4.13}$$

According to the theories described in Chapter 3, the following optimization problem is formulated to estimate the unknown signal:

$$\underset{u \in \mathcal{U}}{\text{minimize}}\ Q(u) \coloneqq H_{\mathbf{s}}(Du) + \frac{\lambda}{2}\|u\|_{\mathcal{U}}^2, \tag{4.14}$$

where $\lambda \in (0, \infty)$ is the regularization parameter and $H_{\mathbf{s}} : \mathbb{R}^N \to \mathbb{R} \cup \{\infty\}$ is defined as

$$H_{\mathbf{s}}(\mathbf{z}) \coloneqq \sum_{n=1}^{N} (F_0(z_n) - s_n z_n) \quad (\mathbf{z} \coloneqq [z_1, \ldots, z_N]^\mathsf{T} \in \mathbb{R}^N) \tag{4.15}$$

with $F_0 : \mathbb{R} \to \mathbb{R}$ being a primitive function of f_0. Then, we can apply the representer theorem to (4.17), which guarantees that the optimal solution $u^{(\mathrm{opt})} \in \mathcal{U}$ admits the form of

$$u^{(\mathrm{opt})} = D^* \boldsymbol{\alpha}^{(\mathrm{opt})} = \sum_{n=1}^{N} \alpha_n^{(\mathrm{opt})} \kappa_n \tag{4.16}$$

with certain $\boldsymbol{\alpha}^{(\mathrm{opt})} \coloneqq [\alpha_1^{(\mathrm{opt})}, \ldots, \alpha_N^{(\mathrm{opt})}]^\mathsf{T} \in \mathbb{R}^N$. Here, $\boldsymbol{\alpha}^{(\mathrm{opt})}$ can be obtained as the optimal solution of

$$\underset{\boldsymbol{\alpha} \in \mathbb{R}^N}{\text{minimize}}\ Q^{(*)}(\boldsymbol{\alpha}) \coloneqq H_{\mathbf{s}}(\mathbf{K}\boldsymbol{\alpha}) + \frac{\lambda}{2}\boldsymbol{\alpha}^\mathsf{T}\mathbf{K}\boldsymbol{\alpha}, \tag{4.17}$$

where $\mathbf{K} \in \mathbb{R}^{N \times N}$ is defined as

$$\mathbf{K} \coloneqq \begin{bmatrix} \kappa(t_1, t_1) & \ldots & \kappa(t_1, t_M) \\ \vdots & \ddots & \vdots \\ \kappa(t_M, t_1) & \ldots & \kappa(t_M, t_M) \end{bmatrix}. \tag{4.18}$$

This objective function is proper, convex, and differentiable, whose gradient is given by

$$\nabla Q^{(*)}(\boldsymbol{\alpha}) \coloneqq \mathbf{K}(f(\mathbf{K}\boldsymbol{\alpha}) - \mathbf{s} + \lambda\boldsymbol{\alpha}) \quad (\boldsymbol{\alpha} \in \mathbb{R}^N). \tag{4.19}$$

4.2.2 Numerical Simulations

Numerical simulations of signal restoration were conducted using Julia v.1.2.0. The following four conditions were compared in the restoration of saturated signals: the proposed method (denoted by **Proposed**), the method with the soft consistency loss function (denoted by **Soft consistency**), the regularized least squares (denoted by **RLS**), and the combination of **Proposed** and **RLS** (denoted by **Proposed+RLS**). The restoration results of unsaturated signals (denoted by **Unsaturated**) were also investigated. The detailed settings are described below.

Table 4.1: Results of bandlimited signal estimation (50 trials).

Condition	NMSE: mean ± standard deviation
Proposed	$-19.67 \pm 3.64\,\mathrm{dB}$
Soft consistency	$-15.94 \pm 3.87\,\mathrm{dB}$
RLS	$-16.84 \pm 2.19\,\mathrm{dB}$
Proposed+RLS	$-21.70 \pm 3.25\,\mathrm{dB}$
Unsaturated	$-25.66 \pm 3.70\,\mathrm{dB}$

The bandlimitation of the target signal was set as $\omega_{\max} \coloneqq 2\pi \mathrm{f}_{\max}$ with $\mathrm{f}_{\max} = 100\,\mathrm{Hz}$. The true signal, denoted by $u_{\mathrm{true}} \in \mathcal{U}$, was defined as

$$u_{\mathrm{true}}(t) \coloneqq \sum_{\nu=0}^{200} a_\nu \mathrm{sinc}(\omega_{\max} t - \nu\pi), \tag{4.20}$$

where $a_0, \ldots, a_{200}$ were sampled independently from the univariate real normal distribution with mean 0 and variance 1. The signal was sampled at $N = 500$ points, where $t_1, \ldots, t_N$ were sampled independently from the uniform distribution on $[0, 1]\,\mathrm{s}$. For **Proposed**, **Soft consistency**, **RLS**, and **Proposed+RLS**, the following saturation function was used:

$$f_0(z) \coloneqq \tanh(z) \quad (z \in \mathbb{R}), \tag{4.21}$$

where $\tanh(\cdot) : \mathbb{R} \to \mathbb{R}$ is the hyperbolic tangent function defined as

$$\tanh(z) \coloneqq \frac{\exp(z) - \exp(-z)}{\exp(z) + \exp(-z)}. \tag{4.22}$$

For **Unsaturated**, on the other hand, f_0 was set as the identity mapping. Observation noises $\epsilon_1, \ldots, \epsilon_N$ were sampled independently from the univariate real normal distribution with mean 0 and variance $10^{-3} \times S$, where S is the average power of the noise-free observed signals (i.e., the signal-to-noise ratio was 30 dB).

In **Proposed** and **Unsaturated**, the unknown signal was estimated by solving the optimization problem of (4.17) with $\lambda = 10^{-3}$ and an initial solution of zero vector. In **Soft consistency**, the optimization problem

$$\underset{u \in \mathcal{U}}{\text{minimize}} \; Q_{\mathrm{Soft}}(u) \coloneqq \frac{1}{2}\|Du - \mathrm{proj}_{f^{-1}(\mathbf{s})}(Du)\|_2^2 + \frac{\lambda}{2}\|u\|_{\mathcal{U}}^2 \tag{4.23}$$

with $\lambda = 10^{-3}$ was used to estimate the signal. Here, for each $n \in [\![1, N]\!]$, the signal s_n was discarded when it was outside the range of f_n owing to the observation noise since $f_n^{-1}(s_n)$ cannot be defined for such s_n. On the basis of the representer theorem, as in **Proposed**, the optimal solution was obtained by solving

$$\underset{\boldsymbol{\alpha} \in \mathbb{R}^N}{\text{minimize}} \; Q_{\mathrm{Soft}}^{(*)}(\boldsymbol{\alpha}) \coloneqq \frac{1}{2}\|\mathbf{K}\boldsymbol{\alpha} - \mathrm{proj}_{f^{-1}(\mathbf{s})}(\mathbf{K}\boldsymbol{\alpha})\|_2^2 + \frac{\lambda}{2}\boldsymbol{\alpha}^\mathsf{T}\mathbf{K}\boldsymbol{\alpha} \tag{4.24}$$

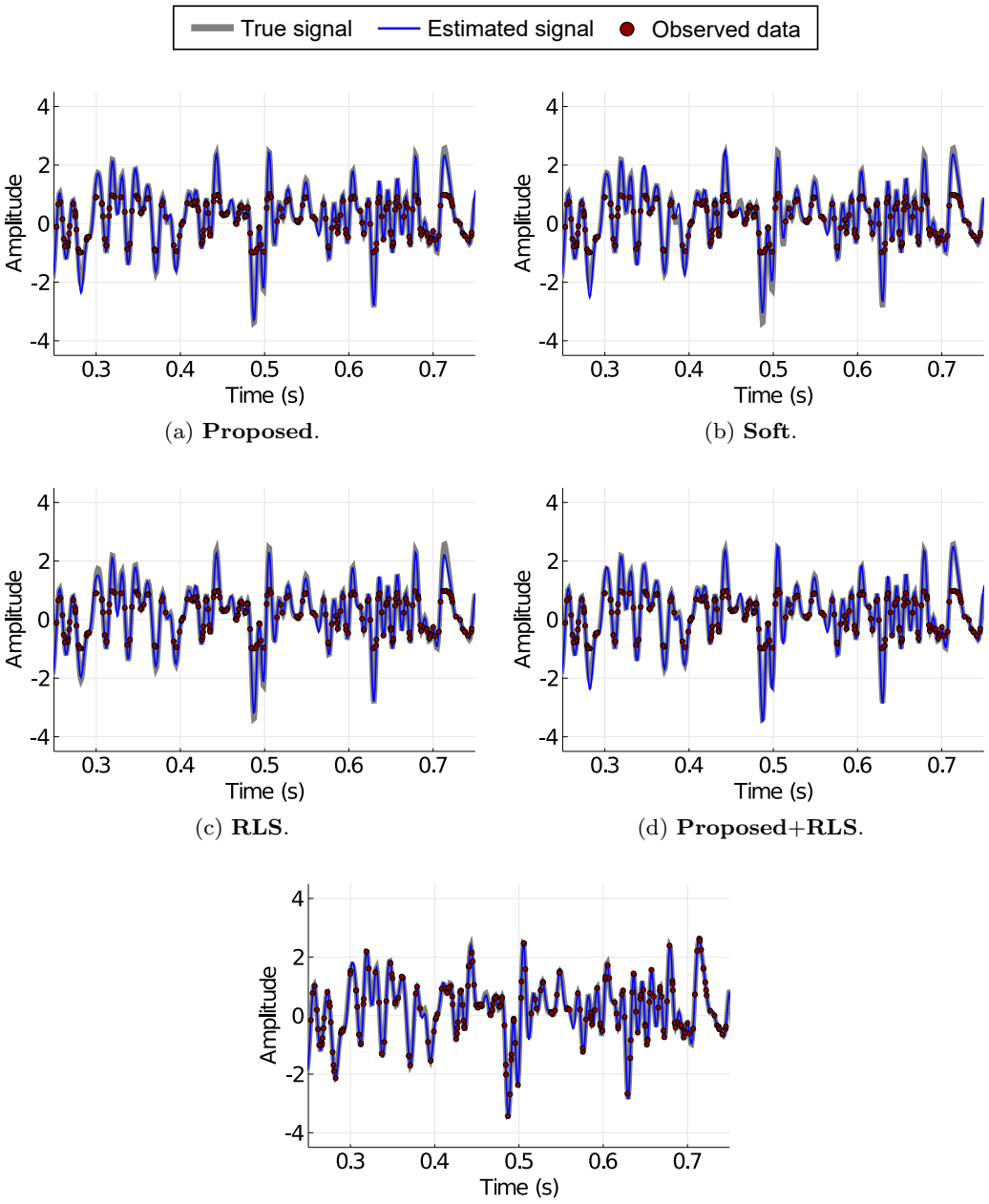

(a) **Proposed**. (b) **Soft**.

(c) **RLS**. (d) **Proposed+RLS**.

(e) **Unsaturated**.

Fig. 4.1: Results of bandlimited signal estimation in $[0.25, 0.75]$ s in the first trial. The NMSEs were (a) -23.33, (b) -18.28, (c) -20.89, (d) -24.20, and (e) -24.56 dB.

with an initial solution of zero vector. In **RLS**, the optimization problem

$$\underset{u \in \mathcal{U}}{\text{minimize}} \; Q_{\mathrm{RLS}}(u) \coloneqq \frac{1}{2}\|f(Du) - \mathbf{s}\|_2^2 + \frac{\lambda}{2}\|u\|_{\mathcal{U}}^2 \tag{4.25}$$

with $\lambda = 10^{-3}$ was used to estimate the signal. On the basis of the representer theorem, the optimal solution was obtained by solving

$$\underset{\boldsymbol{\alpha} \in \mathbb{R}^N}{\text{minimize}} \; Q_{\mathrm{RLS}}^{(*)}(\boldsymbol{\alpha}) \coloneqq \frac{1}{2}\|f(\mathbf{K}\boldsymbol{\alpha}) - \mathbf{s}\|_2^2 + \frac{\lambda}{2}\boldsymbol{\alpha}^{\mathsf{T}}\mathbf{K}\boldsymbol{\alpha} \tag{4.26}$$

with an initial solution of zero vector. In **Proposed+RLS**, (4.17) was solved first, and then (4.26) was solved using the obtained solution of (4.17) as the initial solution. For the optimization method, the nonlinear conjugate gradient method in Optim.jl [77] was used with the default settings.

As an evaluation criterion, the normalized mean squared error (NMSE) was used, which was defined as

$$\mathrm{NMSE} \coloneqq 10\log_{10}\frac{\sum_{\mathrm{i}\in\mathrm{I}_{\mathrm{eval}}}|u_{\mathrm{true}}(t^{(\mathrm{i})}_{\mathrm{eval}})-u_{\mathrm{est}}(t^{(\mathrm{i})}_{\mathrm{eval}})|^2}{\sum_{\mathrm{i}\in\mathrm{I}_{\mathrm{eval}}}|u_{\mathrm{true}}(t^{(\mathrm{i})}_{\mathrm{eval}})|^2}\quad(\mathrm{dB}). \tag{4.27}$$

Here, $u_{\mathrm{est}}\in\mathcal{U}$ denotes the estimated signal, and the evaluation points $\{t^{(\mathrm{i})}_{\mathrm{eval}}\}_{\mathrm{i}\in\mathrm{I}_{\mathrm{eval}}}$ were set as equally spaced points from 0 s to 1 s with intervals of 0.001 s.

The results are provided in Table 4.1, where the mean and standard deviation of the NMSEs were calculated over 50 trials since several parameters were randomly determined. The true and estimated signals in the first trial are also plotted in Figure 4.1. The estimation accuracy for **Soft consistency** was lowest, indicating its lack of robustness against observation noises after saturation effects. Also, the estimation accuracy for **RLS** was low, which was considered to be due to its nonconvexity; the estimated signal might have fallen into local optimal solutions. On the other hand, the estimation accuracy for **Proposed** was higher than that for **RLS**, and it was further improved by **Proposed+RLS**, which was even close to that for **Unsaturated**. One possible reason why **Proposed+RLS** outperformed **Proposed** is the formulation of **RLS** being well suited for Gaussian noises; it can be interpreted formally as a maximum a posteriori (MAP) estimation when the observation noises follow normal distributions. From these results, one can see that an accurate estimation was achieved using the formulation of (4.17), which could also be used as an initial solution in the optimization for a different formulation.

4.3 Restoration of Saturated Sound Signal Based on Signal Sparsity

4.3.1 Formulation

Consider the restoration problem of a discrete-time signal, denoted by $\mathbf{z}\coloneqq[z_1,\dots,z_N]^{\mathsf{T}}\in\mathbb{R}^N$, from its saturated observation, denoted by $\mathbf{s}\coloneqq[s_1,\dots,s_N]^{\mathsf{T}}\in\mathbb{R}^N$. The relationship between $\mathbf{z}$ and $\mathbf{s}$ is given by

$$s_n=f_0(z_n)+\epsilon_n\quad(n\in[\![1,N]\!]), \tag{4.28}$$

where $\epsilon_1,\dots,\epsilon_N\in\mathbb{R}$ denote the observation noises and $f_0:\mathbb{R}\to\mathbb{R}$ is a Lipschitz continuous and monotonically nondecreasing function representing the saturation effect. Hereafter, the following simplified vector notation will be used:

$$\mathbf{s}=f(\mathbf{z})+\boldsymbol{\epsilon}, \tag{4.29}$$

where $f : \mathbb{R}^N \to \mathbb{R}^N$ is defined as the elementwise mapping of f_0 and $\boldsymbol{\epsilon} \in \mathbb{R}^N$ is defined as $\boldsymbol{\epsilon} \coloneqq [\epsilon_1, \ldots, \epsilon_N]$.

Many signals observed in the real world have some "sparse" structure. Here, $\mathbf{z}$ is assumed to be generated by a sparse vector $\mathbf{u} \in \mathbb{R}^M$ via a given linear mapping $\mathbf{D} : \mathbb{R}^M \to \mathbb{R}^N$ called a *synthesis operator*, i.e., $\mathbf{z} = \mathbf{D}\mathbf{u}$. Then, the typical formulation for the sparsity-based signal restoration problem is given by [55]

$$\underset{\mathbf{u}\in\mathbb{R}^M}{\text{minimize}} \ \|\mathbf{u}\|_0 \text{ s.t. } H_{\mathbf{s}}(\mathbf{D}\mathbf{u}) \leq \varepsilon. \tag{4.30}$$

Here, $H_{\mathbf{s}} : \mathbb{R}^N \to \mathbb{R} \cup \{\infty\}$ is a loss function, i.e., $H_{\mathbf{s}}(\mathbf{z})$ evaluates the consistency between $\mathbf{z}$ and $\mathbf{s}$ under f, $\varepsilon \in [0, \infty)$ is a constant parameter representing the maximum allowable inconsistency, and $\|\cdot\|_0 : \mathbb{R}^M \to \mathbb{N}$ is the l_0 pseudonorm, i.e, $\|\mathbf{u}\|_0$ denotes the number of nonzero elements of $\mathbf{u} \in \mathbb{R}^M$. Since the l_0 pseudonorm takes a discrete value in $\mathbb{N}$, (4.30) is equivalent to the problem of seeking the minimum $k \in \mathbb{N}$ satisfying $H_{\mathbf{s}}(\mathbf{D}\hat{\mathbf{u}}^{(k)}) \leq \varepsilon$, where $\hat{\mathbf{u}}^{(k)} \in \mathbb{R}^M$ is the solution of

$$\underset{\mathbf{u}\in\mathbb{R}^M}{\text{minimize}} \ H_{\mathbf{s}}(\mathbf{D}\mathbf{u}) \text{ s.t. } \|\mathbf{u}\|_0 \leq k. \tag{4.31}$$

Therefore, we can solve (4.30) by solving (4.31) for each incremental $k \in \mathbb{N}$ until a stopping criterion, i.e., $H_{\mathbf{s}}(\mathbf{D}\hat{\mathbf{u}}^{(k)}) \leq \varepsilon$, is satisfied. In practice, the stopping criterion can be replaced by another one, as long as it evaluates the consistency between $\mathbf{D}\hat{\mathbf{u}}^{(k)}$ and $\mathbf{s}$. Here, let $R_k(\cdot) : \mathbf{R}^N \to \mathbf{R} \cup \{\infty\}$ be the indicator function defined as

$$R_k(\mathbf{u}) \coloneqq \begin{cases} 0 & \|\mathbf{u}\|_0 \leq k \\ \infty & \text{otherwise} \end{cases}. \tag{4.32}$$

Then, (4.31) is equivalent to

$$\underset{\mathbf{u}\in\mathbb{R}^M}{\text{minimize}} \ H_{\mathbf{s}}(\mathbf{D}\mathbf{u}) + R_k(\mathbf{u}) \tag{4.33}$$

and the proximal operator of R_k, denoted by $\mathcal{H}_k : \mathbb{R}^M \to \mathbb{R}^M$, in particular, is given as the *hard thresholding operator*, which sets all but the largest (in absolute terms) k elements of the input vector to zeros.

In [55], the use of the hard constraint function is proposed, where an ADMM-based approach called the SPADE algorithm is provided. For application to noisy cases, a new algorithm using the loss function given in Section 3.1 is proposed.

4.3.2 Signal Restoration Algorithm

Consider the optimization problem of (4.33) with the loss function $H_{\mathbf{s}} : \mathbb{R}^N \to \mathbb{R} \cup \{\infty\}$ defined as

$$H_{\mathbf{s}}(\mathbf{z}) \coloneqq \sum_{n=1}^{N} (F_0(z_n) - s_n z_n) \quad (\mathbf{z} \coloneqq [z_1, \ldots, z_N]^{\mathsf{T}} \in \mathbb{R}^N). \tag{4.34}$$

Algorithm 5 Proposed signal restoration algorithm

Require: $\mathbf{u} \in \mathbb{R}^M$, $\mathbf{y} \in \mathbb{R}^N$, $\mathbf{v} \in \mathbb{R}^N$, $\rho \in (0, \infty)$, $\gamma \in (0, 1/(\rho\|\mathbf{D}\|_{\mathrm{op}}^2)]$, $\mu \in (0, 1/(\rho + \mathrm{Lip}(f))]$

repeat

$k \leftarrow k + 1$

$\mathbf{u} \leftarrow \mathcal{H}_k\left(\mathbf{u} - \gamma\mathbf{D}^*[\mathbf{v} + \rho(\mathbf{D}\mathbf{u} - \mathbf{y})]\right)$

$\mathbf{y} \leftarrow \mathbf{y} - \mu\left([f(\mathbf{y}) - \mathbf{s}] - [\mathbf{v} + \rho(\mathbf{D}\mathbf{u} - \mathbf{y})]\right)$

$\mathbf{v} \leftarrow \mathbf{v} + \rho(\mathbf{D}\mathbf{u} - \mathbf{y})$

until a stopping criterion is satisfied

return $\mathbf{z} = \mathbf{D}\mathbf{x}$

Table 4.2: Normalized mean squared errors for data 1 (female voice) with $\sigma = 0$.

Condition	$\tau = 0.1$	$\tau = 0.2$
Proposed	−6.89 dB	−14.72 dB
Hard constraint	−11.75 dB	−15.65 dB
Soft consistency	−6.08 dB	−13.26 dB
Minimum norm	−3.24 dB	−6.96 dB

Table 4.3: Normalized mean squared errors for data 1 (female voice) with $\sigma = 10^{-3}$.

Condition	$\tau = 0.1$	$\tau = 0.2$
Proposed	−6.55 dB	−14.08 dB
Hard constraint	−4.79 dB	−10.53 dB
Soft consistency	−4.75 dB	−10.50 dB
Minimum norm	−3.93 dB	−8.30 dB

Its derivative is given by

$$\nabla H_{\mathbf{s}}(\mathbf{z}) = f(\mathbf{z}) - \mathbf{s}. \tag{4.35}$$

Therefore, several algorithms, such as proximal gradient descent [78] and PL-ADMM [66], are available to solve (4.33). Here, a PL-ADMM-based signal restoration algorithm is provided as Algorithm 5.

4.3.3 Numerical Experiments

Numerical experiments of signal restoration were conducted to demonstrate the restoration performance of the proposed method. The proposed method (denoted by **Proposed**)

was compared with similar algorithms where the hard constraint loss function and soft consistency loss function were used (denoted by **Hard constraint** and **Soft consistency**, respectively). Here, in **Hard constraint** and **Soft consistency**, Algorithm 5 was used where the update rule for $\mathbf{y}$ was replaced by

$$\mathbf{y} \leftarrow \mathrm{proj}_{f^{-1}(\mathbf{s})}(\mathbf{v}/\rho + \mathbf{D}\mathbf{u}) \tag{4.36}$$

and

$$\mathbf{y} \leftarrow \mathbf{y} - \mu \left([\mathbf{y} - \mathrm{proj}_{f^{-1}(\mathbf{s})}(\mathbf{y})] - [\mathbf{v} + \rho(\mathbf{D}\mathbf{u} - \mathbf{y})] \right), \tag{4.37}$$

respectively.

For audio examples, i.e., true $\mathbf{z}$, two data of human voices taken from the RWCP-SP99 database [79] were used. Each data was around 3 s, sampled at 16 kHz with 16 bit encoding, and normalized so that its maximum absolute value was equal to 1. The nonlinear saturation effect was set as

$$f_0(z) \coloneqq \begin{cases} -\tau & z \in (-\infty, -\frac{\pi}{2}\tau] \\ \tau \sin(z/\tau) & z \in (-\frac{\pi}{2}\tau, \frac{\pi}{2}\tau) \\ \tau & z \in (\frac{\pi}{2}\tau, \infty) \end{cases} \tag{4.38}$$

with two values of τ, i.e., $\tau = 0.1$ and $\tau = 0.2$. The observational noises $\boldsymbol{\epsilon} \in \mathbb{R}^N$ were added after saturation effects, where each element of $\boldsymbol{\epsilon}$ was determined independently according to the univariate normal distribution with mean 0 and variance σ^2. Here, two values of σ were investigated, i.e., $\sigma = 0$ and $\sigma = 10^{-3}$.

As a preprocessing, $\mathbf{s}$ was projected into $\mathrm{Range}(f)$, i.e., s_n was projected into $[-\tau, \tau]$ for each $n \in [\![1, N]\!]$. In each method, framewise analysis was applied as follows. First, let $N_{\mathrm{frame}} = 1024$ and $N_{\mathrm{shift}} = N_{\mathrm{frame}}/8$. Then, each observed data was first padded with $N_{\mathrm{frame}} - N_{\mathrm{shift}}$ zeros at the beginning. Then, the signal was restored by Algorithm 5 per every N_{frame} samples with shift N_{shift}. The end of the data was also padded with zeros as in the beginning. Finally, each framewise restored data was multiplied by $1/8$, and the whole restored data was obtained by their summation. In the framewise restoration, $\mathbf{D}$ was defined as the inverse discrete cosine transform (IDCT), which is a unitary matrix. The parameters were set as $\rho = 0.1$, $\gamma = 1/\rho$, and $\mu = 1/(\rho + 1)$ since $\|\mathbf{D}\|_{\mathrm{op}} = 1$ and $\mathrm{Lip}(f) = 1$. Note that the update rules of **Hard constraint** correspond to those of the SPADE algorithm [55] in these settings. The initial values for $\mathbf{u}$, $\mathbf{y}$, and $\mathbf{v}$ were set as zero vectors. The stopping condition was defined as $\|f(\mathbf{D}\mathbf{u}) - \mathbf{s}\|_2 \leq \varepsilon$ with $\varepsilon = 0.5$.

As an evaluation criterion, the normalized mean squared error (NMSE) was used, which was defined as

$$\mathrm{NMSE}(\hat{\mathbf{z}}, \mathbf{z}_{\mathrm{true}}) \coloneqq 10 \log_{10} \frac{\|\hat{\mathbf{z}} - \mathbf{z}_{\mathrm{true}}\|_2^2}{\|\mathbf{z}_{\mathrm{true}}\|_2^2}, \tag{4.39}$$

Table 4.4: Normalized mean squared errors for data 2 (male voice) with $\sigma = 0$.

Condition	$\tau = 0.1$	$\tau = 0.2$
Proposed	$-9.28\,\mathrm{dB}$	$-16.98\,\mathrm{dB}$
Hard constraint	$-12.20\,\mathrm{dB}$	$-17.72\,\mathrm{dB}$
Soft consistency	$-8.55\,\mathrm{dB}$	$-16.13\,\mathrm{dB}$
Minimum norm	$-4.46\,\mathrm{dB}$	$-9.05\,\mathrm{dB}$

Table 4.5: Normalized mean squared errors for data 2 (male voice) with $\sigma = 10^{-3}$.

Condition	$\tau = 0.1$	$\tau = 0.2$
Proposed	$-8.74\,\mathrm{dB}$	$-16.15\,\mathrm{dB}$
Hard constraint	$-6.39\,\mathrm{dB}$	$-12.31\,\mathrm{dB}$
Soft consistency	$-6.33\,\mathrm{dB}$	$-12.30\,\mathrm{dB}$
Minimum norm	$-5.26\,\mathrm{dB}$	$-10.29\,\mathrm{dB}$

where $\hat{\mathbf{z}}$ and $\mathbf{z}_{\mathrm{true}}$ respectively denote the restored and true signals. Also, as a baseline, a minimum-norm inversion of f to $\mathbf{s}$, i.e.,

$$\hat{\mathbf{z}}_{\min} = \underset{\mathbf{z}\in f^{-1}(\mathbf{s})}{\arg\min} \left(\|\mathbf{z}\|_2\right), \tag{4.40}$$

was defined (denoted by **Minimum norm**). The results are shown in Tables 4.2, 4.3, 4.4, and 4.5. One can see that **Proposed** achieved the lowest NMSEs for $\sigma = 10^{-3}$, and also that NMSEs for **Proposed** showed relatively little degradation in noisy cases compared with those for **Hard constraint** and **Soft consistency**. This is considered to be due to the continuity of the loss function. In particular, for **Hard constraint** and **Soft consistency**, it is difficult to restore the signal such that its true amplitude is outside $[-\tau, \tau]$ but the observed amplitude is within $[-\tau, \tau]$ owing to the observation noise because of the discontinuity of the loss functions. These results demonstrated the robustness of the proposed method compared with other current methods.

Chapter 5

Measurement of Sound Field

This chapter focuses on practical problems of sound field measurement. As in Chapter 4, the methodological framework is based on Chapter 3; however, several contributions are presented to improve estimation accuracy in comparison with other current sound field estimation methods. In Section 5.1, the research background and related studies on sound field estimation problems are summarized. Sections 5.2 and 5.3 present sound field estimation methods focusing on different topics and also provide the results of their experimental evaluations.

5.1 Research Background

Capturing a sound field is an essential technique for its analysis, visualization, and other related applications. In the field of spatial audio, in particular, sound field estimation techniques using multiple sensors (i.e., microphones) have attracted considerable attention owing to their wide variety of applications, such as the reproduction of a captured sound field using loudspeakers [7, 8, 80, 81] or headphones [5, 6, 19] and spatial active noise control [9, 82, 83].

Sound field estimation methods are classified on the basis of whether sound sources are allowed to exist inside the target region [25, 26, 84–86] or not [8, 17, 18, 20, 21, 87]. In general, the former case is much more difficult than the latter and often requires additional assumptions, such as the spatial sparsity of the source distribution and a reverberant-free condition. This chapter focuses on the sound field estimation inside a source-free target region as shown in Figure 5.1. Note that sound sources may also exist outside the target region in this context.

There are a large number of sound field estimation methods for source-free target regions, which can be further classified on the basis of whether a continuous distribution of sensors is assumed or not. For example, many well-established methods are based on the use of a planar, linear, spherical, cylindrical, or circular array of sensors with specific directivity (e.g., omnidirectional or bidirectional) [7, 88, 89]. In these methods, a sound field is described analytically from the boundary values observed by the sensor arrays

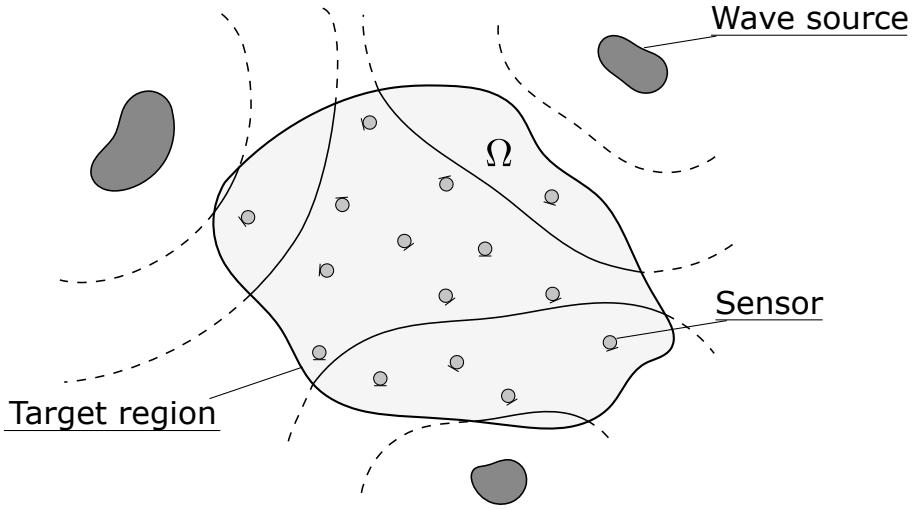

Fig. 5.1: Problem setting of sound field estimation.

on the basis of the Kirchhoff–Helmholtz integral equation or the Rayleigh integral equation [37]. Therefore, the complete reconstruction of the sound field can be achieved in principle as long as errors caused by the discretization of the sensor distribution and the observation noises are small enough to be ignored. However, the implementation of such arrays is difficult except for in a specially designed environment, which limits their scope of practical application.

There have also been several methods allowing a discrete sensor distribution. For example, in [20], a sound field is expanded by spherical wavefunctions [90] up to a certain truncation order, and their coefficients are estimated by solving a linear equation describing the relationship between the unknown coefficients and the observed signals. As seen in this work, most methods allowing a discrete sensor distribution are based on the representation of a sound field using a finite number of certain basis functions and the estimation of their coefficients by solving the linear equation. In this approach, however, basis functions are often chosen in an empirical manner, and their inappropriate setting may degrade estimation accuracy.

This chapter presents sound field estimation methods based on theories of Hilbert space. By considering sound fields as elements of an infinite-dimensional Hilbert space as in Section 2.2, the empirical (and possibly inappropriate) choice of a finite number of basis functions can be avoided in the proposed methods; this is the first such attempt in the literature concerning sound field estimation methods allowing a discrete sensor distribution. Section 5.2 presents a basic framework of the proposed estimation method in cases where linear observation with arbitrary sensor directivity is assumed, which falls into a simple linear inverse problem with Hilbertian regularization described in Section 3.4 from an optimization viewpoint. However, a flexible formulation of an inner product inducing

the regularization function is proposed, from which we can exploit prior information on the source direction if available to improve the estimation accuracy. Section 5.3 presents a field estimation method considering a nonlinear saturation effect; this is also the first such attempt in the field of spatial audio.

5.2 Sound Field Estimation Exploiting Prior Information on Source Direction

This section presents a sound field estimation method exploiting prior information on the source direction. Since linear observation is considered here, sound fields and observed signals are considered in the angular frequency domain for theoretical convenience.

5.2.1 Preliminaries

First, we provide preliminaries on the representation of sound fields and the modeling of sensor directivities.

5.2.1.1 Representation of Sound Fields

Let $\Omega \subseteq \mathbb{R}^3$ be a simply connected open subset of $\mathbb{R}^3$ and $u : \Omega \to \mathbb{C}$ be a sound field in Ω at a fixed angular frequency $\omega \in \mathbb{R}$, i.e., $u(\boldsymbol{r})$ denotes the sound pressure at $\boldsymbol{r} \in \Omega$. If Ω does not include any sound sources, u can be well modeled as a solution of the following (homogeneous) Helmholtz equation [37]:

$$(\Delta + k^2)u = 0, \tag{5.1}$$

where Δ denotes the Laplace operator and $k \coloneqq \omega/c$ is the wavenumber with $c \in (0, \infty)$ being the speed of sound, which is assumed to be constant in Ω. A typical modeling of u satisfying (5.1) is a superposition of plane-wave functions as follows:

$$u(\boldsymbol{r}) = \int_{\boldsymbol{x} \in \mathbb{S}_2} \tilde{u}(\boldsymbol{x}) \exp(-ik\boldsymbol{x} \circ \boldsymbol{r}) \, \mathrm{d}\chi \quad (\boldsymbol{r} \in \Omega). \tag{5.2}$$

Here, $\tilde{u} \in \mathcal{L}_2(\mathbb{S}_2, \mathbb{C})$ represents the complex amplitude of plane waves arriving from each direction. Let $\mathscr{P}$ denote a transform of functions from $\tilde{u}$ to u defined as (5.2) and $\mathcal{U}$ be an infinite-dimensional function space defined as

$$\mathcal{U} \coloneqq \{\mathscr{P}\tilde{u} \mid \tilde{u} \in \mathcal{L}_2(\mathbb{S}_2, \mathbb{C})\}. \tag{5.3}$$

In what follows, the tilde symbol over a letter denotes the inverse of $\mathscr{P}$ (e.g., $\tilde{u} \coloneqq \mathscr{P}^{-1}u$). Although $\mathcal{U}$ does not include all the solutions of (5.1), any solution of (5.1) can be approximated arbitrarily by functions in $\mathcal{U}$ in the sense of the uniform convergence on compact sets (see Appendix B.1 for a proof). Therefore, a sound field estimation problem can be regarded practically as a process of determining a function u within $\mathcal{U}$ on the basis of some criterion.

5.2.1.2 Modeling of Sensor Directivity

Consider a single sensor with a certain directivity located at $\boldsymbol{r}_0 \in \Omega$ in a sound field $u \in \mathcal{U}$. Its directivity can be modeled as the directional function $\gamma \in \mathcal{L}_2(\mathbb{S}_2, \mathbb{C})$, i.e., $\gamma(\boldsymbol{x})$ denotes the sensor's response to the plane wave arriving from the direction $\boldsymbol{x} \in \mathbb{S}_2$. For example, omnidirectional, bidirectional, and first-order sensors are respectively modeled with constant parameters $\boldsymbol{y} \in \mathbb{S}_2$ and $\zeta \in [0, 1]$ as follows.

Omnidirectional:

$$\gamma(\boldsymbol{x}) \coloneqq 1 \quad (\boldsymbol{x} \in \mathbb{S}_2)$$

Bidirectional:

$$\gamma(\boldsymbol{x}) \coloneqq \boldsymbol{y} \circ \boldsymbol{x} \quad (\boldsymbol{x} \in \mathbb{S}_2)$$

First-order:

$$\gamma(\boldsymbol{x}) \coloneqq \zeta + (1 - \zeta)\boldsymbol{y} \circ \boldsymbol{x} \quad (\boldsymbol{x} \in \mathbb{S}_2)$$

In many practical cases including the above examples, the directivity γ can be well represented using finite-order spherical harmonic functions as

$$\gamma(\boldsymbol{x})^* = \sum_{\nu,\mu}^{N} c_{\nu,\mu} Y_{\nu,\mu}(\boldsymbol{x}) \quad (\boldsymbol{x} \in \mathbb{S}_2), \tag{5.4}$$

where $N \in \mathbb{N}$ is the maximum order, $\sum_{\nu,\mu}^{N}$ is the abbreviated form of $\sum_{\nu=0}^{N} \sum_{\mu=-\nu}^{\nu}$, and $Y_{\nu,\mu}(\cdot) : \mathbb{S}_2 \to \mathbb{C}$ denotes the spherical harmonic function of order $\nu \in \mathbb{N}$ and degree $\mu \in [\![-\nu, \nu]\!]$ (see [90] for the definition and [91] for an efficient computational algorithm). Here, the complex conjugate on the right-hand side of (5.4) is used to simplify later discussion.

Since u can be expanded around $\boldsymbol{r}_0$ as

$$u(\boldsymbol{r}) = \int_{\boldsymbol{x} \in \mathbb{S}_2} \tilde{u}(\boldsymbol{x}) \exp(-ik\boldsymbol{x} \circ \boldsymbol{r}_0) \cdot \exp(-ik\boldsymbol{x} \circ (\boldsymbol{r} - \boldsymbol{r}_0)) \, \mathrm{d}\chi \quad (\boldsymbol{r} \in \Omega), \tag{5.5}$$

the observed signal $s_0 \in \mathbb{C}$ of the sensor is given by

$$s_0 = \int_{\boldsymbol{x} \in \mathbb{S}_2} \tilde{u}(\boldsymbol{x}) \exp(-ik\boldsymbol{x} \circ \boldsymbol{r}_0) \gamma(\boldsymbol{x}) \, \mathrm{d}\chi + \epsilon_0, \tag{5.6}$$

where $\epsilon_0 \in \mathbb{C}$ is the observation noise. Hereafter, the simplified notation

$$s_0 = \mathcal{F}u + \epsilon \tag{5.7}$$

is used, where $\mathcal{F} : \mathcal{U} \to \mathbb{C}$ is a functional defined as

$$\mathcal{F}u \coloneqq \int_{\boldsymbol{x} \in \mathbb{S}_2} \tilde{u}(\boldsymbol{x}) \exp(-ik\boldsymbol{x} \circ \boldsymbol{r}_0) \gamma(\boldsymbol{x}) \, \mathrm{d}\chi \quad (u \in \mathcal{U}). \tag{5.8}$$

In addition, $\mathcal{F}$ is referred to as an observation operator of the sensor. Note that $\mathcal{F}$ is a linear functional on $\mathcal{U}$, which means the superposition principle in the observation.

5.2.2 Formulation

Let $M \in \mathbb{N}$ sensors be located arbitrarily in Ω as shown in Figure 5.1. For each $m \in [\![1, M]\!]$, the position, directivity, and observed signal of the mth sensor are respectively denoted by $\boldsymbol{r}_m \in \Omega$, $\gamma_m \in \mathcal{L}_2(\mathbb{S}_2, \mathbb{C})$, and $s_m \in \mathbb{C}$, and they are assumed to be given. In this case, the observation operator of the mth sensor, denoted by $\mathcal{F}_m$, is given for each $m \in [\![1, M]\!]$ by

$$\mathcal{F}_m u \coloneqq \int_{\boldsymbol{x} \in \mathbb{S}_2} \tilde{u}(\boldsymbol{x}) \exp(-ik\boldsymbol{x} \circ \boldsymbol{r}_m) \gamma_m(\boldsymbol{x}) \, \mathrm{d}\chi \quad (u \in \mathcal{U}). \tag{5.9}$$

We consider the following formulation of sound field estimation problems:

$$\underset{u \in \mathcal{U}}{\text{minimize}} \quad Q(u) \coloneqq \sum_{m=1}^{M} \frac{1}{\sigma_m^2} \left| \mathcal{F}_m u - s_m \right|^2 + \lambda \|u\|_{\mathcal{U}}^2, \tag{5.10}$$

where $\sigma_1, \ldots, \sigma_M \in (0, \infty)$ are dispersion parameters representing the observational uncertainty, $\lambda \in (0, \infty)$ is a regularization parameter, and $\| \cdot \|_{\mathcal{U}} : \mathcal{U} \to [0, \infty)$ is a norm on $\mathcal{U}$, which is defined later. The first term of (5.10) is a loss term, which represents the deviation between the predicted values $\mathcal{F}_1 u, \ldots, \mathcal{F}_M u$ and the observed values $s_1, \ldots, s_M$. On the other hand, the second term is a regularization term, which evaluates the reasonability of u independently of the observation. If we can design the norm $\| \cdot \|_{\mathcal{U}}$ so that the sound fields that are likely to occur have small norms, the solution of (5.10) will be induced to such sound fields. Therefore, it is desirable to design an appropriate norm exploiting prior information of sound fields.

On the basis of the above discussion, we introduce the norm $\| \cdot \|_{\mathcal{U}}$ over $\mathcal{U}$ defined as

$$\|u\|_{\mathcal{U}} \coloneqq \left(\int_{\boldsymbol{x} \in \mathbb{S}_2} \frac{|\tilde{u}(\boldsymbol{x})|^2}{w(\boldsymbol{x})} \, \mathrm{d}\chi \right)^{\frac{1}{2}} \quad (u \in \mathcal{U}). \tag{5.11}$$

Here, $w : \mathbb{S}_2 \to (0, \infty)$ is a directional weighting function defined as

$$w(\boldsymbol{x}) \coloneqq \frac{1}{4\pi C(\beta)} \exp(\beta \boldsymbol{\eta} \circ \boldsymbol{x}) \quad (\boldsymbol{x} \in \mathbb{S}_2), \tag{5.12}$$

where $\beta \in [0, \infty)$ and $\boldsymbol{\eta} \in \mathbb{S}_2$ are constant parameters and $C(\beta)$ is a scaling constant (so that w satisfies $\int_{\boldsymbol{x} \in \mathbb{S}_2} w(\boldsymbol{x}) \, \mathrm{d}\chi = 1$) defined as

$$C(\beta) \coloneqq \begin{cases} 1 & (\beta = 0) \\ (\exp(\beta) - \exp(-\beta))/(2\beta) & (\beta \in (0, \infty)) \end{cases}. \tag{5.13}$$

This function w is also known as the probability density function of the von Mises–Fisher distribution used in directional statistics [92]. Note that $w(\boldsymbol{x})$ takes a large value when $\boldsymbol{x}$ is close to $\boldsymbol{\eta}$, especially in the case of large β. Therefore, by using this norm in (5.10), we can impose large penalties for sound fields originating from sound sources in a direction

away from $\boldsymbol{\eta}$ while imposing small penalties for sound fields from sound sources in a direction close to $\boldsymbol{\eta}$. When $\beta = 0$, on the contrary, the solution of (5.10) will be induced relatively to a diffuse field. The weighting function w can be further generalized by using a linear combination of (5.12) for different parameters β and $\boldsymbol{\eta}$, which is useful in cases of multiple sound sources. This extension is discussed in Section 5.2.2.3 after the basic concept of the proposed method is described.

5.2.2.1 Closed-Form Solution

Let $\langle \cdot, \cdot \rangle_{\mathcal{U}}$ be an inner product on $\mathcal{U}$ defined as

$$\langle u_1, u_2 \rangle_{\mathcal{U}} \coloneqq \int_{\boldsymbol{x} \in \mathbb{S}_2} \frac{\tilde{u}_1(\boldsymbol{x})^* \tilde{u}_2(\boldsymbol{x})}{w(\boldsymbol{x})} \, \mathrm{d}\chi \quad (u_1, u_2 \in \mathcal{U}). \tag{5.14}$$

Then, $(\mathcal{U}, \langle \cdot, \cdot \rangle_{\mathcal{U}})$ is a complex Hilbert space because it is isomorphic to the Hilbert space $\mathcal{L}_2(\mathbb{S}_2, \mathbb{C})$ with the weighted $\mathcal{L}_2$ inner product. Therefore, the optimization problem of (5.10) can be solved in a closed form as shown in Section 3.4, which is reiterated as follows.

First, using this inner product $\langle \cdot, \cdot \rangle_{\mathcal{U}}$, we can write the objective function as

$$Q(u) = \sum_{m=1}^{M} \frac{1}{\sigma_m^2} \left| \langle v_m, u \rangle_{\mathcal{U}} - s_m \right|^2 + \lambda \langle u, u \rangle_{\mathcal{U}} \quad (u \in \mathcal{U}), \tag{5.15}$$

where $v_1, \ldots, v_M \in \mathcal{U}$ are given by

$$v_m(\boldsymbol{r}) \coloneqq \int_{\boldsymbol{x} \in \mathbb{S}_2} w(\boldsymbol{x}) \gamma_m(\boldsymbol{x})^* \exp(-ik\boldsymbol{x} \circ (\boldsymbol{r} - \boldsymbol{r}_m)) \, \mathrm{d}\chi \quad (\boldsymbol{r} \in \Omega, \ m \in [\![1, M]\!]). \tag{5.16}$$

Then, we can apply the representer theorem [34, 60], which guarantees that the solution of (5.10), denoted by $u^{(\mathrm{opt})}$, has the form of

$$u^{(\mathrm{opt})} = \sum_{m=1}^{M} \alpha_m^{(\mathrm{opt})} v_m \tag{5.17}$$

with some $\boldsymbol{\alpha}^{(\mathrm{opt})} \coloneqq [\alpha_1^{(\mathrm{opt})}, \ldots, \alpha_M^{(\mathrm{opt})}]^{\mathsf{T}} \in \mathbb{C}^M$. Here, $\boldsymbol{\alpha}^{(\mathrm{opt})}$ can be obtained by solving the following optimization problem:

$$\underset{\boldsymbol{\alpha} \in \mathbb{C}^N}{\text{minimize}} \quad Q^{(*)}(\boldsymbol{\alpha}) \coloneqq (\mathbf{K}\boldsymbol{\alpha} - \mathbf{s})^{\mathsf{H}} \boldsymbol{\Sigma}^{-1} (\mathbf{K}\boldsymbol{\alpha} - \mathbf{s}) + \lambda \boldsymbol{\alpha}^{\mathsf{H}} \mathbf{K} \boldsymbol{\alpha}, \tag{5.18}$$

which is given by substituting $u = \sum_{m=1}^{M} \alpha_m v_m$ with $\boldsymbol{\alpha} \coloneqq [\alpha_1, \ldots, \alpha_M]^{\mathsf{T}}$ in (5.15). Here, $\mathbf{s} \in \mathbb{C}^M$, $\boldsymbol{\Sigma} \in \mathbb{C}^{M \times M}$, and $\mathbf{K} \in \mathbb{C}^{M \times M}$ are defined as

$$\mathbf{s} \coloneqq \begin{bmatrix} s_1 \\ \cdots \\ s_M \end{bmatrix}, \ \boldsymbol{\Sigma} \coloneqq \begin{bmatrix} \sigma_1^2 & & 0 \\ & \ddots & \\ 0 & & \sigma_M^2 \end{bmatrix}, \ \mathbf{K} \coloneqq \begin{bmatrix} K_{1,1} & \cdots & K_{1,M} \\ \vdots & \ddots & \vdots \\ K_{M,1} & \cdots & K_{M,M} \end{bmatrix} \tag{5.19}$$

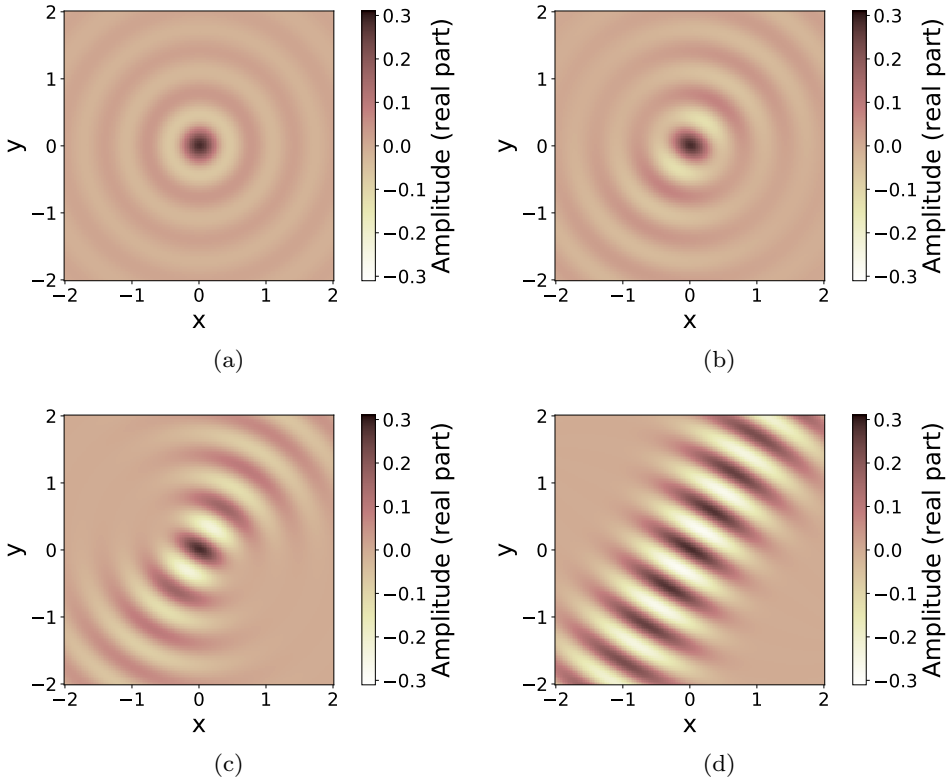

Fig. 5.2: Directionally weighted spherical wavefunctions of order $\nu = 0$ and degree $\mu = 0$ plotted in xy-plane ($\boldsymbol{r} = [\mathrm{x}, \mathrm{y}, 0]^\mathsf{T}$). (a) $\beta = 0$; (b) $\beta = 2$; (c) $\beta = 5$; (d) $\beta = 25$.

with

$$\begin{aligned} K_{m_1,m_2} &\coloneqq \langle v_{m_1}, v_{m_2} \rangle_{\mathcal{U}} \\ &= \int_{\boldsymbol{x} \in \mathbb{S}_2} w(\boldsymbol{x}) \gamma_{m_1}(\boldsymbol{x}) \gamma_{m_2}(\boldsymbol{x})^* \exp(-ik\boldsymbol{x} \circ (\boldsymbol{r}_{m_1} - \boldsymbol{r}_{m_2})) \, \mathrm{d}\chi \\ &\quad (m_1, m_2 \in [\![1, M]\!]). \end{aligned} \tag{5.20}$$

Finally, by solving (5.18), we obtain

$$\boldsymbol{\alpha}^{(\mathrm{opt})} = (\mathbf{K} + \lambda \boldsymbol{\Sigma})^{-1} \mathbf{s}, \tag{5.21}$$

and $u^{(\mathrm{opt})}$ is given by substituting (5.21) into (5.17). Therefore, the remaining problems are the calculations of $v_1, \ldots, v_M$ and $\mathbf{K}$.

5.2.2.2 Directionally Weighted Spherical Wavefunctions and Directionally Weighted Translation Operators

As noted in Section 5.2.1.2, the directivities of various sensors can be well modeled by finite-order spherical harmonic functions. Suppose $\gamma_1, \ldots, \gamma_M$ can be represented as

$$\gamma_m(\boldsymbol{x})^* = \sum_{\nu,\mu}^{N_m} c_{m,\nu,\mu} Y_{\nu,\mu}(\boldsymbol{x}) \quad (\boldsymbol{x} \in \mathbb{S}_2, \ m \in [\![1, M]\!]) \tag{5.22}$$

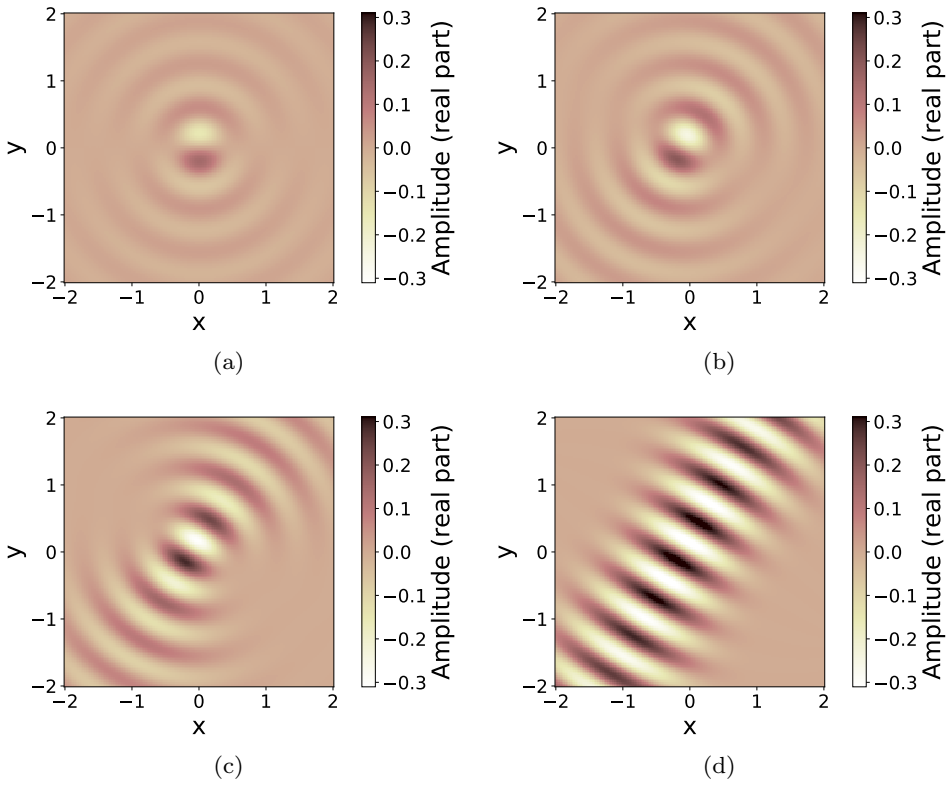

Fig. 5.3: Directionally weighted spherical wavefunctions of order $\nu = 1$ and degree $\mu = 1$ plotted in xy-plane ($\boldsymbol{r} = [\mathrm{x}, \mathrm{y}, 0]^{\mathsf{T}}$). (a) $\beta = 0$; (b) $\beta = 2$; (c) $\beta = 5$; (d) $\beta = 25$.

with $N_1, \ldots, N_M \in \mathbb{N}$. Then, by substituting (5.12) and (5.22) into (5.16) and (5.20) and solving the integrals (see Appendix B.2 for detailed derivations), we obtain

$$v_m(\boldsymbol{r}) = \sum_{\nu,\mu}^{N_m} c_{m,\nu,\mu} \varphi_{\nu,\mu}(\boldsymbol{r} - \boldsymbol{r}_m) \quad (\boldsymbol{r} \in \Omega,\ m \in [\![1, M]\!]), \tag{5.23}$$

$$K_{m_1,m_2} = \sum_{\nu_1,\mu_1}^{N_{m_1}} \sum_{\nu_2,\mu_2}^{N_{m_2}} c^*_{m_1,\nu_1,\mu_1} c_{m_2,\nu_2,\mu_2} T^{\nu_2,\mu_2}_{\nu_1,\mu_1}(\boldsymbol{r}_{m_1} - \boldsymbol{r}_{m_2}) \quad (m_1, m_2 \in [\![1, M]\!]), \tag{5.24}$$

where

$$\varphi_{\nu,\mu}(\boldsymbol{r}) \coloneqq \frac{1}{C(\beta)} \xi_{\nu,\mu}(k\boldsymbol{r} + i\beta\boldsymbol{\eta}) \quad (\boldsymbol{r} \in \mathbb{R}^3,\ \nu \in \mathbb{N},\ \mu \in [\![-\nu, \nu]\!]), \tag{5.25}$$

$$T^{\nu_2,\mu_2}_{\nu_1,\mu_1}(\boldsymbol{r}) \coloneqq \frac{1}{C(\beta)} \Theta^{\nu_2,\mu_2}_{\nu_1,\mu_1}(k\boldsymbol{r} + i\beta\boldsymbol{\eta}) \quad (\boldsymbol{r} \in \mathbb{R}^3,\ \nu_1, \nu_2 \in \mathbb{N},\ \mu_1 \in [\![-\nu_1, \nu_1]\!],\ \mu_2 \in [\![-\nu_2, \nu_2]\!]) \tag{5.26}$$

with

$$\xi_{\nu,\mu}(\boldsymbol{z}) \coloneqq \frac{1}{i^\nu} j_\nu\left(\left(z_1^2+z_2^2+z_3^2\right)^{\frac{1}{2}}\right) y_{\nu,\mu}\left(\frac{\boldsymbol{z}}{\left(z_1^2+z_2^2+z_3^2\right)^{\frac{1}{2}}}\right)$$
$$(\boldsymbol{z} \coloneqq [z_1,z_2,z_3]^\mathsf{T} \in \mathbb{C}^3,\ \nu \in \mathbb{N},\ \mu \in [\![-\nu,\nu]\!]), \tag{5.27}$$

$$\Theta_{\nu_1,\mu_1}^{\nu_2,\mu_2}(\boldsymbol{z}) \coloneqq \sum_{\nu_3,\mu_3}^{\nu_1+\nu_2} \mathcal{G}(\nu_1,\mu_1;\nu_2,\mu_2;\nu_3,\mu_3)\xi_{\nu_3,\mu_3}(\boldsymbol{z})$$
$$(\boldsymbol{z} \in \mathbb{C}^3,\ \nu_1,\nu_2 \in \mathbb{N},\ \mu_1 \in [\![-\nu_1,\nu_1]\!],\ \mu_2 \in [\![-\nu_2,\nu_2]\!]). \tag{5.28}$$

Here, $j_\nu(\cdot) : \mathbb{C} \to \mathbb{C}$ is the νth-order spherical Bessel function of the first kind, $y_{\nu,\mu}(\cdot) : \mathbb{C}^3 \to \mathbb{C}$ is the normalized homogeneous harmonic polynomial [90] of order ν and degree μ (i.e., a homogeneous harmonic polynomial satisfying $y_{\nu,\mu}(\boldsymbol{x}) = Y_{\nu,\mu}(\boldsymbol{x})$ for $\boldsymbol{x} \in \mathbb{S}_2$), and $\mathcal{G}(\cdot)$ denotes the Gaunt coefficient with a slight modification regarding complex conjugation, which is defined as

$$\mathcal{G}(\nu_1,\mu_1;\nu_2,\mu_2;\mu_3;\mu_3)$$
$$\coloneqq \int_{\boldsymbol{x}\in\mathbb{S}_2} Y_{\nu_1,\mu_1}(\boldsymbol{x})^* Y_{\nu_2,\mu_2}(\boldsymbol{x}) Y_{\nu_3,\mu_3}(\boldsymbol{x})^* \,\mathrm{d}\chi$$
$$(\nu_1,\nu_2,\nu_3 \in \mathbb{N},\ \mu_1 \in [\![-\nu_1,\nu_1]\!],\ \mu_2 \in [\![-\nu_2,\nu_2]\!],\ \mu_3 \in [\![-\nu_3,\nu_3]\!]). \tag{5.29}$$

The closed-form expression of (5.29) can be obtained using the formulae in [90], and an efficient computational algorithm is proposed in [93]. Note that (5.27) is well defined independently from branches of the 1/2-power function and can also be defined at $\boldsymbol{z} = [z_1,z_2,z_3]^\mathsf{T} \in \mathbb{C}^3$ such that $z_1^2+z_2^2+z_3^2 = 0$ by using limit values because these points are removable singularities.

When $\beta = 0$, it can be immediately shown that (5.25) and (5.26) correspond respectively to the usual spherical wavefunction and translation operator [21, 81, 87] (except for the constant coefficients). Therefore, (5.25) and (5.26) are hereafter referred to as a *directionally weighted spherical wavefunction* and a *directionally weighted translation operator*, respectively. Several examples of directionally weighted spherical wavefunctions are shown in Figure 5.2, where $k = 10$ and $\boldsymbol{\eta} = [\cos(\pi/3), \sin(\pi/3), 0]^\mathsf{T}$. One can see that these functions become close to the plane-wave function arriving from $\boldsymbol{\eta}$ as β increases.

As a special case, consider the observation with omnidirectional sensors, i.e., $\gamma_m(\boldsymbol{x}) = 1$ $(\boldsymbol{x} \in \mathbb{S}_2,\ m \in [\![1,M]\!])$. Here, we obtain

$$v_m(\boldsymbol{r}) = \sqrt{4\pi}\varphi_{0,0}(\boldsymbol{r}-\boldsymbol{r}_m) \quad (\boldsymbol{r} \in \Omega,\ m \in [\![1,M]\!]), \tag{5.30}$$

$$K_{m_1,m_2} = \sqrt{4\pi}\varphi_{0,0}(\boldsymbol{r}_{m_1}-\boldsymbol{r}_{m_2}) \quad (m_1,m_2 \in [\![1,M]\!]). \tag{5.31}$$

In this case, the proposed method corresponds to kernel ridge regression [94] with the kernel function $\kappa : \Omega \times \Omega \to \mathbb{C}$ defined as

$$\kappa(\boldsymbol{r}_1,\boldsymbol{r}_2) \coloneqq \sqrt{4\pi}\varphi_{0,0}(\boldsymbol{r}_1-\boldsymbol{r}_2) \quad (\boldsymbol{r}_1,\boldsymbol{r}_2 \in \Omega), \tag{5.32}$$

i.e., $(\mathcal{U}, \langle\cdot,\cdot\rangle_{\mathcal{U}})$ is a reproducing kernel Hilbert space [65] generated by κ.

5.2.2.3 Extension to Multiple Sound Sources

The proposed method can be easily extended to cases of multiple sound sources. The weighting function w can be generalized as

$$w(\boldsymbol{x}) \coloneqq \sum_{l=1}^{L} a_l C(\beta_l) \exp(\beta_l \boldsymbol{\eta}_l \circ \boldsymbol{x}) \quad (\boldsymbol{x} \in \mathbb{S}_2), \tag{5.33}$$

where $L \in \mathbb{N}$, $a_1, \ldots, a_L \in [0,1]$, $\beta_1, \ldots, \beta_L \in [0,\infty)$, and $\boldsymbol{\eta}_1, \ldots, \boldsymbol{\eta}_L \in \mathbb{S}_2$ are the constant parameters satisfying $\sum_{l=1}^{L} a_l = 1$. Then, the directionally weighted spherical wavefunctions and directionally weighted translation operators are given by

$$\varphi_{\nu,\mu}(\boldsymbol{r}) \coloneqq \sum_{l=1}^{L} \frac{a_l}{C(\beta_l)} \xi_{\nu,\mu}(k\boldsymbol{r} + i\beta_l \boldsymbol{\eta}_l) \quad (\boldsymbol{r} \in \mathbb{R}^3,\ \nu \in \mathbb{N},\ \mu \in [\![-\nu, \nu]\!]), \tag{5.34}$$

$$T^{\nu_2,\mu_2}_{\nu_1,\mu_1}(\boldsymbol{r}) \coloneqq \sum_{l=1}^{L} \frac{a_l}{C(\beta_l)} \Theta^{\nu_2,\mu_2}_{\nu_1,\mu_1}(k\boldsymbol{r} + i\beta_l \boldsymbol{\eta}_l) \\ (\boldsymbol{r} \in \mathbb{R}^3,\ \nu_1, \nu_2 \in \mathbb{N},\ \mu_1 \in [\![-\nu_1, \nu_1]\!],\ \mu_2 \in [\![-\nu_2, \nu_2]\!]), \tag{5.35}$$

and $v_1, \ldots, v_M$ and $\mathbf{K}$ can be obtained by substituting (5.34) and (5.35) into (5.23) and (5.24), respectively.

5.2.3 Comparison with Previous Methods

This section describes a comparison between the proposed method and the previous method proposed in [20] (also introduced as the *general sampling array approach* in [8]), which is hereafter referred to as the *truncation method*. In the truncation method, the sound field $u \in \mathcal{U}$ is expanded at a given expansion center $\boldsymbol{r}_0 \in \Omega$ by the spherical wavefunctions up to a certain truncation order $N \in \mathbb{N}$ as

$$u(\boldsymbol{r}) \approx \sum_{\nu,\mu}^{N} \mathring{u}_{\nu,\mu} \psi_{\nu,\mu}(\boldsymbol{r}) \quad (\boldsymbol{r} \in \Omega), \tag{5.36}$$

where $\mathring{u}_{\nu,\mu} \in \mathbb{C}$ is the expansion coefficient of order $\nu \in \mathbb{N}$ and degree $\mu \in [\![-\nu, \nu]\!]$, and $\psi_{\nu,\mu} \in \mathcal{U}$ denotes the basis functions given by

$$\psi_{\nu,\mu}(\boldsymbol{r}) \coloneqq \hat{\varphi}_{\nu,\mu}(\boldsymbol{r} - \boldsymbol{r}_0) \quad (\boldsymbol{r} \in \Omega,\ \nu \in [\![0, N]\!],\ \mu \in [\![-\nu, \nu]\!]) \tag{5.37}$$

with $\hat{\varphi}_{\nu,\mu}(\cdot) : \mathbb{R}^3 \to \mathbb{C}$ being the (usual) spherical wavefunction defined as

$$\hat{\varphi}_{\nu,\mu}(\boldsymbol{r}) \coloneqq \xi_{\nu,\mu}(k(\boldsymbol{r} - \boldsymbol{r}_0)) \quad (\boldsymbol{r} \in \mathbb{R}^3,\ \nu \in \mathbb{N},\ \mu \in [\![-\nu, \nu]\!]). \tag{5.38}$$

Then, we obtain the relationship between the expansion coefficients and the observed signals as

$$\mathbf{s} = \mathbf{D}\mathring{\boldsymbol{u}} + \boldsymbol{\epsilon}, \tag{5.39}$$

where $\mathbf{D} \in \mathbb{C}^{M\times(N+1)^2}$ and $\mathring{\boldsymbol{u}} \in \mathbb{C}^{(N+1)^2}$ are defined as

$$\mathbf{D} \coloneqq \begin{bmatrix} \mathcal{F}_1\psi_{0,0} & \cdots & \mathcal{F}_1\psi_{N,N} \\ \vdots & \ddots & \vdots \\ \mathcal{F}_M\psi_{0,0} & \cdots & \mathcal{F}_M\psi_{N,N} \end{bmatrix}, \ \mathring{\boldsymbol{u}} \coloneqq \begin{bmatrix} \mathring{u}_{0,0} \\ \vdots \\ \mathring{u}_{N,N} \end{bmatrix}. \tag{5.40}$$

Here, from [90], we have

$$\mathcal{F}_m\psi_{\nu,\mu} = \sum_{\nu',\mu'}^{N_m} \hat{T}_{\nu,\mu}^{\nu',\mu'}(\boldsymbol{r}_0 - \boldsymbol{r}_m)c_{m,\nu',\mu'} \quad (m \in [\![1, M]\!],\ \nu \in [\![0, N]\!],\ \mu \in [\![-\nu, \nu]\!]) \tag{5.41}$$

with $\hat{T}_{\nu,\mu}^{\nu',\mu'}(\cdot) : \mathbb{R}^3 \to \mathbb{C}$ being the (usual) translation operator defined as

$$\hat{T}_{\nu,\mu}^{\nu',\mu'}(\boldsymbol{r}) \coloneqq \Theta_{\nu,\mu}^{\nu',\mu'}(k\boldsymbol{r}) \quad (\boldsymbol{z} \in \mathbb{C}^3,\ \nu_1, \nu_2 \in \mathbb{N},\ \mu_1 \in [\![-\nu_1, \nu_1]\!],\ \mu_2 \in [\![-\nu_2, \nu_2]\!]). \tag{5.42}$$

From (5.39), $\mathring{\boldsymbol{u}}$ can be obtained by the regularized least squares as

$$\mathring{\boldsymbol{u}} = \mathbf{D}^{\mathsf{H}}(\mathbf{D}\mathbf{D}^{\mathsf{H}} + \lambda\mathbf{I}_M)\mathbf{s}, \tag{5.43}$$

and the estimated sound field $u_{\mathrm{est}} \in \mathcal{U}$ can be written in the form of

$$u_{\mathrm{est}} = \sum_{n=1}^{N} \overline{\alpha}_m \overline{v}_m. \tag{5.44}$$

Here, $\overline{\boldsymbol{\alpha}} \coloneqq [\overline{\alpha}_1, \ldots, \overline{\alpha}_M]^{\mathsf{T}}$ is given by

$$\overline{\boldsymbol{\alpha}} = (\overline{\mathbf{K}} + \lambda\mathbf{I}_M)^{-1}\mathbf{s} \tag{5.45}$$

with $\overline{\mathbf{K}} \coloneqq \mathbf{D}\mathbf{D}^{\mathsf{H}}$, whose (m_1, m_2)th element $\overline{K}_{m_1,m_2} \in \mathbb{C}$ is given by

$$\overline{K}_{m_1,m_2} = \sum_{\nu_1,\mu_1}^{N_{m_1}} \sum_{\nu_2,\mu_2}^{N_{m_2}} c^*_{m_1,\nu_1,\mu_1} c_{m_2,\nu_2,\mu_2} \sum_{\nu',\mu'}^{N} \hat{T}_{\nu_1,\mu_1}^{\nu',\mu'}(\boldsymbol{r}_0 - \boldsymbol{r}_{m_1})^* \hat{T}_{\nu_2,\mu_2}^{\nu',\mu'}(\boldsymbol{r}_0 - \boldsymbol{r}_{m_2}) \tag{5.46}$$

for each $m_1, m_2 \in [\![1, M]\!]$, and $\overline{v}_1, \ldots, \overline{v}_M \in \mathcal{U}$ is given by

$$\overline{v}_m(\boldsymbol{r}) = \sum_{\nu,\mu}^{N_m} c_{m,\nu,\mu} \sum_{\nu',\mu'}^{N} \hat{T}_{\nu,\mu}^{\nu',\mu'}(\boldsymbol{r}_0 - \boldsymbol{r}_m)\hat{\varphi}_{\nu',\mu'}(\boldsymbol{r} - \boldsymbol{r}_m) \quad (\boldsymbol{r} \in \Omega). \tag{5.47}$$

Here, from the addition theorems for spherical Bessel functions [81, 90], we have

$$\sum_{\nu',\mu'} \hat{T}_{\nu_1,\mu_1}^{\nu',\mu'}(\boldsymbol{r}_0 - \boldsymbol{r}_{m_1})^* \hat{T}_{\nu_2,\mu_2}^{\nu',\mu'}(\boldsymbol{r}_0 - \boldsymbol{r}_{m_2}) = \hat{T}_{\nu_1,\mu_1}^{\nu',\mu'}(\boldsymbol{r}_{m_1} - \boldsymbol{r}_{m_2}) \tag{5.48}$$

and

$$\sum_{\nu',\mu'} \hat{T}_{\nu,\mu}^{\nu',\mu'}(\boldsymbol{r}_0 - \boldsymbol{r}_m)\hat{\varphi}_{\nu',\mu'}(\boldsymbol{r} - \boldsymbol{r}_0) = \hat{\varphi}_{\nu,\mu}(\boldsymbol{r} - \boldsymbol{r}_m), \tag{5.49}$$

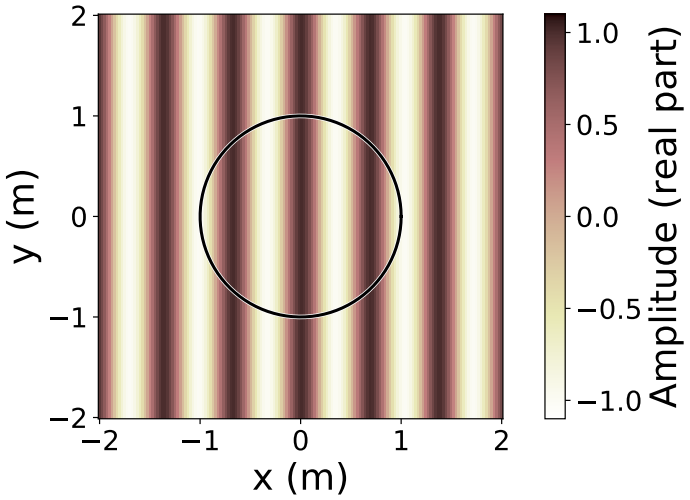

Fig. 5.4: True sound field under free-field condition at 500 Hz plotted in xy-plane ($\boldsymbol{r} = [\mathrm{x}, \mathrm{y}, 0]^{\mathsf{T}}\,\mathrm{m}$).

where $\sum_{\nu,\mu}$ is the abbreviated form of $\sum_{\nu=0}^{\infty}\sum_{\mu=-\nu}^{\nu}$. These equalities mean that $\overline{\mathbf{K}}$ and $\overline{v}_1, \ldots, \overline{v}_M$ respectively converges to $\mathbf{K}$ and $v_1, \ldots, v_M$ in the proposed method with $\beta = 0$ (and $\boldsymbol{\Sigma} = \mathbf{I}_M$) as $N \to \infty$ independently of the setting of $\boldsymbol{r}_0$. In the truncation method, the estimation depends on the position $\boldsymbol{r}_0$ and the truncation order N. In the proposed method, on the other hand, the infinite-dimensional modeling of sound fields enables us to estimate the sound field independently of $\boldsymbol{r}_0$ and N.

5.2.4 Numerical Experiments

Numerical experiments of sound field estimation using a microphone array were conducted to demonstrate the performance of the proposed method. The sound field in air was considered, and the speed of sound was set as $c = 340\,\mathrm{m/s}$. The proposed method was compared with the truncation method [20] described in Section 5.2.3. In addition, the proposed method for $\beta = 0$ (no prior information) was also investigated for comparison. Hereafter, the notation of temporal frequency is used instead of angular frequency.

5.2.4.1 Estimation of Plane-Wave Field under Free-Field Condition

In a three-dimensional free field, 64 microphones were located on a sphere with a radius of 1.0 m centered at the origin. Their positions were determined according to the spherical t-design [95]. Each microphone was modeled as a cardioid microphone oriented outward, i.e., the observed signals $s_1, \ldots, s_M$ in a sound field u were given by

$$s_m = \frac{1}{2}u(\boldsymbol{r}_m) - \frac{1}{2ik}\frac{\partial}{\partial \boldsymbol{y}_m}u(\boldsymbol{r}_m) + \epsilon_m \quad (m \in [\![1, M]\!]). \tag{5.50}$$

Here, for each $m \in [\![1, M]\!]$, $\boldsymbol{y}_m$ denotes the outward unit normal vector on the sphere at $\boldsymbol{r}_m$, $\partial/\partial \boldsymbol{y}_m$ denotes the directional derivative along the direction $\boldsymbol{y}_m$, and ϵ_m denotes

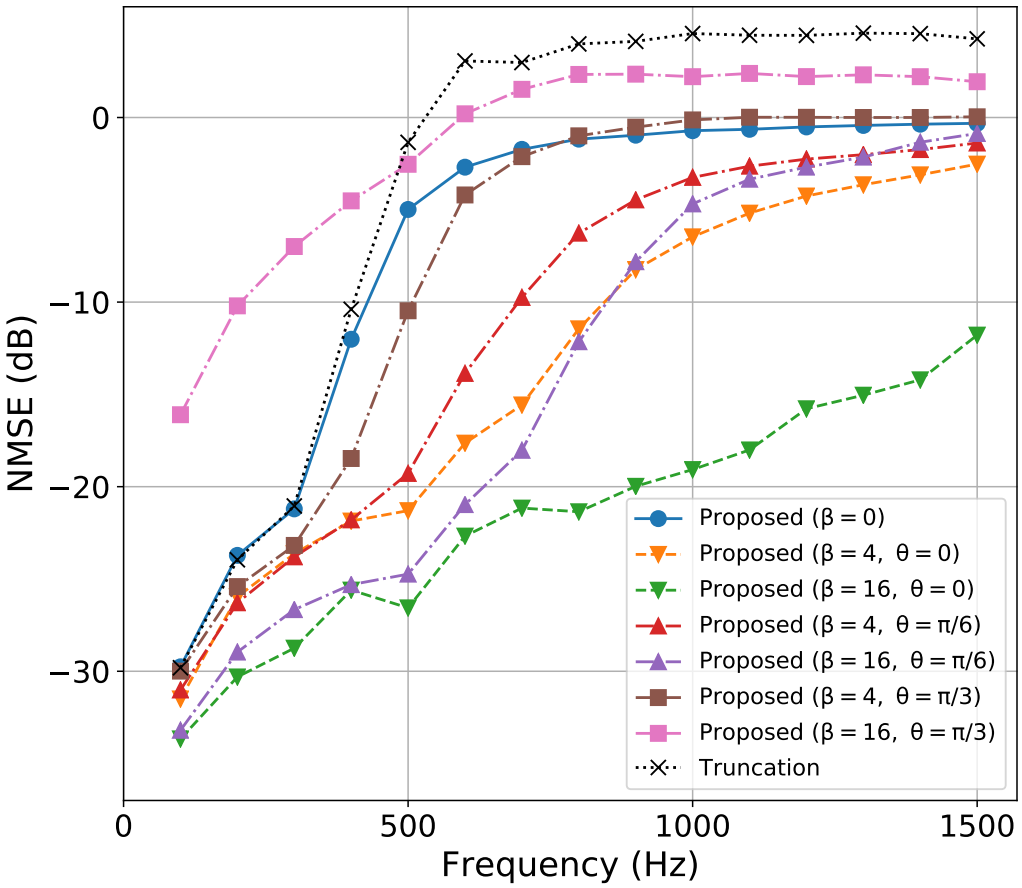

Fig. 5.5: NMSE plotted against frequency under free-field condition.

the observation noise of the mth microphone. For $u \in \mathcal{U}$, these microphones can be equivalently modeled by the following directivities:

$$\gamma_m(\boldsymbol{x}) = \frac{1}{2} + \frac{1}{2}\boldsymbol{y}_m \circ \boldsymbol{x} \quad (\boldsymbol{x} \in \mathbb{S}_2,\ m \in [\![1, M]\!]). \tag{5.51}$$

Furthermore, these directivities $\gamma_1, \ldots, \gamma_M$ can be represented as (5.22) with

$$c_{m,\nu,\mu} = \begin{cases} \sqrt{\pi} & (\nu = 0) \\ \frac{2\pi}{3} Y_{1,\mu}(\boldsymbol{y}_m)^* & (\nu = 1) \\ 0 & (\nu \geq 2) \end{cases} \quad (m \in [\![1, M]\!]). \tag{5.52}$$

The true sound field u_{true} was set as a single plane wave, which was defined as

$$u_{\mathrm{true}}(\boldsymbol{r}) \coloneqq \exp(-ik\boldsymbol{x}_{\mathrm{inc}} \circ \boldsymbol{r}) \quad (\boldsymbol{r} \in \mathbb{R}^3) \tag{5.53}$$

with $\boldsymbol{x}_{\mathrm{inc}} = [1, 0, 0]^\mathsf{T}$ (note that $\boldsymbol{x}_{\mathrm{inc}}$ denotes the incident direction, not the traveling direction). An example of the true sound field is shown in Figure 5.4, where the black line denotes the boundary of the microphone array. The observed signals were calculated using (5.50), and the observation noises were sampled independently from the circularly symmetric complex normal distribution with zero mean and a variance of $10^{-2} \times S$, where

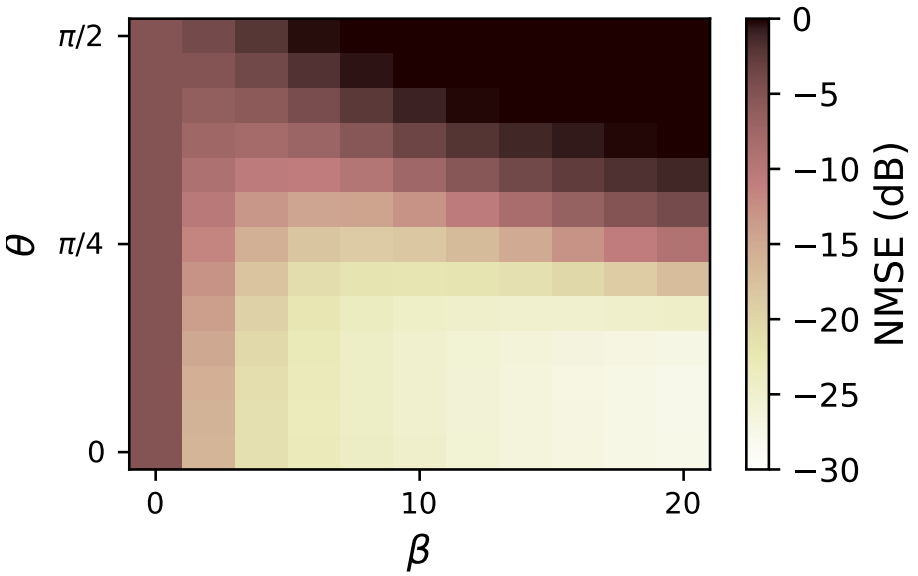

(a)

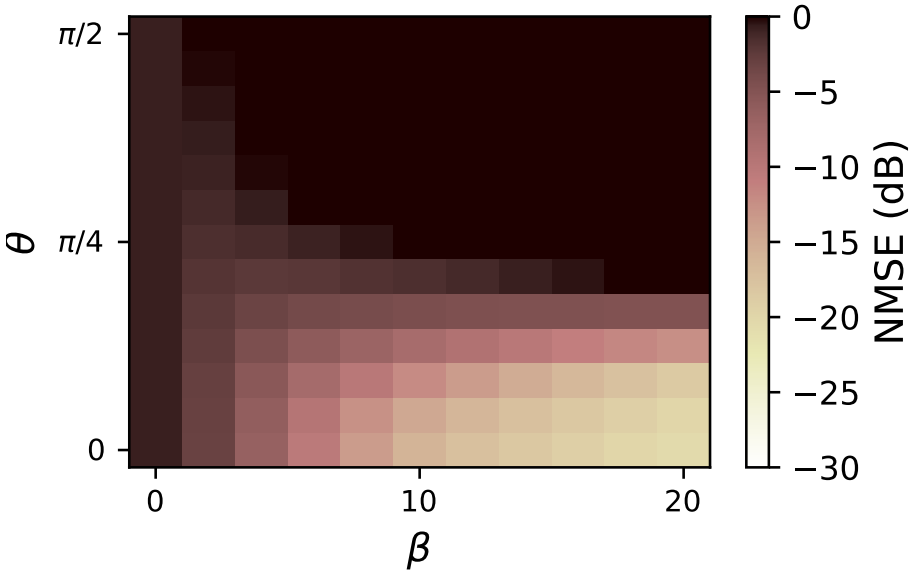

(b)

Fig. 5.6: Relationship between parameters and NMSE under free-field condition. (a) 500 Hz; (b) 1000 Hz.

S denotes the average power of the noise-free signals (i.e., the signal-to-noise ratio was 20 dB).

In the proposed method, $\sigma_1, \ldots, \sigma_N$ were set as 1 and λ was set as 10^{-2}. For prior information, we used the weighting function defined in (5.12). Here, we defined $\boldsymbol{\eta} := [\cos\theta, \sin\theta, 0]^\mathsf{T}$ for $\theta \in [0, \pi/2]$ ($\theta = 0$ means accurate prior information and a large θ means inaccurate information), and different values of β and θ were investigated.

In the truncation method, the truncation order was determined as $N = 7$ so that the

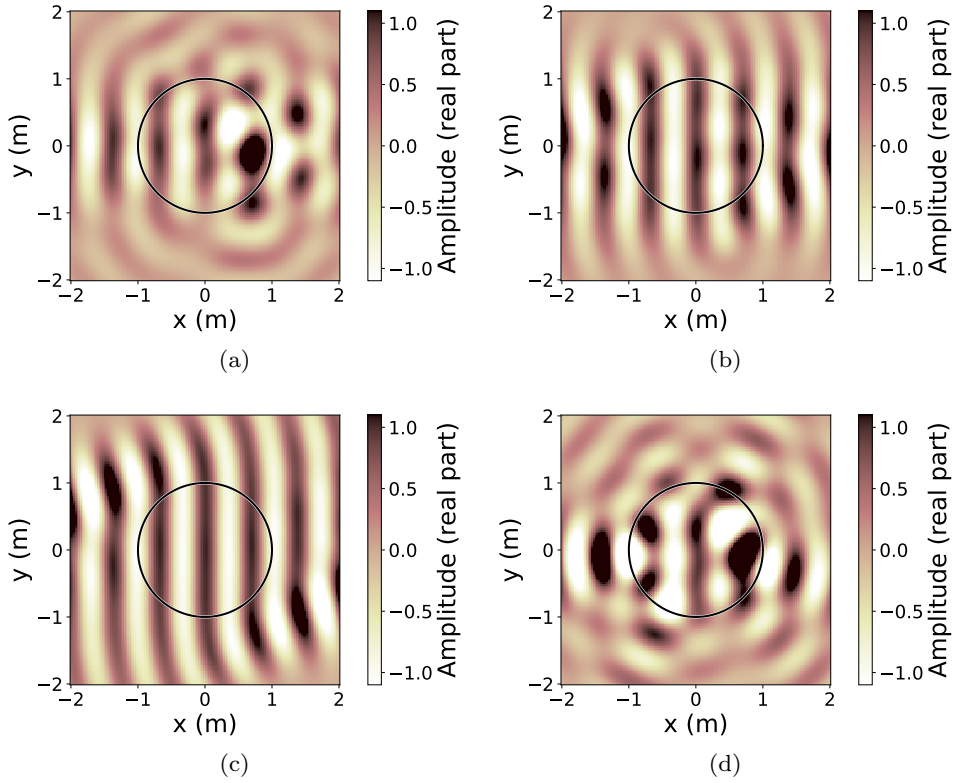

Fig. 5.7: Estimated sound fields under free-field condition at 500 Hz plotted in xy-plane ($\boldsymbol{r} = [\mathrm{x}, \mathrm{y}, 0]^{\mathsf{T}}$ m). (a) Proposed method ($\beta = 0$); (b) proposed method ($\beta = 4$, $\theta = \pi/6$); (c) proposed method ($\beta = 16$, $\theta = \pi/6$); (d) truncation method.

number of unknown coefficients corresponds to the number of microphones, i.e., 64. The global origin $\boldsymbol{r}_0$ (center of the spherical wavefunction expansion) was set at the center of the spherical microphone array. The regularization parameter in the matrix inversion was set at $\lambda = 10^{-2}$ as in the proposed method.

As an evaluation criterion, the normalized mean squared error (NMSE) was used, which was defined as

$$\mathrm{NMSE} \coloneqq 10 \log_{10} \frac{\sum_{\mathrm{i} \in \mathrm{I}_{\mathrm{eval}}} |u_{\mathrm{true}}(\boldsymbol{r}_{\mathrm{eval}}^{(\mathrm{i})}) - u_{\mathrm{est}}(\boldsymbol{r}_{\mathrm{eval}}^{(\mathrm{i})})|^2}{\sum_{\mathrm{i} \in \mathrm{I}_{\mathrm{eval}}} |u_{\mathrm{true}}(\boldsymbol{r}_{\mathrm{eval}}^{(\mathrm{i})})|^2} \quad (\mathrm{dB}). \tag{5.54}$$

Here, u_{est} denotes the estimated sound field, and the evaluation points $\{\boldsymbol{r}_{\mathrm{eval}}^{(\mathrm{i})}\}_{\mathrm{i} \in \mathrm{I}_{\mathrm{eval}}}$ were set as all grid points with an interval of 0.1 m on and inside the surface of the spherical microphone array.

First, the relationship between frequency and NMSE is plotted in Figure 5.5. We can see that the NMSEs for the proposed method ($\beta = 0$) were almost the same as those for the truncation method at low frequencies and were lower than those for the truncation method at high frequencies. This is considered to be because the finite number of basis functions used in the truncation method is not sufficient to represent the true sound field at high

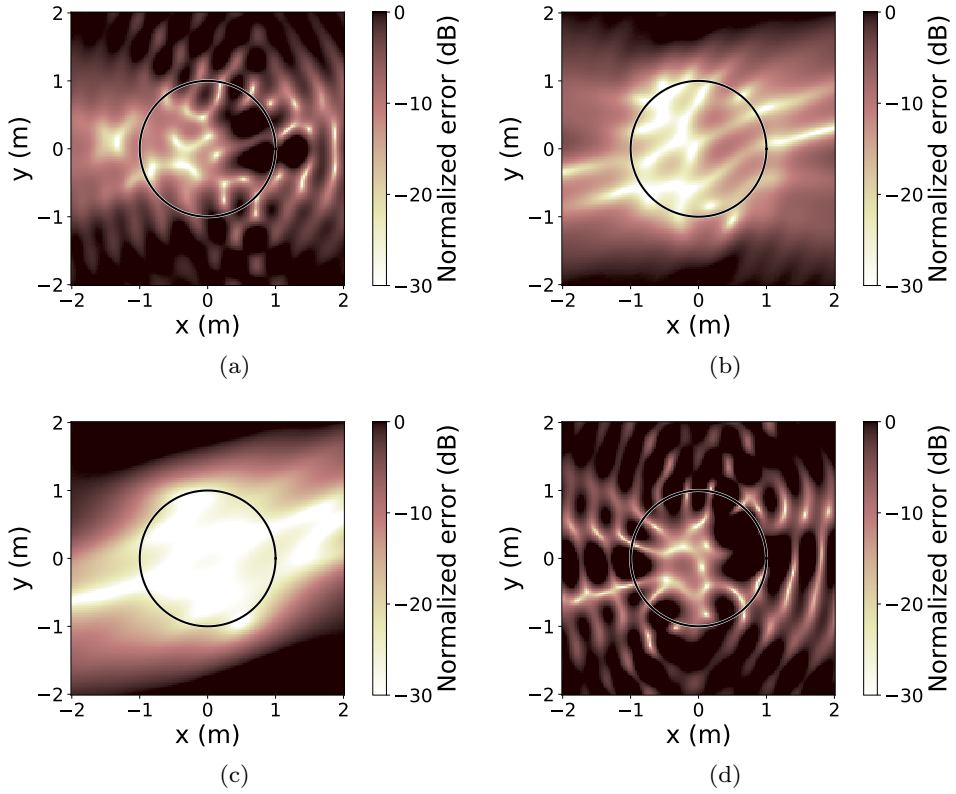

Fig. 5.8: Normalized error distributions under free-field condition at 500 Hz plotted in xy-plane ($\boldsymbol{r} = [\mathrm{x}, \mathrm{y}, 0]^{\mathsf{T}}$ m). (a) Proposed method ($\beta = 0$); (b) proposed method ($\beta = 4$, $\theta = \pi/6$); (c) proposed method ($\beta = 16$, $\theta = \pi/6$); (d) truncation method.

frequencies. Among the proposed methods, the NMSEs for $\theta = 0$ were lower than those for the other conditions, and even the NMSEs for $\theta = \pi/6$ (i.e., inaccurate prior information) were lower than those for $\beta = 0$. For further investigation, the NMSEs at different θ and β are plotted at frequencies of 500 and 1000 Hz in Figure 5.6. It can be seen that for $\theta = 0$, the NMSE decreased as β increased, and for $\theta > 0$, the NMSE took a minimum value at a certain value of β. This is considered to be because the estimation was strongly affected by inaccurate prior information in cases of large β for $\theta > 0$. The best value of β varied depending on θ and the frequency, and their quantitative relationship seems complex; however, at least, many conditions achieved lower NMSEs than the condition of $\beta = 0$. These results indicate that even rough prior information on the source direction improves the estimation accuracy in the proposed method. We also show examples of the estimated sound fields and (pointwise) normalized error distributions at 500 Hz in Figures 5.7 and 5.8, respectively. In this example, the NMSEs were (a) -4.87, (b) -18.20, (c) -24.74, and (d) -1.18 dB. The tendencies described above can also be seen in these results.

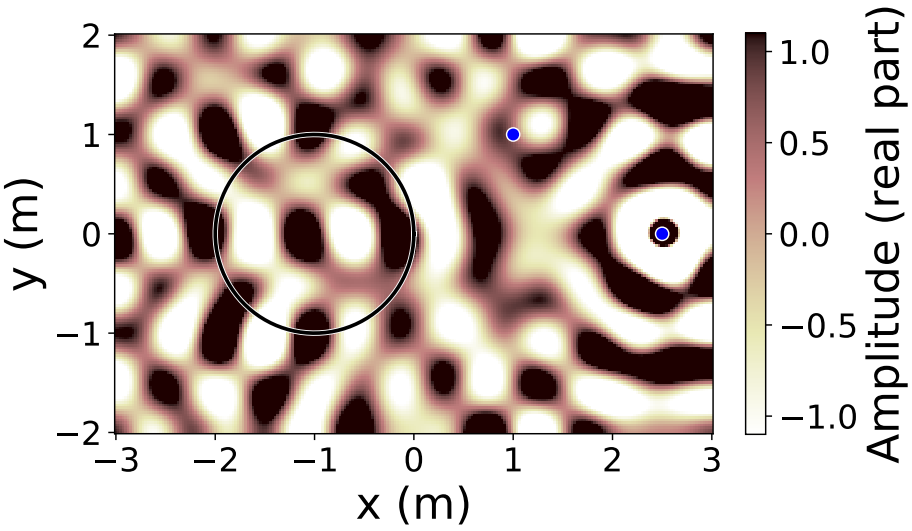

Fig. 5.9: True sound field under reverberant condition ($\Gamma_{\mathrm{reflect}} = 0.8$) at 500 Hz plotted in xy-plane ($\boldsymbol{r} = [\mathrm{x}, \mathrm{y}, 0]^\mathsf{T}$ m).

5.2.4.2 Estimation of Monopole Field under Free-Field and Reverberant Condition

In a 6 m × 4 m × 3 m rectangular room with its center defined as the origin, the same spherical microphone array as used in the previous experiments was placed with its center positioned at $[-1, 0, 0]^\mathsf{T}$ m. The reverberation in the room was simulated by the image-source method [96], where image sources were considered up to the 20th reflection order. Here, the reflection coefficients were set as $\Gamma_{\mathrm{reflect}} \in \{0, 0.4, 0.8\}$ for all six wall surfaces, where each of the above three values was investigated ($\Gamma_{\mathrm{reflect}} = 0$ corresponds to the free-field condition). In these settings, the reverberation time (from Sabine's formula) and reverberation radius (critical distance) [97] were respectively 0.13 s and 1.35 m for $\Gamma_{\mathrm{reflect}} = 0.4$, and 0.30 s and 0.88 m for $\Gamma_{\mathrm{reflect}} = 0.8$.

The true sound field u_{true} was set as a superposition of two monopole functions, whose direct wave component was defined as

$$u_{\mathrm{true}}(\boldsymbol{r}) = \sum_{q=1}^{2} A^{(q)} \frac{\exp(ik\|\boldsymbol{r} - \boldsymbol{r}_{\mathrm{src}}^{(q)}\|_2)}{4\pi\|\boldsymbol{r} - \boldsymbol{r}_{\mathrm{src}}^{(q)}\|_2} \quad (\boldsymbol{r} \in \mathbb{R}^3) \tag{5.55}$$

with $A^{(1)} = 15$ m, $\boldsymbol{r}_{\mathrm{scr}}^{(1)} = [2.5, 0, 0]^\mathsf{T}$ m, $A^{(2)} = 10i$ m, and $\boldsymbol{r}_{\mathrm{scr}}^{(1)} = [1, 1, 1]^\mathsf{T}$ m. An example of the true sound field is shown in Figure 5.9, where the black line denotes the boundary of the microphone array and the blue dots denote the positions of the sound sources projected into the xy-plane. The observed signals were calculated using (5.50), and the observation noises were added in the same way as in the previous experiments.

In the proposed method, $\sigma_1, \ldots, \sigma_N$ and λ were set to be the same as in the previous experiments. For prior information, we used the weighting function defined in (5.33) with

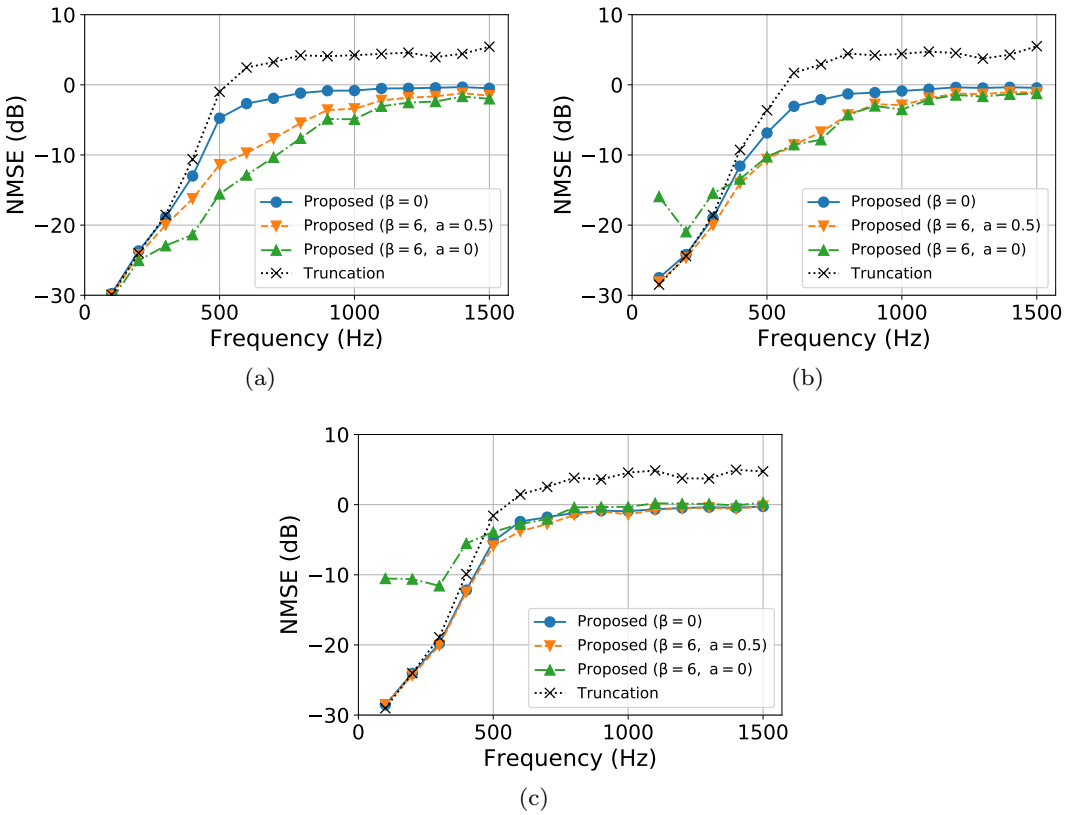

Fig. 5.10: NMSE plotted against frequency. (a) $\Gamma_{\mathrm{reflect}} = 0$; (b) $\Gamma_{\mathrm{reflect}} = 0.4$; (c) $\Gamma_{\mathrm{reflect}} = 0.8$.

$L = 3$, where we defined

$$\beta_1 = \beta_2 = \beta, \ \beta_3 = 0, \tag{5.56}$$

$$\boldsymbol{\eta}_1 = [1, 0, 0]^{\mathsf{T}}, \ \boldsymbol{\eta}_2 = \left[\frac{2}{\sqrt{6}}, \frac{1}{\sqrt{6}}, \frac{1}{\sqrt{6}}\right]^{\mathsf{T}}, \tag{5.57}$$

$$a_1 = a_2 = \frac{1-a}{2}, \ a_3 = a \tag{5.58}$$

using the parameters $\beta \in [0, \infty)$ and $a \in [0, 1]$. We defined $\beta_3 = 0$ for the third weighting to represent the reverberant component and investigated different β and a. In the truncation method, the same parameters as in the previous experiments were used. The NMSE was used as an evaluation criterion.

First, the relationship between frequency and NMSE is plotted in Figure 5.10. Under the free-field condition, i.e., $\Gamma_{\mathrm{reflect}} = 0$, one can see tendencies similar to the previous experimental results. Under the reverberant conditions, the NMSEs for the proposed method ($\beta = 6$, $a = 0$) increased with $\Gamma_{\mathrm{reflect}}$, which was due to the fact that the regularization term for $a = 0$ takes a large value for reverberant components. On the other hand, the proposed method ($\beta = 6$, $a = 0.5$) achieved lower NMSEs than the proposed method ($\beta = 0$) at most frequencies, although the performance improvement decreased

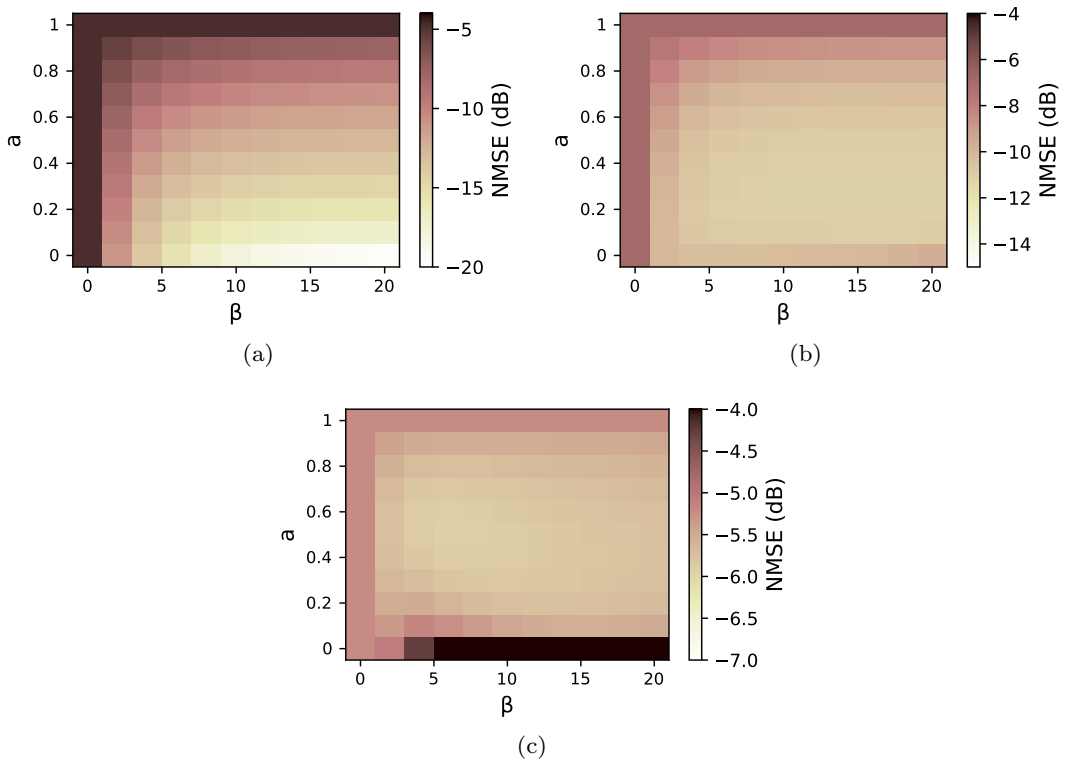

Fig. 5.11: Relationship between parameters and NMSE. (a) $\Gamma_{\mathrm{reflect}} = 0$; (b) $\Gamma_{\mathrm{reflect}} = 0.4$; (c) $\Gamma_{\mathrm{reflect}} = 0.8$.

as $\Gamma_{\mathrm{reflect}}$ increased. The reduced effectiveness is considered to be related to the extent of reverberation; in highly reverberant environments, even sound fields originating from monopole sources become close to diffuse fields, which makes it difficult to improve the estimation performance by using a directional weighting.

For further investigation, the NMSEs for different a and β at 500 Hz are plotted in Figure 5.11. Also, in this case, most conditions achieved lower NMSEs than $\beta = 0$, which indicates again that even rough prior information contributes to the improvement of estimation performance. We also show examples of the estimated sound fields and normalized error distributions for $\Gamma_{\mathrm{reflect}} = 0.8$ at 500 Hz in Figures 5.12 and 5.13, respectively. In this example, the NMSEs were (a) -5.22, (b) -5.90, and (c) -3.90 dB. The tendencies described above can also be seen in these results.

Finally, to investigate how the above results generalize, we conducted the same evaluations for two different source positions, i.e., $\boldsymbol{r}_{\mathrm{src}}^{(1)}$ and $\boldsymbol{r}_{\mathrm{src}}^{(2)}$, and several accuracies of prior information, i.e., $\boldsymbol{\eta}_1$ and $\boldsymbol{\eta}_2$. The source positions were sampled randomly according to the uniform distribution on the entire room excluding a ball with a radius of 2.0 m centered at $[-1, 0, 0]^{\mathsf{T}}$ m. The directions $\boldsymbol{\eta}_1$ and $\boldsymbol{\eta}_2$ were sampled randomly so that the angle between $\boldsymbol{\eta}_l$ and the true direction of the lth source from the center of the spherical microphone array was $\theta \in \{0, \pi/6, \pi/3\}$ for each $l \in \{1, 2\}$, where each of the three values of θ was

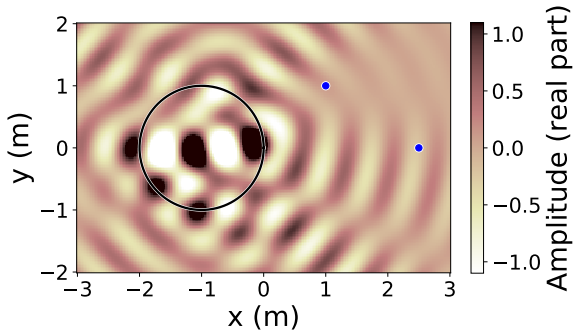

(a)

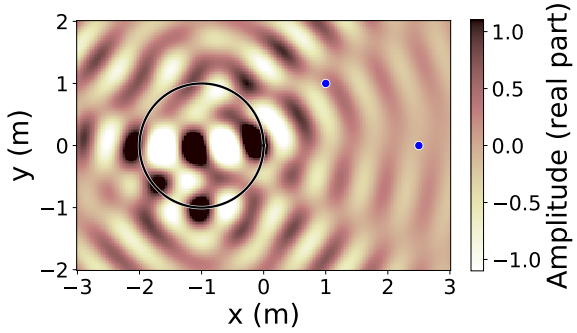

(b)

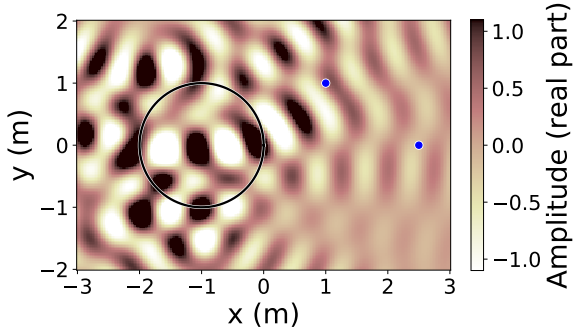

(c)

Fig. 5.12: Estimated sound fields under reverberant condition ($\Gamma_{\mathrm{reflect}} = 0.8$) at 500 Hz plotted in xy-plane ($\boldsymbol{r} = [\mathrm{x}, \mathrm{y}, 0]^{\mathsf{T}}$ m). (a) Proposed method ($\beta = 0$); (b) proposed method ($\beta = 6$, $a = 0$); (c) proposed method ($\beta = 6$, $a = 0.5$).

investigated. Figure 5.14 shows the relationship between NMSE averaged over 20 trials and frequency for different values of a, β, and Γ. For $\theta = 0$ (i.e., accurate prior information), one can see that the performance improvement using the directional weighting can be generalized in various settings of source positions. Moreover, the proposed method ($\beta = 6$, $a = 0.5$, $\theta = \pi/6$) exhibited lower NMSEs than the proposed method ($\beta = 0$). For $\Gamma = 0.8$, the NMSEs for these two conditions were very close; however, the proposed method ($\beta = 6$, $a = 0.5$, $\theta = \pi/6$) showed slightly lower NMSEs at most frequencies. These results mean that a certain degree of inaccurate prior information can be used in

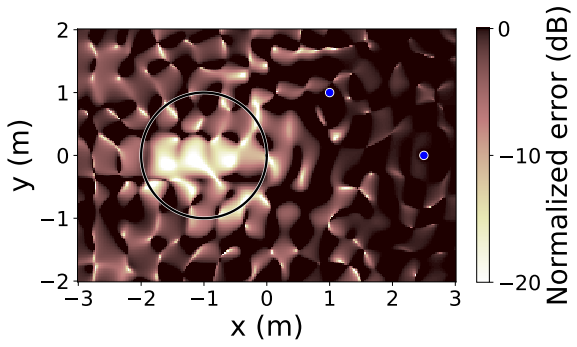

(a)

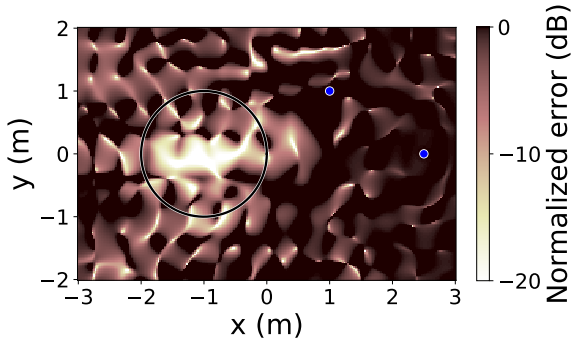

(b)

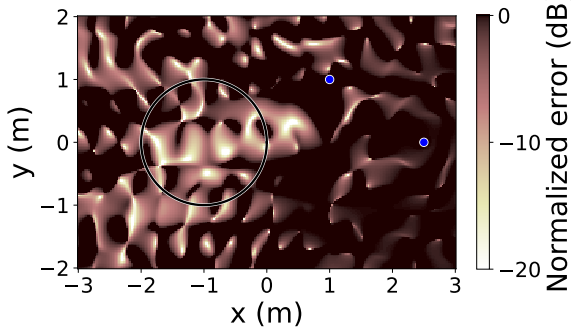

(c)

Fig. 5.13: Normalized error distributions under reverberant condition ($\Gamma_{\mathrm{reflect}} = 0.8$) at 500 Hz plotted in xy-plane ($\boldsymbol{r} = [\mathrm{x}, \mathrm{y}, 0]^{\mathsf{T}}$ m). (a) Proposed method ($\beta = 0$); (b) proposed method ($\beta = 4$, $a = 0.5$); (c) proposed method ($\beta = 4$, $a = 0$).

the proposed method.

5.3 Sound Field Estimation Considering Saturation Effect

This section presents a sound field estimation method from saturated observation. Although two-dimensional time-harmonic sound fields are considered and sensors with specific directivity are used here for theoretical simplicity, this method can be extended to three-dimensional sound fields with multiple frequency components and arbitrary sensor

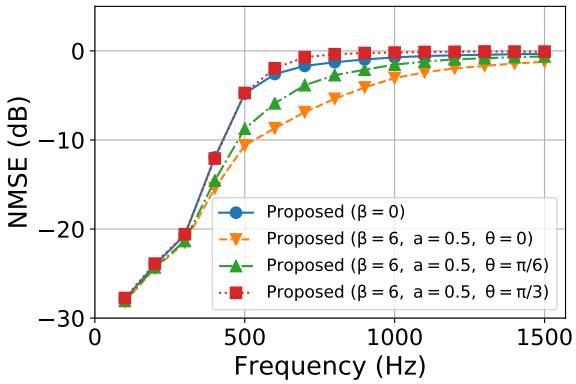

(a)

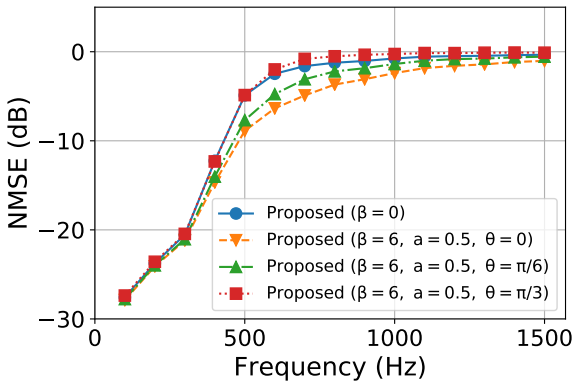

(b)

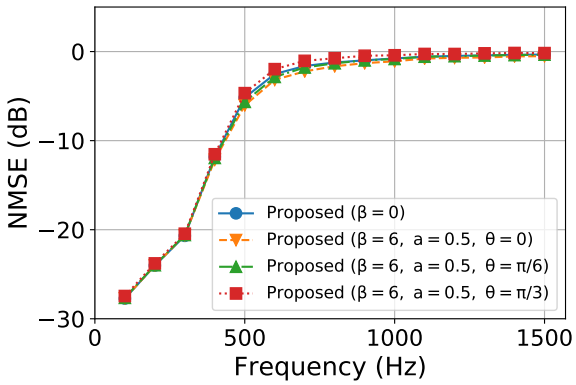

(c)

Fig. 5.14: Relationship between parameters and NMSE averaged over 20 trials. (a) $\Gamma_{\text{reflect}} = 0$; (b) $\Gamma_{\text{reflect}} = 0.4$; (c) $\Gamma_{\text{reflect}} = 0.8$.

directivity. Since the nonlinear saturation effect is considered, sound fields are described here in the time domain, in contrast to that in Section 5.2.

5.3.1 Formulation

Consider the following two-dimensional acoustic wave equation:

$$\left(\Delta - \frac{1}{c^2}\frac{\partial^2}{\partial t^2}\right) u(\boldsymbol{r}, t) = 0 \quad (\boldsymbol{r} \in \mathbb{R}^2,\ t \in \mathbb{R}). \tag{5.59}$$

Here, $u(\boldsymbol{r}, t) \in \mathbb{R}$ denotes the sound pressure at a position $\boldsymbol{r} \in \mathbb{R}^2$ and a time $t \in \mathbb{R}$, and $c \in (0, \infty)$ denotes the speed of sound. One of the solutions for (5.59) is a complex sinusoidal plane wave function defined as

$$u_{\mathrm{pw}}(\boldsymbol{r}, t) \coloneqq \exp\left(-ik\boldsymbol{x} \circ \boldsymbol{r} - i\omega t\right) \quad (\boldsymbol{r} \in \mathbb{R}^2,\ t \in \mathbb{R}), \tag{5.60}$$

where $\omega \in (0, \infty)$ denotes an angular frequency, $k \coloneqq \omega/c$ is the wavenumber, and $\boldsymbol{x} \in \mathbb{S}_1$ denotes a unit vector representing the incident direction of the plane wave. As a superposition of plane waves, the time-harmonic incident sound field with angular frequency ω can be well modeled as

$$u(\boldsymbol{r}, t) = \int_{\boldsymbol{x} \in \mathbb{S}_1} \mathrm{Re}\left(\tilde{u}(\boldsymbol{x})\left(-ik\boldsymbol{x} \circ \boldsymbol{r} - i\omega t\right)\right) \mathrm{d}\chi \quad (\boldsymbol{r} \in \mathbb{R}^2,\ t \in \mathbb{R}) \tag{5.61}$$

with $\tilde{u} \in \mathcal{L}_2(\mathbb{S}_1, \mathbb{C})$. Let $\mathscr{P}$ denote a transform of functions from $\tilde{u}$ to u defined as (5.61) and $(\mathcal{U}, \langle \cdot, \cdot \rangle_{\mathcal{U}})$ be an infinite-dimensional real Hilbert space defined as

$$\mathcal{U} = \{\mathscr{P}\tilde{u} \mid \tilde{u} \in \mathcal{L}_2(\mathbb{S}_1, \mathbb{C})\} \tag{5.62}$$

and

$$\langle u_1, u_2 \rangle_{\mathcal{U}} \coloneqq \int_{\boldsymbol{x} \in \mathbb{S}_1} \mathrm{Re}\left(\tilde{u}_1(\boldsymbol{x})^* \tilde{u}_2(\boldsymbol{x})\right) \mathrm{d}\chi, \tag{5.63}$$

respectively, where $\tilde{u}_1, \tilde{u}_2 \in \mathcal{L}_2(\mathbb{S}_1, \mathbb{C})$ are functions satisfying $u_1 = \mathscr{P}\tilde{u}_1$ and $u_2 = \mathscr{P}\tilde{u}_2$.

Suppose $M \in \mathbb{N}$ pressure-gradient microphones are located at $\boldsymbol{r}_1, \ldots, \boldsymbol{r}_M \in \mathbb{R}^2$, and let $t_1, \ldots, t_{P_m} \in \mathbb{R}$ with $P_m \in \mathbb{N}$ be the sampling times of the mth microphone for each $m \in [\![1, M]\!]$. Moreover, for each $m \in [\![1, M]\!]$, let $f_m : \mathbb{R} \to \mathbb{R}$ be defined as

$$f_m(z) \coloneqq \begin{cases} -\tau_m & z \in (-\infty, -\tau_m] \\ z & z \in (-\tau_m, \tau_m) \\ \tau_m & z \in [\tau_m, \infty) \end{cases} \quad (m \in [\![1, M]\!]) \tag{5.64}$$

with $\tau_m \in [0, \infty]$, which denotes the nonlinear saturation effect of the mth microphone. Then, the relationship between the unknown sound field $u \in \mathcal{U}$ and the observed signal of the mth microphone at the sampling time t_p, denoted by $s_{m,p} \in \mathbb{R}$, is given by

$$s_{m,p} = f_m(D_{m,p}u) + \epsilon_{m,p} \tag{5.65}$$

for each $m \in [\![1, M]\!]$ and $p \in [\![1, P_m]\!]$, where $\epsilon_{m,p} \in \mathbb{R}$ denotes the observation noise and $D_{m,p}$ is a linear functional defined as

$$D_{m,p}u \coloneqq G_m \frac{\partial}{\partial \boldsymbol{y}_m} u(\boldsymbol{r}_m, t_p) \quad (u \in \mathcal{U}). \tag{5.66}$$

Here, for each $m \in [\![1, M]\!]$, $G_m \in \mathbb{R}$ and $\boldsymbol{y}_m \in \mathbb{R}$ denote the gain and the direction of the mth microphone, respectively, and $\partial/\partial \boldsymbol{y}_m$ denotes the directional derivative along the direction $\boldsymbol{y}_m$.

According to the theories described in Chapter 3, the following optimization problem is formulated to estimate the sound field:

$$\underset{u \in \mathcal{U}}{\text{minimize}} \; Q(u) \coloneqq \sum_{m=1}^{M} \sum_{p=1}^{P_m} \frac{1}{\sigma_m^2} \left(F_m(D_{m,p}u) - s_{m,p} D_{m,p} u\right) + \frac{\lambda}{2}\|u\|_{\mathcal{U}}^2. \tag{5.67}$$

Here, $F_1, \ldots, F_M : \mathbb{R} \to \mathbb{R}$ are primitive functions of $f_1, \ldots, f_M$, respectively, $\sigma_1, \ldots, \sigma_M \in (0, \infty)$ are dispersion parameters representing the observational uncertainty, and $\lambda \in (0, \infty)$ is a regularization parameter. For each $m \in [\![1, M]\!]$ and $p \in [\![1, P_m]\!]$, the functional $D_{m,p}$ can be represented as

$$D_{m,p}u = \langle v_{m,p}, u \rangle_{\mathcal{U}} \quad (u \in \mathcal{U}) \tag{5.68}$$

with

$$v_{m,p}(\boldsymbol{r}, t) = 2\pi k G_m J_1(k\|\boldsymbol{r} - \boldsymbol{r}_m\|_2) \cos(\angle(\boldsymbol{r} - \boldsymbol{r}_m) - \angle \boldsymbol{y}_m) \cos(\omega(t - t_p)), \tag{5.69}$$

where $J_\nu(\cdot) : \mathbb{R} \to \mathbb{R}$ is the νth-order Bessel function of the first kind for $\nu \in \mathbb{N}$ and $\angle(\cdot) : \mathbb{R}^2 \to [0, 2\pi)$ denotes the polar angle of the vector. The derivation is given in Appendix B.3. Therefore, we can apply the representer theorem to (5.67), and the optimal solution $u^{(\mathrm{opt})} \in \mathcal{U}$ is guaranteed to admit the form of

$$u^{(\mathrm{opt})} = \sum_{m=1}^{M} \sum_{p=1}^{P_m} \alpha_{m,p} v_{m,p} \tag{5.70}$$

with certain $\boldsymbol{\alpha}^{(\mathrm{opt})} \coloneqq [\alpha_{1,1}^{(\mathrm{opt})}, \ldots, \alpha_{1,P_1}^{(\mathrm{opt})}, \ldots, \alpha_{M,1}^{(\mathrm{opt})}, \ldots, \alpha_{M,P_M}^{(\mathrm{opt})}] \in \mathbb{R}^N$, where $N \coloneqq \sum_{m=1}^{M} P_m$. Here, $\boldsymbol{\alpha}^{(\mathrm{opt})}$ can be obtained as the solution of the following optimization problem:

$$\underset{\boldsymbol{\alpha} \in \mathbb{R}^N}{\text{minimize}} \; Q^{(*)}(\boldsymbol{\alpha}) \coloneqq H(\mathbf{K}\boldsymbol{\alpha}) + \frac{\lambda}{2} \boldsymbol{\alpha}^{\mathsf{T}} \mathbf{K} \boldsymbol{\alpha}, \tag{5.71}$$

where

$$\mathbf{s} \coloneqq \begin{bmatrix} \mathbf{s}_1 \\ \vdots \\ \mathbf{s}_M \end{bmatrix} \tag{5.72}$$

with $\mathbf{s}_m \coloneqq [s_{m,1}, \ldots, s_{m,P_m}]^{\mathsf{T}}$ for each $m \in [\![1, M]\!]$, $H_{\mathbf{s}} : \mathbb{R}^N \to \mathbb{R}$ is defined as

$$H_{\mathbf{s}}(\mathbf{z}) \coloneqq \sum_{m=1}^{M} \sum_{p=1}^{P_m} \frac{1}{\sigma_m^2} \left(F_m(z_{m,p}) - s_{m,p} z_{m,p}\right) \quad (\mathbf{z} \coloneqq [z_{1,1}, \ldots, z_{1,P_1}, \ldots, z_{M,1}, \ldots, z_{M,P_M}] \in \mathbb{R}^N), \tag{5.73}$$

Table 5.1: Results of sound field estimation (50 trials).

Condition	NMSE: mean ± standard deviation
Proposed	$-12.33 \pm 5.01\,\mathrm{dB}$
Soft consistency	$-6.97 \pm 3.65\,\mathrm{dB}$
Unsaturated	$-17.25 \pm 4.30\,\mathrm{dB}$

and $\mathbf{K} \in \mathbb{R}^{N \times N}$ is defined as

$$\mathbf{K} \coloneqq \begin{bmatrix} \mathbf{K}_{1,1} & \dots & \mathbf{K}_{1,M} \\ \vdots & \ddots & \vdots \\ \mathbf{K}_{M,1} & \dots & \mathbf{K}_{M,M} \end{bmatrix} \tag{5.74}$$

with $\mathbf{K}_{m_1,m_2} \in \mathbb{R}^{P_{m_1} \times P_{m_2}}$ given by

$$\mathbf{K}_{m_1,m_2} \coloneqq \begin{bmatrix} K_{m_1,m_2}^{1,1} & \dots & K_{m_1,m_2}^{1,P_{m_2}} \\ \vdots & \ddots & \vdots \\ K_{m_1,m_2}^{P_{m_1},1} & \dots & K_{m_1,m_2}^{P_{m_1},P_{m_2}} \end{bmatrix} \tag{5.75}$$

for each $m_1, m_2 \in [\![1, M]\!]$. Furthermore, $K_{m_1,m_2}^{p_1,p_2} \in \mathbb{R}$ is given by

$$\begin{aligned} K_{m_1,m_2}^{p_1,p_2} = -\pi k^2 G_{m_1} G_{m_2} [&J_2(k\|\boldsymbol{r}_{m_2} - \boldsymbol{r}_{m_1}\|_2) \cos(2\angle(\boldsymbol{r}_2 - \boldsymbol{r}_1) - \angle \boldsymbol{y}_{m_1} - \angle \boldsymbol{y}_{m_2}) \\ &- J_0(k\|\boldsymbol{r}_{m_2} - \boldsymbol{r}_{m_1}\|_2) \cos(\angle \boldsymbol{y}_{m_2} - \angle \boldsymbol{y}_{m_1})] \cdot \cos(\omega(t_{p_2} - t_{p_1})) \end{aligned} \tag{5.76}$$

for each $m_1, m_2 \in [\![1, M]\!]$, $p_1 \in [\![1, P_{m_1}]\!]$, and $p_2 \in [\![1, P_{m_2}]\!]$ (see Appendix B.3 for derivation). Then, the objective function of (5.71) is convex and partially differentiable, whose gradient is given by

$$\nabla Q^{(*)}(\boldsymbol{\alpha}) = \mathbf{K}\boldsymbol{\Sigma}^{-1}(f(\mathbf{K}\boldsymbol{\alpha}) - \mathbf{s}) + \lambda \mathbf{K}\boldsymbol{\alpha} \quad (\boldsymbol{\alpha} \in \mathbb{R}^N). \tag{5.77}$$

Here, $\boldsymbol{\Sigma} \in \mathbb{R}^{N \times N}$ is given by

$$\boldsymbol{\Sigma} \coloneqq \begin{bmatrix} \sigma_1^2 \mathbf{I}_1 & & 0 \\ & \ddots & \\ 0 & & \sigma_M^2 \mathbf{I}_M \end{bmatrix}. \tag{5.78}$$

5.3.2 Numerical Experiments

Numerical experiments were conducted using Julia v.1.2.0. In the two-dimensional free field $\mathbb{R}^2$, $M = 12$ pressure-gradient microphones were located, whose positions $\boldsymbol{r}_1, \dots, \boldsymbol{r}_M$ were determined according to the uniform distribution on the square region $[-2, 2]\,\mathrm{m} \times [-2, 2]\,\mathrm{m}$. The true sound field was determined as

$$u_{\mathrm{true}}(\boldsymbol{r}, t) \coloneqq \sum_{\nu=-10}^{10} \mathrm{Re}\,(a_\nu J_\nu(k\|\boldsymbol{r}\|_2) \exp(i\nu\angle\boldsymbol{r} - i\omega t)) \tag{5.79}$$

with $c = 340\,\mathrm{m/s}$, $\omega = 2\pi\mathrm{f}$, $\mathrm{f} = 100\,\mathrm{Hz}$, and $a_{-10}, \dots, a_{10}$ sampled independently from the univariate circular-symmetric complex normal distribution with mean 0 and variance 1. With respect to the microphones' parameter, for each $m \in [\![1, M]\!]$, P_m was set as 10, $t_{m,1}, \dots, t_{m,P_m}$ were sampled independently from the uniform distribution on $[0, 0.01]\,\mathrm{s}$, $\boldsymbol{y}_m$ was sampled from the uniform distribution on $\mathbb{S}_1$, and A_m was set as $1/k$. The following two conditions were compared: the proposed method (denoted by **Proposed**) and the method with the soft consistency loss function (denoted by **Soft consistency**). The restoration results of unsaturated signals (denoted by **Unsaturated**) were also investigated. For **Proposed** and **Soft consistency**, τ_m was set as 0.5 for each $m \in [\![1, M]\!]$. For **Unsaturated**, τ_m was set as ∞ for each $m \in [\![1, M]\!]$. Observation noises were added to the observed signals, which were sampled independently from the circularly symmetric complex normal distribution with mean 0 and variance $10^{-3} \times S$, where S denotes the average power of the noise-free signals (i.e., the signal-to-noise ratio was 30 dB). In **Proposed** and **Unsaturated**, the unknown signal was estimated by solving the optimization problem of (5.67) with an initial solution of zero vector. In **Soft consistency**, the optimization problem

$$\underset{u \in \mathcal{U}}{\text{minimize}}\ Q_{\mathrm{Soft}}(u) \coloneqq \sum_{m=1}^{M} \sum_{p=1}^{P_m} \frac{1}{2\sigma_m^2} (D_{m,p} u - \mathrm{proj}_{f_m^{-1}(s_{m,p})}(D_{m,p} u))^2 + \frac{\lambda}{2} \|u\|_{\mathcal{U}}^2 \quad (5.80)$$

was used to estimate the signal. As a preprocessing, $\mathbf{s}$ was projected into the range of f. On the basis of the representer theorem, as in **Proposed**, the optimal solution was obtained by solving

$$\underset{\boldsymbol{\alpha} \in \mathbb{R}^N}{\text{minimize}}\ Q_{\mathrm{Soft}}^{(*)}(\boldsymbol{\alpha}) \coloneqq \frac{1}{2} \|\mathbf{K}\boldsymbol{\alpha} - \mathrm{proj}_{f^{-1}(\mathbf{s})}(\mathbf{K}\boldsymbol{\alpha})\|_{\boldsymbol{\Sigma}^{-1}}^2 + \frac{\lambda}{2} \boldsymbol{\alpha}^{\mathsf{T}} \mathbf{K} \boldsymbol{\alpha} \quad (5.81)$$

with an initial solution of zero vector. For all conditions, the parameters in the optimization problem were set as $\lambda = 10^{-3}$ and $\sigma_m = 1$ for each $m \in [\![1, M]\!]$. For the optimization method, the nonlinear conjugate gradient method in Optim.jl [77] was used with the default settings.

As an evaluation criterion, the normalized mean squared error (NMSE) was used, which was defined as

$$\mathrm{NMSE} \coloneqq 10 \log_{10} \frac{\sum_{\mathrm{i} \in \mathrm{I}_{\mathrm{eval}}} \sum_{\mathrm{j} \in \mathrm{J}_{\mathrm{eval}}} |u_{\mathrm{true}}(\boldsymbol{r}_{\mathrm{eval}}^{(\mathrm{i})}, t_{\mathrm{eval}}^{(\mathrm{j})}) - u_{\mathrm{est}}(\boldsymbol{r}_{\mathrm{eval}}^{(\mathrm{i})}, t_{\mathrm{eval}}^{(\mathrm{j})})|^2}{\sum_{\mathrm{i} \in \mathrm{I}_{\mathrm{eval}}} \sum_{\mathrm{j} \in \mathrm{J}_{\mathrm{eval}}} |u_{\mathrm{true}}(\boldsymbol{r}_{\mathrm{eval}}^{(\mathrm{i})}, t_{\mathrm{eval}}^{(\mathrm{j})})|^2} \quad (\mathrm{dB}). \quad (5.82)$$

Here, u_{est} denotes the estimated sound field, and the evaluation points $\{\boldsymbol{r}_{\mathrm{eval}}^{(\mathrm{i})}\}_{\mathrm{i} \in \mathrm{I}_{\mathrm{eval}}}$ and $\{t_{\mathrm{eval}}^{(\mathrm{i})}\}_{\mathrm{j} \in \mathrm{J}_{\mathrm{eval}}}$ were set respectively as all grid points with an interval of 0.05 m in the square region $[-2, 2]\,\mathrm{m} \times [-2, 2]\,\mathrm{m}$ and equally spaced points from 0 s to 0.01 s with an interval of 0.001 s.

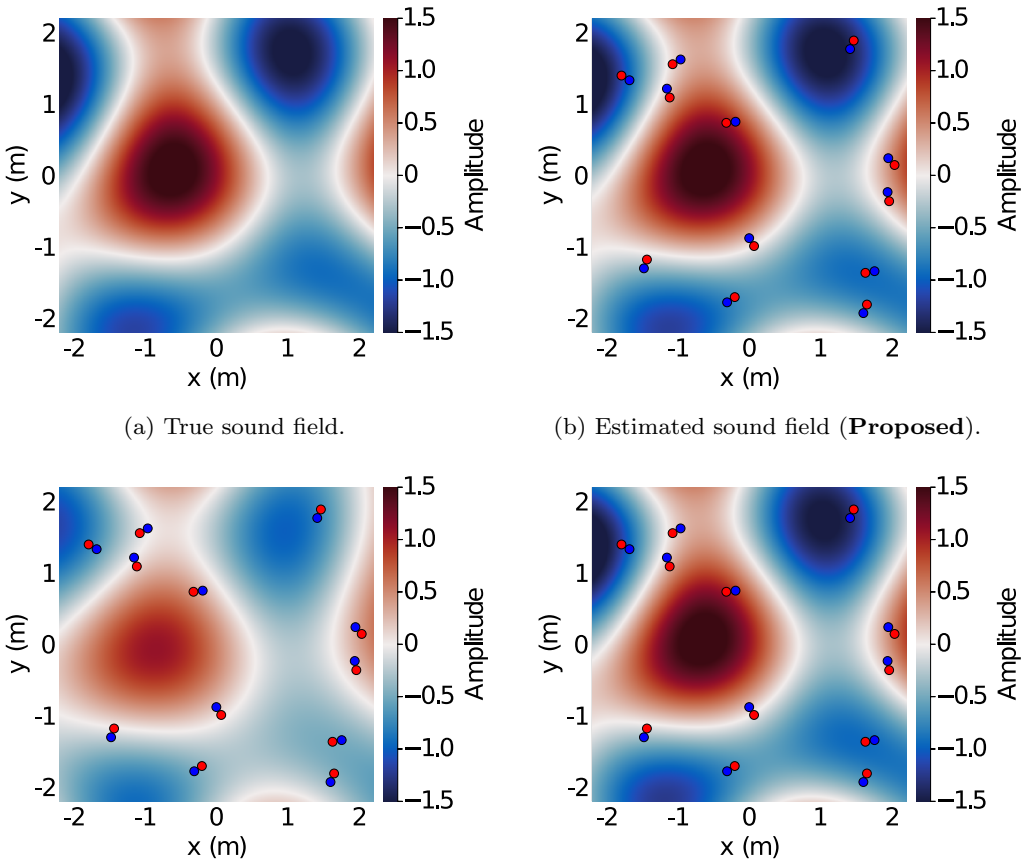

(a) True sound field.

(b) Estimated sound field (**Proposed**).

(c) Estimated sound field (**Soft consistency**).

(d) Estimated sound field (**Unsaturated**).

Fig. 5.15: Results of sound field estimation at $t = 0\,\mathrm{s}$ in the first trial. The NMSEs were (b) -17.15, (c) -6.82, and (d) $-17.83\,\mathrm{dB}$. The saturation distortion was $-8.07\,\mathrm{dB}$.

The results from 50 trials are shown in Table 5.1. The saturation distortion defined as $10\log_{10}\|\mathbf{s}_{\mathrm{sat}} - \mathbf{s}_{\mathrm{unsat}}\|_2^2 / \|\mathbf{s}_{\mathrm{unsat}}\|_2^2$ was also calculated, where $\mathbf{s}_{\mathrm{sat}}$ and $\mathbf{s}_{\mathrm{unsat}}$ denote the saturated and unsaturated noise-free observed signals, respectively. Its mean $\pm$ standard deviation for 50 trials was $-10.18 \pm 3.87\,\mathrm{dB}$. In addition, we show the true and estimated sound fields in the first trial in Figure 5.15. Here, pairs of red and blue circles represent the position and orientation of the pressure-gradient microphones; the direction from the blue circle to the red circle corresponds to the direction of the derivative observed using the pressure-gradient microphone. Even under the saturation effects, **Proposed** achieved an estimation performance relatively close to that of **Unsaturated**, compared with the value of the saturation distortion. We can also see that **Proposed** outperformed clipped **Soft consistency**, as was the case in the experiments in Section 4.2.

Chapter 6

Conclusion

The objectives of this thesis were (1) to establish a unifying framework of inverse problems for acoustic measurement, especially considering nonlinear saturation effects, and (2) to propose efficient estimation methods for sound signals and sound fields, where existing and proposed theories on inverse problems are fully utilized.

In Chapter 2, the mathematical framework of an inverse problem for acoustic measurement was introduced. The inverse problem of interest was formulated as an optimization problem of a certain class, whose objective function consists of a loss function and a regularization function, and its related studies were summarized. Finally, current problems to be addressed to achieve the objectives given above were clarified.

To overcome the theoretical difficulties shown in Chapter 2, a new formulation for inverse problems of interest was presented in Chapter 3. A theoretical comparison between the proposed formulation and other current formulations was given, and it was shown that the proposed formulation achieves both robustness against observation noise and mathematical tractability from an optimization viewpoint, which are not achieved simultaneously in other current formulations. Efficient optimization algorithms for the proposed formulation were also provided for various classes of regularization functions.

Chapters 4 and 5 focused on different specific topics of acoustic measurement problems, both on the basis of the theoretical framework provided in Chapters 2 and 3. In Chapter 4, signal restoration methods for saturated sound signals were proposed. In this chapter, two different methods were proposed: one based on the bandlimitation of the target signal and the other based on the sparsity of the target signal. In Chapter 5, sound field estimation methods were proposed. First, an estimation method exploiting prior information on the source direction was presented. In this method, linear observation was assumed; however, several contributions were made by utilizing theories on Hilbert spaces in comparison with other current methods. Second, a sound field estimation method considering nonlinear saturation effects was also proposed. The experimental results indicated that the proposed method achieved high estimation accuracy even from saturated observed signals.

Acknowledgement (in Japanese)

本論文は，筆者が東京大学大学院情報理工学系研究科システム情報学専攻修士課程及び博士課程に在学中に，猿渡・小山研究室で行った研究の成果をまとめたものです．

まず初めに，修士課程及び博士課程の計 5 年間の間，親身に指導して頂いた，筆者の指導教員かつ学位審査の主査でいらっしゃる猿渡洋教授に，心より感謝を申し上げます．猿渡先生には，修士研究，博士研究に関して，研究室内ゼミで様々なご指導を頂いただけでなく，日頃のよりインフォーマルな場においても様々な話題の学問，研究に関する議論をさせて頂きました．猿渡先生の，何より研究を愛する姿勢には，強く感銘を受けたとともに，筆者の目指す研究者像にも大きな影響を与えて下さったと感じております．

小山翔一講師には，研究テーマの相談から，理論，実装までにおいて，沢山のご指導を頂きました．小山先生の音場収録・再現に関する研究に強く興味を持ったことが，筆者が本研究に取り組むきっかけとなりました．筆者の研究アイデアを常に尊重して頂く一方で，時には進むべき方向を正して頂いたりと，数えきれない程の助言を頂けたことを深く感謝しております．時には数々のご迷惑をおかけしてしまいましたが，辛抱強く指導頂いたおかげで今の自分があると感じております．

お忙しい中にも関わらず，学位審査員を引き受けて下さった，奈良高明教授，成瀬誠教授，田中健一郎准教授に感謝申し上げます．予備審査及び本審査では数々の有益なご指摘，ご意見などを頂きました．おかげで本学位論文がより充実したものになったと感じております．奈良先生には，研究に関する議論の場を設けて頂いたこともあり，大変有意義な議論をさせて頂いたことを深く感謝いたします．

高道慎之介助教授，中村友彦特任助教授，郡山知樹助教授には，研究室内ゼミにて幅広い視点から助言を頂きました．また，猿渡・小山研究室の学術支援専門職員でいらっしゃる高宗典玄さんには，特に数理理論に関しての沢山の議論を交わす機会を頂きました．さらに，猿渡・小山研究室の学術支援職員でいらっしゃる丹治尚子さんには，研究室生活における沢山の事務的なサポートを頂きました．心より感謝を申し上げます．

他にも，本研究を成し遂げるにあたり，数多くの方々から助言を頂きました．また，逆に他の方々の研究内容に関する議論の機会も数多く頂きましたが，そのすべてが今の自分と，この研究成果に繋がっていると感じております．これまでに議論して頂いたすべての方々に感謝いたします．

最後に，筆者の大学院での研究生活を陰ながらも惜しみなく支え続けて下さった両親に，感謝申し上げます．

Bibliography

[1] L. Rabiner, *Fundamentals of Speech Recognition*, Prentice Hall, Upper Saddle River, 1993.

[2] D. Yu and L. Deng, *Automatic Speech Recognition*, Springer, London, 2016.

[3] G. J. Brown and M. Cooke, "Computational auditory scene analysis," *Computer Speech and Language*, vol. 8, no. 4, pp. 297–336, 1994.

[4] D. Wang and G. J. Brown, *Computational Auditory Scene Analysis: Principles, Algorithms, and Applications*, Wiley–IEEE Press, New York, 2006.

[5] R. Duraiwami, D. N. Zotkin, Z. Li, E. Grassi, N. A. Gumerov, and L. S. Davis, "High order spatial audio capture and its binaural head-tracked playback over headphones with HRTF cues," in *Proceedings of AES Convention*, New York, October 2005.

[6] D. Menzies and M. Al-Akaidi, "Nearfield binaural synthesis and ambisonics," *The Journal of the Acoustical Society of America*, vol. 121, no. 3, pp. 1559–1563, 2007.

[7] A. J. Berkhout, D. de Vries, and P. Vogel, "Acoustic control by wave field synthesis," *The Journal of the Acoustical Society of America*, vol. 93, no. 5, pp. 2764–2778, 1993.

[8] M. A. Poletti, "Three-dimensional surround sound systems based on spherical harmonics," *Journal of the Audio Engineering Society*, vol. 53, no. 11, pp. 1004–1025, 2005.

[9] J. Zhang, T. D. Abhayapala, W. Zhang, P. N. Samarasinghe, and S. Jiang, "Active noise control over space: A wave domain approach," *IEEE/ACM Transactions on Audio, Speech, and Language Processing*, vol. 26, no. 4, pp. 774–786, 2018.

[10] H. W. Engl, M. Hanke, and A. Neubauer, *Regularization of Inverse Problems*, Kluwer Academic Publishers, Dordrecht, 1996.

[11] C. R. Vogel, *Computational Methods for Inverse Problems*, SIAM, Philadelphia, 2002.

[12] J. Kaipio and E. Somersalo, *Statistical and Computational Inverse Problems*, Springer, New York, 2005.

[13] A. Kirsch, *An Introduction to the Mathematical Theory of Inverse Problems*, Springer Science & Business Media, New York, 2011.

[14] K. Yao, "Applications of reproducing kernel Hilbert spaces–bandlimited signal models," *Information and Control*, vol. 11, no. 4, pp. 429–444, 1967.

[15] M. Z. Nashed and G. G. Walter, "General sampling theorems for functions in

reproducing kernel Hilbert spaces," *Mathematics of Control, Signals, and Systems*, vol. 4, pp. 363–390, 1991.

[16] M. Unser, "Sampling—50 years after Shannon," *Proceedings of the IEEE*, vol. 88, no. 4, pp. 569–587, 2000.

[17] T. D. Abhayapala and D. B. Ward, "Theory and design of high order sound field microphones using spherical microphone array," in *Proceedings of IEEE International Conference on Acoustics, Speech, and Signal Processing (ICASSP)*, Orlando, May 2002, pp. II–1949–1952.

[18] J. Meyer and G. Elko, "A highly scalable spherical microphone array based on an orthogonal decomposition of the soundfield," in *Proceedings of IEEE International Conference on Acoustics, Speech, and Signal Processing (ICASSP)*, Orlando, May 2002, pp. II–1781–1784.

[19] J. Daniel, "Spatial sound encoding including near field effect: Introducing distance coding filters and a viable, new ambisonics format," in *Proceedings of AES International Conference*, Copenhagen, May 2003.

[20] A. Laborie, R. Bruno, and S. Montoya, "A new comprehensive approach of surround sound recording," in *Proceedings of AES Convention*, Amsterdam, March 2003.

[21] P. N. Samarasinghe, T. D. Abhayapala, and M. A. Poletti, "Wavefield analysis over large areas using distributed higher order microphones," *IEEE/ACM Transactions on Audio, Speech, and Language Processing*, vol. 22, no. 3, pp. 647–658, 2014.

[22] S. Kitić, L. Albera, N. Bertin, and R. Gribonval, "Physics-driven inverse problems made tractable with cosparse regularization," *IEEE Transactions on Signal Processing*, vol. 64, no. 2, pp. 335–348, 2016.

[23] D.-Y. Hu, H.-B. Li, Y. Hu, and Y. Fang, "Sound field reconstruction with sparse sampling and the equivalent source method," *Mechanical Systems and Signal Processing*, vol. 108, pp. 317–325, 2018.

[24] N. Murata, S. Koyama, N. Takamune, and H. Saruwatari, "Sparse representation using multidimensional mixed-norm penalty with application to sound field decomposition," *IEEE Transactions on Signal Processing*, vol. 66, no. 12, pp. 3327–3338, 2018.

[25] S. Koyama and L. Daudet, "Sparse representation of a spatial sound field in a reverberant environment," *IEEE Journal of Selected Topics in Signal Processing*, vol. 13, no. 1, pp. 172–184, 2019.

[26] A. E. Badia and T. Nara, "An inverse source problem for Helmholtz's equation from the Cauchy data with a single wave number," *Inverse Problems*, vol. 27, no. 10, 2011.

[27] S. Argentieri, P. Danès, and P. Souères, "A survey on sound source localization in robotics: From binaural to array processing methods," *Computer Speech and*

Language, vol. 34, no. 1, pp. 87–112, 2015.

[28] F. Antonacci, A. Alexandridis, A. Mouchtaris, and B. Lee, "A survey on sound source localization methods in wireless acoustic sensor networks," *Wireless Communications and Mobile Computing*, vol. 2017, 2017.

[29] N. Patwari, J. N. Ash, S. Kyperountas, A. O. Hero, R. L. Moses, and N. S. Correal, "Locating the nodes: cooperative localization in wireless sensor networks," *IEEE Signal Processing Magazine*, vol. 22, no. 4, pp. 54–69, 2005.

[30] V. C. Raykar, I. V. Kozintsev, and R. Lienhart, "Position calibration of microphones and loudspeakers in distributed computing platforms," *IEEE Transactions on Speech and Audio Processing*, vol. 13, no. 1, pp. 70–83, 2005.

[31] J. Liu, *Nonlinear Dynamics of a Dual-Backplate Capacitive MEMS Microphone*, dissertation, University of Florida, 2007.

[32] W. Sansen, "Distortion in elementary transistor circuits," *IEEE Transactions on Circuits and Systems II: Analog and Digital Signal Processing*, vol. 46, no. 3, pp. 315–325, 1999.

[33] J. Liu, D. T. Martin, K. Kadirvel, T. Nishida, M. Sheplak, and B. P. Mann, "Nonlinear identification of a capacitive dual-backplate MEMS microphone," in *Proceedings of International Design Engineering Technical Conferences and Computers and Information in Engineering Conference*, California, September 2005.

[34] F. Dinuzzo and B. Schölkopf, "The representer theorem for Hilbert spaces: a necessary and sufficient condition," in *Advances in Neural Information Processing Systems (NIPS)*, Lake Tahoe, December 2012, pp. 189–196.

[35] R. A. Kennedy and P. Sadeghi, *Hilbert Space Methods in Signal Processing*, Cambridge University Press, Cambridge, 2013.

[36] J. Hadamard, "Sur les problèmes aux dérivées partielles et leur signification physique," *Princeton University Bulletin*, vol. 13, pp. 49–52, 1902.

[37] E. G. Williams, *Fourier Acoustics: Sound Radiation and Nearfield Acoustical Holography*, Academic Press, London, 1999.

[38] C. T. Kelley, *Iterative Methods for Linear and Nonlinear Equations*, SIAM, Philadelphia, 1995.

[39] J. E. Dennis Jr. and R. B. Schnabel, *Numerical Methods for Unconstrained Optimization and Nonlinear Equations*, SIAM, Philadelphia, 1996.

[40] S. Boyd and L. Vandenberghe, *Convex Optimization*, Cambridge University Press, Cambridge, 2004.

[41] W. W. Hager and H. Zhang, "A survey of nonlinear conjugate gradient methods," *Pacific Journal of Optimization*, vol. 2, no. 1, pp. 35–58, 2006.

[42] P. L. Combettes and J.-C. Pesquet, "Proximal splitting methods in signal processing," *Fixed-Point Algorithms for Inverse Problems in Science and Engineering*, pp.

185–212, 2011.

[43] N. Parikh and S. Boyd, "Proximal algorithms," *Foundations and Trends in Optimization*, vol. 1, no. 3, pp. 127–239, 2014.

[44] K. Lange, *MM Optimization Algorithms*, SIAM, Philadelphia, 2016.

[45] L. Armijo, "Minimization of functions having Lipschitz continuous first partial derivatives," *Pacific Journal of Mathematics*, vol. 16, no. 1, pp. 1–3, 1966.

[46] Y. E. Nesterov, "A method of solving a convex programming problem with convergence rate $O(1/k^2)$," *Doklady Akademii Nauk SSSR*, vol. 269, no. 3, pp. 543–547, 1983.

[47] M. Elad, *Sparse and Redundant Representations*, Springer Science & Business Media, New York, 2010.

[48] M. Benning and M. Burger, "Modern regularization methods for inverse problems," *Acta Numerica*, vol. 27, no. 1, pp. 1–111, 2018.

[49] K. Lange, D. R. Hunter, and I. Yang, "Optimization transfer using surrogate objective functions," *Journal of Computational and Graphical Statistics*, vol. 9, no. 1, pp. 1–20, 2000.

[50] S. Boyd, N. Parikh, E. Chu, B. Peleato, and J. Eckstein, "Distributed optimization and statistical learning via the alternating direction method of multipliers," *Foundations and Trends in Machine Learning*, vol. 3, no. 1, pp. 1–122, 2011.

[51] I. Daubechies, M. Defrise, and C. De Mol, "An iterative thresholding algorithm for linear inverse problems with a sparsity constraint," *Communications on Pure and Applied Mathematics*, vol. 57, no. 11, pp. 1413–1457, 2004.

[52] J. A. Tropp and S. J. Wright, "Computational methods for sparse solution of linear inverse problems," *Proceedings of the IEEE*, vol. 98, no. 6, pp. 948–958, 2010.

[53] W. Munk, P. Worcester, and C. Wunsch, *Ocean Acoustic Tomography*, Cambridge University Press, Cambridge, 2009.

[54] S. Kitić, L. Jacques, N. Madhu, M. P. Hopwood, A. Spriet, and C. De Vleeschouwer, "Consistent iterative hard thresholding for signal declipping," in *Proceedings of IEEE International Conference on Acoustics, Speech, and Signal Processing (ICASSP)*, Vancouver, May 2013, pp. 5939–5943.

[55] S. Kitić, N. Bertin, and R. Gribonval, "Sparsity and cosparsity for audio declipping: a flexible non-convex approach," in *Proceedings of International Conference on Latent Variable Analysis and Signal Separation (LVA/ICA)*, Liberec, 2015, pp. 243–250.

[56] L. Rencker, F. Bach, W. Wang, and M. D. Plumbley, "Fast iterative shrinkage for signal declipping and dequantization," in *Proceedings of iTWIST'18*, Marseille, November 2018.

[57] L. Rencker, F. Bach, W. Wang, and M. D. Plumbley, "Sparse recovery and dictionary

learning from nonlinear compressive measurements," *IEEE Transactions on Signal Processing*, vol. 67, no. 21, pp. 5659–5670, 2019.

[58] R. T. Rockafellar, *Convex Analysis*, Princeton University Press, Princeton, 1970.

[59] G. Wahba, *Spline Models for Observational Data*, SIAM, Philadelphia, 1990.

[60] B. Schölkopf, R. Herbrich, and A. J. Smola, "A generalized representer theorem," in *Proceedings of Computational Learning Theory (COLT)*, Amsterdam, July 2001, pp. 416–426.

[61] C. A. Micchelli and M. Pontil, "Kernels for multi-task learning," in *Advances in Neural Information Processing Systems (NIPS)*, 2004, pp. 921–928.

[62] M. Unser, "A unifying representer theorem for inverse problems and machine learning," *arXiv:1903.00687*, 2019.

[63] R. Wang and Y. Xu, "Functional reproducing kernel Hilbert spaces for non-point-evaluation functional data," *Applied and Computational Harmonic Analysis*, vol. 46, no. 3, pp. 569–623, 2019.

[64] K. P. Murphy, *Machine Learning: a Probabilistic Perspective*, The MIT Press, Cambridge, 2012.

[65] N. Aronszajn, "Theory of reproducing kernels," *Transactions of the American Mathematical Society*, vol. 68, no. 3, pp. 337–404, 1950.

[66] R. I. Boţ and D.-K. Nguyen, "The proximal alternating direction method of multipliers in the nonconvex setting: Convergence analysis and rates," *Mathematics of Operations Research*, vol. 45, no. 2, pp. 682–712, 2020.

[67] C.-T. Tan, B. C. J. Moore, and N. Zacharov, "The effect of nonlinear distortion on the perceived quality of music and speech signals," *Journal of the Audio Engineering Society*, vol. 51, no. 11, pp. 1012–1031, 2003.

[68] L. W. Lee and E. R. Geddes, "Auditory perception of nonlinear distortion," in *Proceedings of AES Convention*, New York, October 2003.

[69] M. J. Harvilla and R. M. Stern, "Efficient audio declipping using regularized least squares," in *Proceedings of IEEE International Conference on Acoustics, Speech, and Signal Processing (ICASSP)*, Brisbane, April 2015, pp. 221–225.

[70] J. S. Abel and J. O. Smith, "Restoring a clipped signal," in *Proceedings of IEEE International Conference on Acoustics, Speech, and Signal Processing (ICASSP)*, Toronto, April 1991, pp. 1745–1748.

[71] P. Weiss, L. Blanc-Féraud, T. André, and M. Antonini, "Compression artifacts reduction using variational methods: algorithms and experimental study," in *Proceedings of IEEE International Conference on Acoustics, Speech, and Signal Processing (ICASSP)*, Las Vegas, March 2008, pp. 1173–1176.

[72] A. Dahimene, M. Noureddine, and A. Azrar, "A simple algorithm for the restoration of clipped speech signal," *Informatica*, vol. 32, no. 2, pp. 183–188, 2008.

[73] J. N. Laska, P. T. Boufounos, M. A. Davenport, and R. G. Baraniuk, "Democracy in action: Quantization, saturation, and compressive sensing," *Applied and Computational Harmonic Analysis*, vol. 31, no. 3, pp. 429–443, 2011.

[74] A. Adler, V. Emiya, M. G. Jafari, M. Elad, R. Gribonval, and M. D. Plumbley, "Audio inpainting," *IEEE Transactions on Audio, Speech, and Language Processing*, vol. 20, no. 3, pp. 922–932, 2012.

[75] B. Defraene, N. Mansour, S. De Hertogh, T. van Waterschoot, M. Diehl, and M. Moonen, "Declipping of audio signals using perceptual compressed sensing," *IEEE Transactions on Audio, Speech, and Language Processing*, vol. 21, no. 12, pp. 2627–2637, 2013.

[76] F. Wen, L. Adhikari, L. Pei, R. F. Marcia, P. Liu, and R. C. Qiu, "Nonconvex regularization-based sparse recovery and demixing with application to color image inpainting," *IEEE Access*, vol. 5, pp. 11513–11527, 2017.

[77] P. K. Mogensen and A. N. Riseth, "Optim: A mathematical optimization package for Julia," *The Journal of Open Source Software*, vol. 3, no. 24, 2018.

[78] A. Beck and M. Teboulle, "A fast iterative shrinkage-thresholding algorithm for linear inverse problems," *SIAM Journal on Imaging Sciences*, vol. 2, no. 1, pp. 183–202, 2009.

[79] RWCP Intellectual Resources Working Group, "RWCP news speech corpus (RWCP-SP99)," http://research.nii.ac.jp/src/en/RWCP-SP99.html (Accessed on November 13, 2020).

[80] J. Ahrens and S. Spors, "An analytical approach to sound field reproduction using circular and spherical loudspeaker distributions," *Acta Acustica united with Acustica*, vol. 94, pp. 988–999, 2008.

[81] N. Ueno, S. Koyama, and H. Saruwatari, "Three-dimensional sound field reproduction based on weighted mode-matching method," *IEEE/ACM Transactions on Audio, Speech, and Language Processing*, vol. 27, no. 12, pp. 1852–1867, 2019.

[82] Y. Maeno, Y. Mitsufuji, P. N. Samarasinghe, N. Murata, and T. D. Abhayapala, "Spherical-harmonic-domain feedforward active noise control using sparse decomposition of reference signals from distributed sensor arrays," *IEEE/ACM Transactions on Audio, Speech, and Language Processing*, vol. 28, pp. 656–670, 2020.

[83] H. Ito, S. Koyama, N. Ueno, and H. Saruwatari, "Feedforward spatial active noise control based on kernel interpolation of sound field," in *Proceedings of IEEE International Conference on Acoustics, Speech, and Signal Processing (ICASSP)*, Brighton, May 2019, pp. 466–470.

[84] Y. Takida, S. Koyama, N. Ueno, and H. Saruwatari, "Reciprocity gap functional in spherical harmonic domain for gridless sound field decomposition," *Signal Processing*, vol. 169, 2020.

[85] Z. Dogan, V. Tsiminaki, I. Jovanovic, T. Blu, and D. Van De Ville, "Localization of point sources for systems governed by the wave equation," in *Proceedings of Wavelets and Sparsity XIV*, San Diego, August 2011.

[86] Z. Dogan, I. Jovanovic, T. Blu, and D. Van De Ville, "3D reconstruction of wave-propagated point sources from boundary measurements using joint sparsity and finite rate of innovation," in *Proceedings of IEEE International Symposium on Biomedical Imaging (ISBI)*, Barcelona, May 2012, pp. 1575–1578.

[87] N. Ueno, S. Koyama, and H. Saruwatari, "Sound field recording using distributed microphones based on harmonic analysis of infinite order," *IEEE Signal Processing Letters*, vol. 25, no. 1, pp. 135–139, 2018.

[88] A. J. Berkhout, D. de Vries, J. Baan, and B. W. van den Oetelaar, "A wave field extrapolation approach to acoustical modeling in enclosed spaces," *The Journal of the Acoustical Society of America*, vol. 105, no. 3, pp. 1725–1733, 1999.

[89] E. Hulsebos, D. de Vries, and E. Bourdillat, "Improved microphone array configurations for auralization of sound fields by Wave-Field Synthesis," *Journal of the Audio Engineering Society*, vol. 50, no. 10, pp. 779–790, 2002.

[90] P. A. Martin, *Multiple Scattering: Interaction of Time-Harmonic Waves with N Obstacles*, Cambridge University Press, New York, 2006.

[91] M. Guy and R.-D. Keith, "On the efficient calculation of ordinary and generalized spherical harmonics," *Geophysical Journal International*, vol. 135, no. 1, pp. 307–309, 1998.

[92] K. V. Mardia and P. E. Jupp, *Directional Statistics*, John Wiley & Sons, Chichester, 2009.

[93] Y. L. Xu, "Fast evaluation of Gaunt coefficients: recursive approach," *Journal of Computational and Applied Mathematics*, vol. 85, no. 1, pp. 53–65, 1997.

[94] T. Hofmann, B. Schölkopf, and A. J. Smola, "Kernel methods in machine learning," *The Annals of Statistics*, vol. 36, no. 3, pp. 1171–1220, 2008.

[95] X. Chen and R. Womersley, "Spherical t-design with d=(t+1)^2 points," http://www.polyu.edu.hk/ama/staff/xjchen/sphdesigns.html (Accessed on November 13, 2020).

[96] J. B. Allen and D. A. Berkley, "Image method for efficiently simulating small-room acoustics," *The Journal of the Acoustical Society of America*, vol. 65, no. 4, pp. 943–950, 1979.

[97] H. Kuttruff, *Room Acoustics*, Spon Press, London, 5th edition, 2009.

[98] R. Narasimhan, *Analysis on Real and Complex Manifolds*, North-Holland, Amsterdam, 2nd edition, 1985.

[99] A. Dufresnoy, P. N. Gauthier, and W. H. Ow, "Uniform approximation on closed sets by solutions of elliptic partial differential equations," *Complex Variables and*

Elliptic Equations, vol. 6, no. 2-4, pp. 235–247, 1986.

[100] A. Kirsch and F. Hettlich, *The Mathematical Theory of Time-Harmonic Maxwell's Equations*, Springer International Publishing, Cham, 2015.

[101] J. S. Avery, "Harmonic polynomials, hyperspherical harmonics, and atomic spectra," *Journal of Computational and Applied Mathematics*, vol. 233, no. 6, pp. 1366–1379, 2010.

[102] G. N. Watson, *A Treatise on the Theory of Bessel Functions*, Cambridge University Press, Cambridge, 2nd edition, 1995.

A

Mathematical Definitions

A.1 Hilbert Space

Definition A.1. A set $\mathcal{U}$ is called a linear space over $\mathbb{K} \in \{\mathbb{R}, \mathbb{C}\}$ if the following conditions are satisfied:

- $u + (v + w) = u + (v + w)$ for all $u, v, w \in \mathcal{U}$.
- $u + v = v + u$ for all $u, v \in \mathcal{U}$.
- There exists an element $0 \in \mathcal{U}$ such that $u + 0 = u$ for all $u \in \mathcal{U}$.
- For each $u \in \mathcal{U}$, there exists an element $-u \in \mathcal{U}$ such that $u + (-u) = 0$.
- $a(u + v) = au + av$ for all $a \in \mathbb{K}$ and $u, v \in \mathcal{U}$.
- $(a + b)u = au + bu$ for all $a, b \in \mathbb{K}$ and $u \in \mathcal{U}$.
- $a(bu) = (ab)u$ for all $a, b \in \mathbb{K}$ and $u \in \mathcal{U}$.
- $1u = u$ for all $u \in \mathcal{U}$, where 1 denotes the multiplicative identity of $\mathbb{K}$.

Definition A.2. A set $\mathcal{U}$ is called an inner product space over $\mathbb{K} \in \{\mathbb{R}, \mathbb{C}\}$ with an inner product $\langle \cdot, \cdot \rangle_{\mathcal{U}} : \mathcal{U} \times \mathcal{U} \to \mathbb{K}$ if the following conditions hold:

- $\langle u, a(v + w) \rangle_{\mathcal{U}} = a \langle u, v \rangle_{\mathcal{U}} + a \langle u, w \rangle_{\mathcal{U}}$ for all $a \in \mathbb{K}$ and $u, v, w \in \mathcal{U}$.
- $\langle v, u \rangle_{\mathcal{U}} = \langle u, v \rangle_{\mathcal{U}}^*$ for all $u, v \in \mathcal{U}$.
- $\langle u, u \rangle_{\mathcal{U}} > 0$ for all $u \in \mathcal{U} \setminus \{0\}$.

In addition, $\mathcal{U}$ is called a Hilbert space over $\mathbb{K}$ with an inner product $\langle \cdot, \cdot \rangle_{\mathcal{U}}$ if the following condition is satisfied:

- Every Cauchy sequence $(u_n)_{n \in \mathbb{N}} \in \mathcal{U}^{\mathbb{N}}$ (with respect to the distance induced by the inner product $\langle \cdot, \cdot \rangle_{\mathcal{U}}$) converges to some point in $\mathcal{U}$.

Here, a sequence $(u_n)_{n \in \mathbb{N}} \in \mathcal{U}^{\mathbb{N}}$ is called a Cauchy sequence if for every $\varepsilon \in (0, \infty)$,

there exists some $N \in \mathbb{N}$ such that $\|u_n - u_m\|_{\mathcal{U}} < \varepsilon$ for all $n, m \in \mathbb{N}$ satisfying $n \geq N$ and $m \geq N$.

Definition A.3. Let $\mathcal{U}$ and $\mathcal{V}$ be Hilbert spaces over $\mathbb{K} \in \{\mathbb{R}, \mathbb{C}\}$ with inner products $\langle \cdot, \cdot \rangle_{\mathcal{U}} : \mathcal{U} \times \mathcal{U} \to \mathbb{K}$ and $\langle \cdot, \cdot \rangle_{\mathcal{V}} : \mathcal{V} \times \mathcal{V} \to \mathbb{K}$, respectively. A mapping $\Phi : \mathcal{U} \to \mathcal{V}$ is called a linear mapping if the following conditions are satisfied:

- $\Phi(u + u') = \Phi u + \Phi u'$ for all $u, u' \in \mathcal{U}$.
- $\Phi(au) = a(\Phi u)$ for all $a \in \mathbb{K}$ and $u \in \mathcal{U}$.

Furthermore, a linear mapping φ is said to be bounded if the following condition is satisfied:

- There exists some $M \in (0, \infty)$ such that $\|\varphi u\|_{\mathcal{V}} \leq M \|u\|_{\mathcal{U}}$ for all $u \in \mathcal{U}$.

Definition A.4. Let $\mathcal{U}$ be a Hilbert space over $\mathbb{K} \in \{\mathbb{R}, \mathbb{C}\}$ with an inner product $\langle \cdot, \cdot \rangle_{\mathcal{U}} : \mathcal{U} \times \mathcal{U} \to \mathbb{K}$. For $u \in \mathcal{U}$, the adjoint of u, denoted by $u^* : \mathcal{U} \to \mathbb{K}$ is defined as the bounded linear mapping given by

$$u^* v = \langle u, v \rangle_{\mathcal{U}} \quad (v \in \mathcal{V}). \tag{A.1}$$

Definition A.5. Let $\mathcal{U}$ and $\mathcal{V}$ be Hilbert spaces over $\mathbb{K} \in \{\mathbb{R}, \mathbb{C}\}$ with inner products $\langle \cdot, \cdot \rangle_{\mathcal{U}} : \mathcal{U} \times \mathcal{U} \to \mathbb{K}$ and $\langle \cdot, \cdot \rangle_{\mathcal{V}} : \mathcal{V} \times \mathcal{V} \to \mathbb{K}$, respectively. For a bounded linear mapping $\Phi : \mathcal{U} \to \mathcal{V}$, the adjoint of Φ, denoted by $\Phi^* : \mathcal{V} \to \mathcal{U}$ is defined as the unique bounded linear mapping satisfying

$$\langle \Phi u, v \rangle_{\mathcal{V}} = \langle u, \Phi^* v \rangle_{\mathcal{U}} \quad \forall u \in \mathcal{U},\ v \in \mathcal{V}. \tag{A.2}$$

A.2 Optimization Theory

Definition A.6. Let $\mathcal{U}$ be a linear space over $\mathbb{K} \in \{\mathbb{R}, \mathbb{C}\}$. A function $Q : \mathcal{U} \to \mathbb{R} \cup \{\infty\}$ is said to be convex if the following condition is satisfied.

- $Q(tu + (1-t)v) \leq tQ(u) + (1-t)Q(v)$ for all $u, v \in \mathcal{U}$ and $t \in [0,1]$.

Definition A.7. Let $\mathcal{U}$ be a Hilbert space over $\mathbb{K} \in \{\mathbb{R}, \mathbb{C}\}$ with an inner product $\langle \cdot, \cdot \rangle_{\mathcal{U}} : \mathcal{U} \times \mathcal{U} \to \mathbb{K}$. A function $Q : \mathcal{U} \to \mathbb{R} \cup \{\infty\}$ is said to be (Fréchet) differentiable at $u \in \mathcal{U}$ if there exists some $v \in \mathcal{U}$ satisfying

$$\lim_{h \to 0} \frac{Q(u+h) - Q(u) - \langle v, h \rangle_{\mathcal{U}}}{\|h\|_{\mathcal{U}}} = 0,$$

and such v, denoted by $\nabla Q(u)$ and called the (Fréchet) derivative, is unique if it exists.

Definition A.8. Let $\mathcal{U}$ be a Hilbert space over $\mathbb{K} \in \{\mathbb{R}, \mathbb{C}\}$ with an inner product $\langle \cdot, \cdot \rangle_{\mathcal{U}} : \mathcal{U} \times \mathcal{U} \to \mathbb{K}$. For a function $Q : \mathcal{U} \to \mathbb{R} \cup \{\infty\}$, the proximal operator of Q, denoted by $\operatorname{prox}_Q^\gamma \mathcal{S} \to \mathcal{U}$, is defined for $\gamma \in (0, \infty)$ as

$$\operatorname{prox}_Q^\gamma(u) \coloneqq \arg\min_{v \in \mathcal{U}} \left(Q(v) + \frac{1}{2\gamma} \|v - u\|_{\mathcal{U}}^2 \right).$$

B

Theories on Wave Equation and Helmholtz Equation

This appendix provides supporting mathematical theories for Chapter 5. The mathematical notations used in this appendix follow those in Chapter 5.

B.1 Approximation by Plane-Wave Functions

This section shows that for any solution u of (5.1), bounded closed set $\Omega_K \subset \Omega$, and positive number ε, there is a function u_{approx} in $\mathcal{U}$ (defined as (5.3)) satisfying

$$|u(\boldsymbol{r}) - u_{\mathrm{approx}}(\boldsymbol{r})| < \varepsilon \quad \forall \boldsymbol{r} \in \Omega_K. \tag{B.1}$$

First, from the boundedness of Ω_K, there is an open ball $B \supset \Omega_K$ centered at the origin. For such B, from the Lax–Malgrange theorem [98, 99] (note that the Helmholtz equation is an elliptic partial differential equation), there is a function $u_{\mathrm{LM}} : B \to \mathbb{C}$ satisfying $(\Delta + k^2)u_{\mathrm{LM}} = 0$ and

$$|u(\boldsymbol{r}) - u_{\mathrm{LM}}(\boldsymbol{r})| < \varepsilon/2 \quad \forall \boldsymbol{r} \in \Omega_K. \tag{B.2}$$

Moreover, from [100], u_{LM} admits the spherical wavefunction expansion

$$u_{\mathrm{LM}}(\boldsymbol{r}) = \sum_{\nu,\mu} \mathring{u}_{\mathrm{LM},\nu,\mu} \hat{\varphi}_{\nu,\mu}(\boldsymbol{r}) \quad (\boldsymbol{r} \in B). \tag{B.3}$$

Here, for $\nu \in \mathbb{N}$ and $\mu \in [\![-\nu, \nu]\!]$, $\mathring{u}_{\mathrm{LM},\nu,\mu} \in \mathbb{C}$ denotes the expansion coefficients, and $\hat{\varphi}_{\nu,\mu}(\cdot) : \mathbb{C}^3 \to \mathbb{C}$ is defined in (5.38). This series converges uniformly on Ω_K; therefore, there is some $N \in \mathbb{N}$ satisfying

$$|u_{\mathrm{LM}}(\boldsymbol{r}) - u_{\mathrm{LM},N}(\boldsymbol{r})| < \varepsilon/2 \quad \forall \boldsymbol{r} \in \Omega_K, \tag{B.4}$$

where $u_{\mathrm{LM},N} : \Omega \to \mathbb{C}$ is defined as

$$u_{\mathrm{LM},N}(\boldsymbol{r}) \coloneqq \sum_{\nu,\mu}^{N} \mathring{u}_{\mathrm{LM},\nu,\mu} \hat{\varphi}_{\nu,\mu}(\boldsymbol{r}) \quad (\boldsymbol{r} \in \Omega). \tag{B.5}$$

From (B.2) and (B.4), we obtain

$$|u(\boldsymbol{r}) - u_{\mathrm{LM},N}(\boldsymbol{r})| < \varepsilon \quad \forall \boldsymbol{r} \in \Omega_K. \tag{B.6}$$

On the other hand, from the equality (see Appendix B.2)

$$\hat{\varphi}_{\nu,\mu}(\boldsymbol{r}) = \frac{1}{4\pi} \int_{\boldsymbol{x}\in\mathbb{S}_2} \exp(-ik\boldsymbol{r}\circ\boldsymbol{x}) Y_{\nu,\mu}(\boldsymbol{x})\,\mathrm{d}\chi \quad (\boldsymbol{r}\in\mathbb{R}^3), \tag{B.7}$$

$u_{\mathrm{LM},N}$ is shown to be in $\mathcal{U}$. Therefore, by taking $u_{\mathrm{approx}} \coloneqq u_{\mathrm{LM},N}$, we obtain (B.1).

B.2 Derivation of Directionally Weighted Spherical Integrals

First, the equality

$$\xi_{\nu,\mu}(\boldsymbol{z}) = \frac{1}{4\pi} \int_{\boldsymbol{x}\in\mathbb{S}_2} \exp(-i\boldsymbol{z}\circ\boldsymbol{x}) Y_{\nu,\mu}(\boldsymbol{x})\,\mathrm{d}\chi \quad (\boldsymbol{z}\in\mathbb{C}^3,\ \nu\in\mathbb{N},\ \mu\in[\![-\nu,\nu]\!]) \tag{B.8}$$

will be proved as follows. Let $\Xi(\cdot):\mathbb{C}^3\to\mathbb{C}$ be defined as

$$\Xi(\boldsymbol{z}) \coloneqq \frac{1}{4\pi} \int_{\boldsymbol{x}\in\mathbb{S}_2} \exp(-i\boldsymbol{z}\circ\boldsymbol{x})\,\mathrm{d}\chi \quad (\boldsymbol{z}\in\mathbb{C}^3). \tag{B.9}$$

Since $\exp(-i\boldsymbol{z}\circ\boldsymbol{x})$ can be represented as a convergent power series with respect to $\boldsymbol{x}$, we can apply the integral formula in [101] and obtain the following equality:

$$\begin{aligned}\Xi(\boldsymbol{z}) &= \sum_{n=0}^{\infty} \frac{(-1)^n n!}{(2n+1)!} (z_1^2+z_2^2+z_3^2)^n \\ &= j_0\left((z_1^2+z_2^2+z_3^2)^{\frac{1}{2}}\right) \quad (\boldsymbol{z}\coloneqq[z_1,z_2,z_3]^{\mathsf{T}}\in\mathbb{C}^3).\end{aligned} \tag{B.10}$$

Moreover, let $\mathcal{Y}_{\nu,\mu}$ be differential operators obtained by replacing variables of the polynomials $y_{\nu,\mu}$ formally with the corresponding partial differentials. Then, from (B.9), we obtain

$$(\mathcal{Y}_{\nu,\mu}\Xi)(\boldsymbol{z}) = \frac{(-i)^\nu}{4\pi} \int_{\boldsymbol{x}\in\mathbb{S}_2} \exp(-i\boldsymbol{z}\circ\boldsymbol{x}) Y_{\nu,\mu}(\boldsymbol{x})\,\mathrm{d}\chi \quad (\boldsymbol{z}\in\mathbb{C}^3,\ \nu\in\mathbb{N},\ \mu\in[\![-\nu,\nu]\!]). \tag{B.11}$$

On the other hand, from Hobson's theorem [90] and (B.10), the following equality holds:

$$\begin{aligned}(\mathcal{Y}_{\nu,\mu}\Xi)(\boldsymbol{z}) &= \left[\left(\frac{1}{z}\frac{\mathrm{d}}{\mathrm{d}z}\right)^{\nu} j_0(z)\Big|_{z=\left(z_1^2+z_2^2+z_3^2\right)^{\frac{1}{2}}}\right] y_{\nu,\mu}(\boldsymbol{z}) \\ &= \frac{(-1)^\nu}{\left(z_1^2+z_2^2+z_3^2\right)^{\frac{\nu}{2}}} j_\nu\left(\left(z_1^2+z_2^2+z_3^2\right)^{\frac{1}{2}}\right) y_{\nu,\mu}(\boldsymbol{z}) \\ &= (-1)^\nu j_\nu\left(\left(z_1^2+z_2^2+z_3^2\right)^{\frac{1}{2}}\right) y_{\nu,\mu}\left(\frac{\boldsymbol{z}}{\left(z_1^2+z_2^2+z_3^2\right)^{\frac{1}{2}}}\right) \\ &\quad (\boldsymbol{z}\coloneqq[z_1,z_2,z_3]^{\mathsf{T}}\in\mathbb{C}^3,\ \nu\in\mathbb{N},\ \mu\in[\![-\nu,\nu]\!]).\end{aligned} \tag{B.12}$$

From (B.11) and (B.12), we obtain (B.8).

Next, the equality

$$\Theta_{\nu_1,\mu_2}^{\nu_2,\mu_2}(\boldsymbol{z}) = \frac{1}{4\pi}\int_{\boldsymbol{x}\in\mathbb{S}_2} \exp(-i\boldsymbol{z}\circ\boldsymbol{x}) Y_{\nu_1,\mu_1}(\boldsymbol{x})^* Y_{\nu_2,\mu_2}(\boldsymbol{x})\,\mathrm{d}\chi \\ (\boldsymbol{z}\in\mathbb{C}^3,\ \nu_1,\nu_2\in\mathbb{N},\ \mu_1\in[\![-\nu_1,\nu_1]\!],\ \mu_2\in[\![-\nu_2,\nu_2]\!]) \tag{B.13}$$

will be proved as follows. From the linearization formula of the spherical harmonic functions [90], we obtain

$$Y_{\nu_1,\mu_1}(\boldsymbol{x})^* Y_{\nu_2,\mu_2}(\boldsymbol{x}) = \sum_{\nu_3,\mu_3}^{\nu_1+\nu_2} \mathcal{G}(\nu_1,\mu_1;\nu_2,\mu_2;\nu_3,\mu_3) Y_{\nu_3,\mu_3}(\boldsymbol{x}) \\ (\boldsymbol{x}\in\mathbb{S}_2,\ \nu_1,\nu_2\in\mathbb{N},\ \mu_1\in[\![-\nu_1,\nu_1]\!],\ \mu_2\in[\![-\nu_2,\nu_2]\!]). \tag{B.14}$$

Using this formula and (B.8), we obtain (B.13) as

$$\begin{aligned}
&\frac{1}{4\pi}\int_{\boldsymbol{x}\in\mathbb{S}_2} \exp(-i\boldsymbol{z}\circ\boldsymbol{x}) Y_{\nu_1,\mu_1}(\boldsymbol{x})^* Y_{\nu_2,\mu_2}(\boldsymbol{x})\,\mathrm{d}\chi \\
&= \sum_{\nu_3,\mu_3}^{\nu_1+\nu_2} \mathcal{G}(\nu_1,\mu_1;\nu_2,\mu_2;\nu_3,\mu_3)\cdot\frac{1}{4\pi}\int_{\boldsymbol{x}\in\mathbb{S}_2} \exp(-i\boldsymbol{z}\circ\boldsymbol{x}) Y_{\nu_3,\mu_3}(\boldsymbol{x})\,\mathrm{d}\chi \\
&= \sum_{\nu_3,\mu_3}^{\nu_1+\nu_2} \mathcal{G}(\nu_1,\mu_1;\nu_2,\mu_2;\nu_3,\mu_3)\xi_{\nu_3,\mu_3}(\boldsymbol{z}) \\
&\quad (\boldsymbol{z}\in\mathbb{C}^3,\ \nu_1,\nu_2\in\mathbb{N},\ \mu_1\in[\![-\nu_1,\nu_1]\!],\ \mu_2\in[\![-\nu_2,\nu_2]\!]).
\end{aligned} \tag{B.15}$$

B.3 Derivation of Adjoint Representation of Pressure-Gradient Microphone

Let $u\in\mathcal{U}$ be represented as (5.2) with $\tilde{u}\in\mathcal{L}_2(\mathbb{S}_1,\mathbb{C})$. Then, we have

$$D_{m,p}u = G_m\int_{\boldsymbol{x}\in\mathbb{S}_1}\tilde{u}(\boldsymbol{x})(-ik\boldsymbol{x}\circ\boldsymbol{y}_m)\exp(-i\boldsymbol{x}\circ\boldsymbol{r}_m - i\omega t_p)\,\mathrm{d}\chi \\ (u\in\mathcal{U},\ m\in[\![1,M]\!],\ p\in[\![1,P_m]\!]). \tag{B.16}$$

Therefore, $v_{m,p}$ can be represented as

$$\begin{aligned}
v_{m,p}(\boldsymbol{r},t) &= G_m\int_{\boldsymbol{x}\in\mathbb{S}_1}\mathrm{Re}\left((ik\boldsymbol{x}\circ\boldsymbol{y}_m)\exp(i\boldsymbol{x}\circ\boldsymbol{r}_m + i\omega t_p)\exp(-i\boldsymbol{x}\circ\boldsymbol{r} - i\omega t)\right)\mathrm{d}\chi \\
&= G_m\int_{\boldsymbol{x}\in\mathbb{S}_1}\mathrm{Re}\left(\exp(-i\boldsymbol{x}\circ(\boldsymbol{r}-\boldsymbol{r}_m))(ik\boldsymbol{x}\circ\boldsymbol{y}_m)\exp(-\omega(t-t_p)\right)\mathrm{d}\chi \\
&\quad (\boldsymbol{r}\in\mathbb{R}^2,\ t\in\mathbb{R})
\end{aligned} \tag{B.17}$$

for each $m\in[\![1,M]\!]$ and $p\in[\![1,P_m]\!]$. Here, from the formulae for Bessel functions for the first kind [102]

$$\frac{1}{2\pi}\int_{\boldsymbol{x}\in\mathbb{S}_1}\exp(-i\boldsymbol{x}\circ\boldsymbol{z})\exp(i\nu\angle\boldsymbol{x})\,\mathrm{d}\chi = \frac{1}{i^\nu}J_\nu(\|\boldsymbol{z}\|_2)\exp(i\nu\angle\boldsymbol{z}) \quad (\boldsymbol{z}\in\mathbb{R}^2,\ \nu\in\mathbb{Z}), \tag{B.18}$$

$$J_{-\nu}(z) = (-1)^{\nu} J_{\nu}(z) \quad (z \in \mathbb{R},\ \nu \in \mathbb{Z}), \tag{B.19}$$

and the equality

$$\boldsymbol{x} \circ \boldsymbol{y}_m = \cos(\angle \boldsymbol{x} - \angle \boldsymbol{y}_m) \quad (\boldsymbol{x} \in \mathbb{S}_1,\ m \in [\![1, M]\!]), \tag{B.20}$$

the integral in (B.17) can be calculated as

$$\begin{aligned} v_{m,p}(\boldsymbol{r}, t) = 2\pi k G_m J_1(k\|\boldsymbol{r} - \boldsymbol{r}_m\|_2) \cos(\angle(\boldsymbol{r} - \boldsymbol{r}_m) - \angle \boldsymbol{y}_m) \cos(\omega(t - t_p)) \\ (\boldsymbol{r} \in \mathbb{R}^2,\ t \in \mathbb{R},\ m \in [\![1, M]\!],\ p \in [\![1, P_m]\!]). \end{aligned} \tag{B.21}$$

Furthermore, $K_{m_1,m_2}^{p_1,p_2}$ can be represented as

$$\begin{aligned} K_{m_1,m_2}^{p_1,p_2} &= \langle v_{m_1,p_1}, v_{m_2,p_2} \rangle_{\mathcal{U}} \\ &= G_{m_1} G_{m_2} \int_{\boldsymbol{x} \in \mathbb{S}_1} \mathrm{Re}((ik\boldsymbol{x} \circ \boldsymbol{y}_{m_2})(-ik\boldsymbol{x} \circ \boldsymbol{y}_{m_1}) \exp(i\boldsymbol{x} \circ (\boldsymbol{r}_{m_2} - \boldsymbol{r}_{m_1})) \\ &\qquad \cdot \exp(i\omega(t_{p_2} - t_{p_1}))) \, \mathrm{d}\chi \\ &\quad (m_1, m_2 \in [\![1, M]\!],\ p_1 \in [\![1, P_{m_1}]\!],\ p_2 \in [\![1, P_{m_2}]\!]). \end{aligned} \tag{B.22}$$

Here, from (B.18), (B.19), and

$$\begin{aligned} (\boldsymbol{x} \circ \boldsymbol{y}_{m_1})(\boldsymbol{x} \circ \boldsymbol{y}_{m_2}) &= \cos(\angle \boldsymbol{x} - \angle \boldsymbol{y}_{m_1}) \cos(\angle \boldsymbol{x} - \angle \boldsymbol{y}_{m_1}) \\ &= \frac{1}{2} \left(\cos(2\angle \boldsymbol{x} - \angle \boldsymbol{y}_{m_1} - \angle \boldsymbol{y}_{m_2}) - \cos(\angle \boldsymbol{y}_{m_2} + \angle \boldsymbol{y}_{m_1})\right) \\ &\quad (\boldsymbol{x} \in \mathbb{S}_1,\ m_1, m_2 \in [\![1, M]\!]), \end{aligned} \tag{B.23}$$

the integral in (B.22) can be calculated as

$$\begin{aligned} K_{m_1,m_2}^{p_1,p_2} = -\pi k^2 G_{m_1} G_{m_2} [J_2(k\|\boldsymbol{r}_{m_2} - \boldsymbol{r}_{m_1}\|_2) \cos(2\angle(\boldsymbol{r}_2 - \boldsymbol{r}_1) - \angle \boldsymbol{y}_{m_1} - \angle \boldsymbol{y}_{m_2}) \\ - J_0(k\|\boldsymbol{r}_{m_2} - \boldsymbol{r}_{m_1}\|_2) \cos(\angle \boldsymbol{y}_{m_2} - \angle \boldsymbol{y}_{m_1})] \cdot \cos(\omega(t_{p_2} - t_{p_1})) \\ (m_1, m_2 \in [\![1, M]\!],\ p_1 \in [\![1, P_{m_1}]\!],\ p_2 \in [\![1, P_{m_2}]\!]). \end{aligned} \tag{B.24}$$